

**Elementary Reaction Steps of NO_x Trapping and SO_x Deactivation of
NO_x Storage Reduction Catalysts**

Christian Sedlmair

2002

Ph.D. thesis
University of Twente



Twente University Press

Also available in print:

<http://www.tup.utwente.nl/catalogue/book/index.jsp?isbn=9036518199>

ELEMENTARY REACTION STEPS OF
NO_x TRAPPING AND SO_x DEACTIVATION OF
NO_x STORAGE REDUCTION CATALYSTS

Leden van de promotiecommissie:

Voorzitter/Secretaris:	Prof.dr. J. Feijen	U. Twente
Promotor:	Prof.dr. J.A. Lercher	TU München
Assistent-promotor:	Dr. K. Seshan	U. Twente
Leden:	Prof.dr.ir. L. Lefferts	U. Twente
	Prof.dr.ir. J.A.M Kuipers	U. Twente
	Prof.dr. F. Kapteijn	TU Delft
	Prof.dr. B. Weckhuysen	U. Utrecht
Deskundige:	Dr. A. Jentys	TU München

The research described in this thesis was funded by the European Community within the project, STORECAT, BriteEuram BRPR-CT98-0613.



Twente University **Press**

Publisher:
Twente University Press
P.O. Box 217, 7500 AE Enschede
www.tup.utwente.nl

Printing and binding by Océ Facility Services, Enschede

Copyright © 2002 by Christian Sedlmair, Enschede, The Netherlands

ISBN 90 365 1819 9

ELEMENTARY REACTION STEPS OF
NO_x TRAPPING AND SO_x DEACTIVATION OF
NO_x STORAGE REDUCTION CATALYSTS

PROEFSCHRIFT

ter verkrijging van
de graad van doctor aan de Universiteit Twente,
op gezag van de rector magnificus,
prof. dr. F.A. van Vught,
volgens besluit van het College voor Promoties
in het openbaar te verdedigen
op vrijdag 15 november 2002 te 16.45 uur

door

Christian Sedlmair

geboren op 4 mei 1972

te Buchloe, Duitsland

Dit Proefschrift is goedgekeurd door de promotor

Prof. Dr. J. A. Lercher

en assistent-promotor

Dr. K. Seshan

to my family

Catalysts should always be benchmarked against state-of-the-art materials. Reports of improved catalyst life without some reference point to established catalysts under similar operating conditions only adds confusion to the growing literature in this area.

J.N. Armor, Catal. Today **38** (1997) 163

Table of Contents

<i>Chapter 1</i>	Introduction	1
	Vehicle emissions and environmental problems	
	Vehicle emissions legislation	
	Catalytic emission aftertreatment systems	
	Structure and Scope of the thesis	
<i>Chapter 2</i>	Experimental section	17
	Catalyst preparation	
	Characterization techniques	
<i>Chapter 3</i>	An <i>in situ</i> IR study of the NO_x adsorption/ reduction mechanism on modified Y zeolites	25
	Introduction	
	Experimental	
	Results and discussion	
	NO ₂ adsorption on NaHY, NaY	
	Thermal stability of NO _x surface species on NaHY and NaY	
	NO ₂ adsorption on BaY	
	Thermal stability of NO _x surface species on BaY	
	Effect of different gas mixtures – NO, NO+O ₂ and NO ₂	
	Adsorption of NO, NO+O ₂ and NO ₂ under non isothermal conditions	
	Mechanistic model for NO _x adsorption	
	Reduction of surface NO _x species by propene	
	Conclusions	

Chapter 4 **Elementary steps of NO_x adsorption and surface reaction on a commercial storage reduction catalyst** **53**

Introduction

Experimental

Results

 Catalyst characterization

 IR spectroscopic study of the NO_x storage process

 Exposure to NO

 Exposure to NO₂

 Simultaneous exposure to NO and O₂

 Thermal stability of NO_x surface species

Discussion

Conclusion

Chapter 5 **Influence of sulfur dioxide on the catalytic performance of a commercial NO_x-storage reduction catalyst** **77**

Introduction

Experimental

Results and discussion

 XRD study of the interaction of SO₂ with a NSR catalyst

 Sorption and retention of SO₂ under varying reaction conditions

 Adsorption of SO₂ under lean conditions

 Adsorption of SO₂ under fuel-rich conditions

 Stability of SO_x species formed

 Effect of sulfation on the NO_x adsorption capacity

Conclusions

<i>Chapter 6</i>	Mechanistic aspects on the sulfur deactivation of NO_x storage reduction catalysts	95
	Introduction	
	Experimental	
	Results	
	Interaction of SO _x with the storage component	
	Interaction of SO _x with the oxidation/reduction function	
	Discussion	
	Conclusion	
<i>Chapter 7</i>	Summary and conclusions	109
	Summary and conclusions	
	Samenvatting en conclusies	
	Zusammenfassung und Schlußfolgerungen	
	<i>Acknowledgements</i>	123
	<i>Curriculum Vitae</i>	124

Chapter 1

Introduction

Abstract

This chapter gives a background on the concerns associated with vehicle emissions, the trends in regulation and the approaches developed for their reduction.

1. INTRODUCTION

Motor vehicles emit significant quantities of carbon monoxide (CO), hydrocarbons (HC), nitrogen oxides (NO_x), sulfur oxides (SO_x) and fine particles (PM). The negative impact of these emissions on the environment, on human health and on the climate led to the introduction of emission control standards and the development of exhaust aftertreatment systems. This resulted in a 90% reduction of the major pollutants CO, hydrocarbons and NO_x from passenger car emissions per vehicle and kilometres.

However, the increasing concentration of carbon dioxide (CO₂) in the atmosphere and its contribution to the global warming (greenhouse effect) is also of general concern. The transportation sector is responsible for about 17% of global CO₂ emissions.

Lean-burn and diesel engines possess a high effective fuel efficiency and hence lower fuel consumption, which contributes to the reduction of CO₂ emissions. Due to the surplus of oxygen in their exhausts NO_x reduction by conventional three-way catalysts (TWCs) is hindered, and new aftertreatment technologies are required. Besides selective catalytic reduction with hydrocarbons (HC-SCR) or ammonia (NH₃-SCR), a promising new technology for aftertreatment systems for lean-burn exhausts is based on the concept of NO_x storage reduction (NSR).

In this chapter, a brief summary about the concerns associated with vehicle emissions, the trends in regulation and the approaches developed for their reduction is given. Emphasis is placed on the NO_x storage reduction technology.

1.1 Vehicle emissions and environmental problems

One of the most important issues concerning our environment is air pollution. Emissions of mobile sources, such as automobiles, aircrafts, trains and ships

contribute a significant fraction of the total amount of emissions. In Europe, the transportation sector contributes about 60 % of carbon monoxide emissions and about 25 % of energy-related CO₂ emissions and more than half of total nitrogen oxide emissions come from road traffic alone [1]. The major air pollutants emitted by the transport sector are nitrogen oxides (NO_x), carbon monoxide (CO), hydrocarbons (HC), particulate matter (PM), sulfur oxides (SO_x) and carbon dioxide (CO₂) [2]. In table 1 the exhaust compositions of different engines are given [3].

Table 1: Indicative values of the exhaust composition for different engine types [3].

	CO (%)	HC (ppm C)	NO _x (ppm)	Particulates (g/kWh)	O ₂ (%)
Diesel	0.01-0.2	100-2000	200-1000	0.15-0.5	3-15
Otto lean-burn	0.05-0.5	1000-5000	100-1000	-	0.5-5
Otto	0.3-1	1000-5000	50-2500	-	0.1-0.5

The negative influence of *nitrogen oxide* (NO_x) emissions to the environment is caused by their contributions to acid rain, smog and the greenhouse effect (especially N₂O) and to the depletion of the earth protective ozone layer. Nitrogen oxides produce several negative health effects through NO_x intrusion in the respiratory system.

Carbon monoxide (CO) is a tasteless, odourless and colourless gas produced through the incomplete combustion of carbon-based fuels. CO enters the bloodstream through the lungs and reduces the delivery of oxygen to the organs and tissues.

Hydrocarbons (HCs) are known to be involved in the formation of ozone as a photochemical precursor. HC derivatives, as for example benzene, are toxic to the human body and extremely carcinogen.

During combustion the sulfur containing impurities react with oxygen forming sulfur *oxides* (SO_x). In the atmosphere these species undergo further oxidation and interact with water [4], producing acid rain that kills vegetation and corrodes buildings.

Particulate matter (PM) is the term for the mixture of solid particles and liquid droplets found in the air. PM includes dust, dirt, soot, smoke and liquid droplets emitted from motor vehicles or formed by condensation or transportation of emitted exhaust gases in the atmosphere. The small particles (less than 2.5 μm in diameter) could penetrate the respiratory defence system and could be linked to a series of health problems, like chronic bronchitis, premature death and even lung cancer.

Besides CH₄ and N₂O, *carbon dioxide* (CO₂) is known to be the major greenhouse gas. In the most countries, over 90% of the global warming potential of the direct acting greenhouse gases from transportation sector comes from CO₂ [5]. The transportation sector is responsible for approximately 17% of global CO₂ emissions and these emissions are still increasing due to the rapid increasing numbers of vehicles.

1.2 Vehicle emissions legislation

The growing knowledge of the impact of automotive emissions on the environment and human health and the increasing environmental awareness of the public led to the introduction of emission control standards for motor vehicle starting at the sixties in the US [6]. In Europe, the first passenger car emissions directive was enacted in 1970 [7, 8]. Since then the introduction of exhaust catalysts for vehicles has led to an overall reduction of emissions of the order of 90% for the pollutant

carbon monoxide (CO), unburned hydrocarbons (HC) and nitrogen oxides (NO_x) [9]. These improvements are illustrated in figure 1.

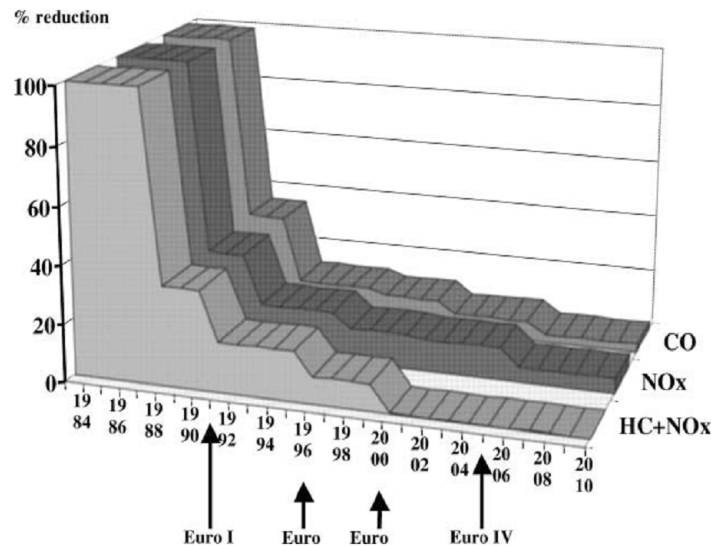


Fig. 1: Evolution of emission standards – gasoline passenger cars.

However, due to the fast increase of world motor vehicle production more stringent emission standards have to be legislated to reduce the world air pollution. In the EU the next step for lower emission standards for passenger cars (EURO IV) is scheduled for 2005 (Table 2).

Table 2: Euro III and EURO IV legislation for diesel and gasoline passenger cars [10].

State	Year	CO (g/km)	HC (g/km)	HC+NO _x (g/km)	NO _x (g/km)	PM (g/km)
Diesel						
Euro III	2000	0.64	-	0.56	0.50	0.05
Euro IV	2005	0.50	-	0.30	0.25	0.025
Petrol (Gasoline)						
Euro III	2000	2.30	0.20	-	0.15	-
Euro IV	2005	1.0	0.10	-	0.08	-

In conjunction with the further tightening of emission limits a new aspect is the reduction of CO₂ emission levels. Due to the Kyoto Protocol, approved in 1997, the EU commit on reducing their greenhouse gas emissions from 1990 by 8 per cent until 2012. Achievement of the lower limits for emissions from vehicles requires both, a further reduction of CO, HC and NO_x by more efficient aftertreatment catalyst and engine technologies with an improved fuel economy such as diesel or lean-burn Otto engines to reduce the CO₂ emissions.

1.3 Catalytic emission aftertreatment systems

1.3.1 Three-way catalyst –catalyst for stoichiometric working engines

Since 1975 catalytic emission control systems have been used on passenger cars to reduce engine exhaust pollutants (i.e. NO_x, CO and HC). The first technology was based on oxidation catalyst, followed in the early 1980s by the three-way conversion catalyst (TWC) [11]. This system consists of an oxygen sensor (lambda-sensor), a three-way catalytic converter, an electronic control unit and a controllable fuel-metering unit. This system provides a very efficient control of hydrocarbon (HC), carbon monoxide (CO) and nitrogen oxide (NO_x) exhaust emissions, by a simultaneous oxidation of CO and HC and the reduction of NO_x [12]. The key problem to advancing this technology was to control the air to fuel ratio within a narrow window of about ± 0.05 around the stoichiometric air to fuel ratio point of about 14.6 (wt basis) (see Fig. 2).

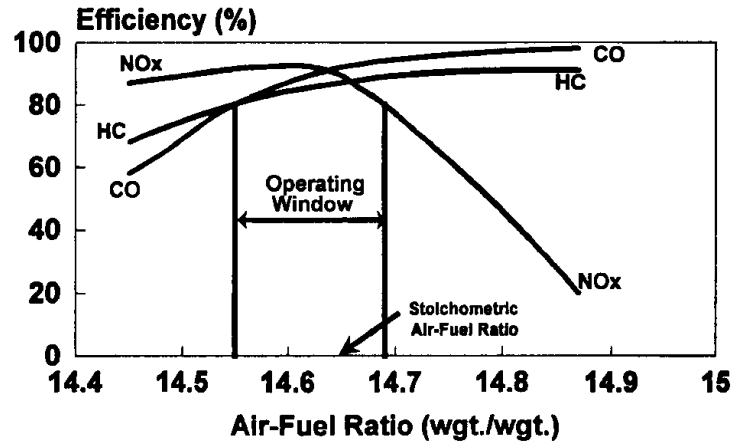


Figure 2: Three way catalyst simultaneous conversion of NO_x , CO and HCs [13].

The more stringent emission standards require a higher efficiency and a further development. The liberation of unburned HCs from the exhaust during the cold start period is one of the key problems. To shortening of the cold-start period to reach earlier the HC light-off temperature (above 300°C) several new technologies are under investigation. One promising technology is to install an additional catalyst close to the exhaust port to benefit from the hot exhaust and thus reach the light-off temperature within shorter time [14]. Alternative technologies are (i) to electrically heat the pre-converter during the cold start period [15-17], (ii) to trap the HCs during the cold start period and release it when the catalyst reached the light-off temperature [18] (iii) to increase the HC concentration at the beginning and ignite it electrically upstream of the catalyst [19].

1.3.2 Catalysts for lean burn gasoline and diesel engines

Lean burn engines operations, i.e. engine operations with excess oxygen have promising advantages for meeting the stricter emission standards. Raw NO_x emissions are lowered, due to a reduced combustion temperature [18]. Furthermore, lean burn engines have a higher efficiency and hence a lower fuel consumption. The potential fuel saving and therefore reduction in CO_2 emissions

compared to stoichiometric gasoline engines is for lean burn gasoline engines up to 20% and for diesel engines even up to 32%.

However, three way catalysts are unable to convert NO_x to N_2 under the large excess of O_2 present in the exhaust stream (oxidizing conditions) [20, 21]. Research and development of materials and methods of NO_x conversion in exhaust gas with excess air for use in lean burn gasoline and diesel engines has gained in significance in recent years.

1.3.2.1 HC-Selective Reduction

Lean burn and diesel engine exhausts contain low levels of reductant (CO , HC) in the presence of a large excess of oxygen. These small amounts of reductants could only reduce a small amount of NO_x under catalyzed conditions. Additional HCs added to the exhaust could raise the NO_x reduction to more adequate levels. From intensive research it was found that metal (mainly transition metals such as Cu or Co), supported on specific zeolites are able to convert NO_x [22-25]. Also metal oxides supported on silica or alumina [26-29] were reported to be active for the HC-SCR of NO_x . However their drawbacks for a commercial application is the low durability, especially the stability at high temperature, the small temperature activity range [20] and a low resistance against water in the exhaust and sulfur poisoning [30].

1.3.2.2 Urea/ NH_3 -SCR

Selective catalytic reduction of NO_x using ammonia (NH_3) or urea ($\text{CO}(\text{NH}_2)_2$) has been used for many years in industrial processes, as well as in stationary diesel engine applications. In the NH_3 -SCR process, NO_x reacts with ammonia, which is injected into the exhaust gas stream before the catalyst. Several types of catalysts based on platinum, vanadium oxides or zeolites are used. The different operating

temperature window of these catalysts determines the choice for a particular SCR process.

Urea is potentially a convenient source of ammonia and urea-based SCR systems are already applied for heavy-duty diesel trucks [31]. The system consists of a platinum pre-oxidation catalyst, a hydrolysis catalyst and a vanadium based SCR catalyst, followed by a platinum guard catalyst to prevent traces of ammonia from escaping into the environment by oxidizing it to NO which is environmentally less sensitive (see Fig. 3).

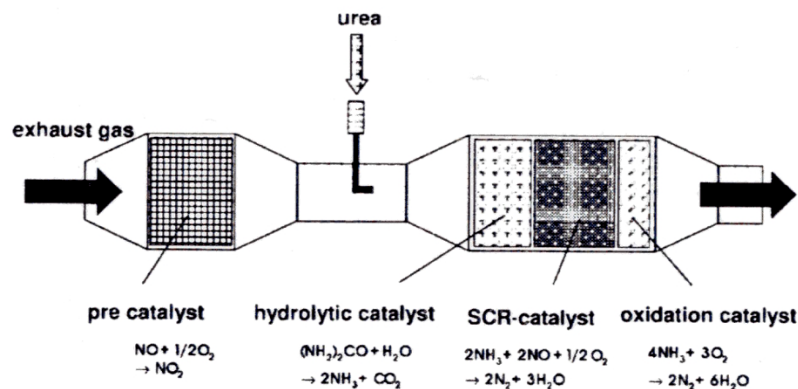


Figure 3: Selective catalytic reduction with urea.

The use of urea-SCR, especially in passenger cars present however the following problems [18, 32]:

- Additional space for urea tank and the more complex aftertreatment system.
- Creation of necessary infrastructure for refilling with urea.
- Efficiency limits at low exhaust gas temperatures in part-load range.
- Operation at low ambient temperatures due to the high freezing point (-10°C) of urea.

1.3.2.3 Non Thermal-Plasma exhaust treatment

A new approach to control NO_x emissions in lean exhaust is plasma-assisted catalytic NO_x reduction

[33]. NO_x control using non-thermal plasma is achieved as followed

(Fig.4). A high voltage is applied across two plates

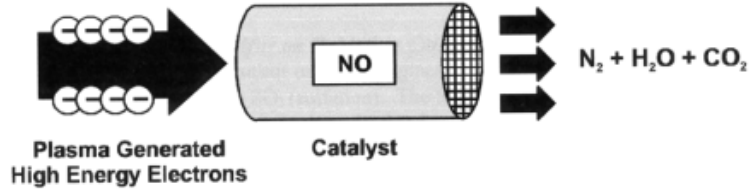


Figure 4: Concept of non-thermal plasma treatment

positioned in the exhaust. Electrons of molecules are energized and ionic chemical species are formed – oxygen and water are the easiest species to be ionised. Under certain conditions of voltage and current density the generated ions oxidize NO to NO_2 . catalytic reductions of NO_x emissions then proceed efficiently on a selective NO_x catalyst with HC as the reductant. The selective NO_x catalyst using HC as reductant works more efficiently in the reduction of NO_2 as compared to NO [34, 35].

Additionally, this technology is found to reduce PM, presumably by NO_2 oxidation of carbon. This promising technology is still in the research and development stage. The mechanisms for the whole process are not fully understood and significant additional development efforts are needed to optimise this technology for commercial application.

1.3.2.4 NO_x Storage Reduction

The most promising aftertreatment technology for lean burn and diesel engines is based on the concept of NO_x storage-reduction (NSR) explored in the early 90s for lean burn engines operating alternatively under lean and fuel-rich conditions [36-40]. The NSR catalyst consists mainly of noble metals (mainly Pt) for the three-way function, alkali and alkaline earth metals (mainly Ba) or rare earth metals for

the storage function and alumina as a high surface area support [41]. During the

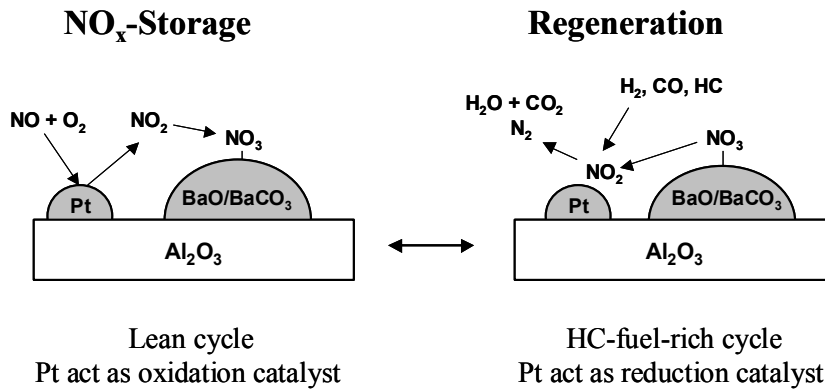


Fig. 5: Concept of NO_x storage reduction.

nitrogen oxide storage phase (lean operation) the NO_x from the engine, primarily in the form of NO is oxidized to NO₂ on the noble

metal component and reacts further with the storage component of the catalyst to form nitrate (Fig. 5). When the available storage component is saturated the engine is briefly operated with sub-stoichiometric air to fuel ratio (fuel-rich operation) to regenerate the storage function. The excess exhaust components H₂, CO and HC convert the released NO_x on the noble metal to nitrogen [42-45]. This concept shows a high efficiency in reducing NO_x from exhausts of lean burn engines. For example, an average NO_x conversion of 90,5% can be obtained using 60 sec lean ($\lambda = 1.35$) and 0.3 sec fuel-rich ($\lambda = 0.7$) cycles on a fresh catalyst at 350°C [46].

The NSR concept has been the subject of intensive research and development activities [47-54] and has now reached high development standard and commercial applications in Japan [13] and Europe [18] in direct-injection petrol engines.

The main drawback of NSR catalysts is their high sensitivity to sulfur due to the fact that the NO_x storage component forms a stable sulfate with SO_x present in a typical European exhaust emission from gasoline and particularly from diesel engines [40, 55]. These sulfates are not removable during a normal NO_x regeneration cycle and accumulate on the catalysts, which result in a drastic loss of the NO_x storage ability [56]. A desulfurization requires fuel-rich operation at high temperatures for several minutes. However these represents extremely critical

operation conditions in view of detriment to the vehicle performance, driving convenience, secondary emissions (mainly H₂S) and especially an increase in fuel consumption [18].

The reduction of the amount of sulfur in the fuel down to a technically sulfur-free level will help to preserve the activity of NSR catalysts. However, a slow poisoning effect occurs even on a fuel with very low sulfur content (<10 ppm). Therefore, improvements to catalyst design and technology will also be required to create systems, which either totally preclude the possibility of sulfur poisoning or significantly facilitate regeneration.

1.4 Scope and structure of the thesis

The NO_x storage reduction concept offers a promising strategy for exhaust aftertreatment of lean-burn and diesel engines. However, to meet further more stringent emission regulations, the sulfur resistance of these catalysts has to be improved. Therefore, a detailed knowledge of the NO_x storage reduction mechanism and the SO_x deactivation mechanism is important to achieve suitable catalysts.

The aim of this thesis is, therefore, to obtain a fundamental insight in the NO_x adsorption/reduction mechanism and the SO_x deactivation mechanism occurring on NSR catalysts to be able structure the complex reaction sequences into specific key elementary steps.

In **chapter 2** the experimental details employed in this thesis are given. The adsorption and reduction mechanisms of NO_x on sodium and barium metal exchanged zeolite Y used as model storage components are elucidated in **chapter 3**. With this knowledge, a detailed investigation of the mechanism of NO_x storage on a commercial NSR catalyst was carried out and discussed in **chapter 4**. The influence of SO₂ on the catalytic performance of the catalyst is explored in **chapter**

5. The information obtained in Chapter 5 was used for a detailed investigation of the interaction of SO_x with the storage and the oxidation/reduction component (**Chapter 6**). Finally, in **Chapter 7** the results of these study are summarized and general conclusions are given.

References

- [1] European Commission: [http:// europa.eu.int/comm/environment](http://europa.eu.int/comm/environment).
- [2] Walsh M.P., *Platinum Metals Rev.* **44**, 22 (2000).
- [3] Koltsakis G.C., Stamatelos A.M., *Prog. Energy Combust. Sci.* **23**, 1 (1997).
- [4] Stern A.C., Boubel R.W., Turner D.B., Fox D.L., “Fundamental of Air Pollution”, 2nd ed., Academic Press, Orlando, 1984.
- [5] Second Assessment Report of the Intergovernmental Panel on Climate Change (IPCC), “Climate Change 1995: The Science of Climate Change”, ed. J.T. Houghton, Cambridge University Press, Cambridge, 1996.
- [6] Armor J.N., *Appl. Catal. B* **1**, 221 (1992).
- [7] Ertl G., Knözinger H., Weitkamp J., “Handbook of Heterogeneous Catalysis”, Wiley-VCH, Weinheim (1997).
- [8] Greening P., *Topics in Catal.* **16/17**, 5 (2001).
- [9] Rainbow R., Tan H., “Meeting the demand for mobility”, Shell selected paper (1993).
- [10] Docquier N., Candel S., *Prog. Energy Combust. Sci.* **28**, 107 (2002).
- [11] Shelef M., Graham G.W., *Catal. Rev.-Sci. Eng.* **36**, 433 (1994).
- [12] Taylor K.C., *Catal. Rev.-Sci. Eng.* **35**, 457 (1993).
- [13] Farrauto R.J., Heck R.M., *Catal. Today* **51**, 351 (1999).
- [14] Hu Z., Heck R., *SAE 950254* (1995).
- [15] Shimasaki Y., Kato H., Abe F., Hashimoto S., Kaneko T., *SAE 971031* (1997).
- [16] Oh S.H., Bissett E.J., Battison P.A., *Ind. Eng. Chem. Res.* **32**, 1560 (1993).
- [17] Kirchner T., Eigenberger G., *Chem. Eng. Sci.* **10**, 2409 (1996).
- [18] König A., Herding G., Hupfeld B., Richter Th., Weidmann K., *Topics in Catal.* **16/17**, 23 (2001).
- [19] Ma T., Collins N., Hands T., *SAE 920400* (1992).
- [20] Kreuzer T., Lox E.S., Lindner D., Leyrer J., *Catal. Today* **29**, 17 (1996).
- [21] Shelef, M., *Catal. Rev.-Sci. Eng.* **95**, 209 (1995).

- [22] Iwamoto M., Furukawa H., Mine Y., Uemura F., Mikuriya S., Kagawa S., *J. Chem. Soc. Chem. Commun.*, 1272 (1986).
- [23] Held W., König A., Richter T., Puppe L., *SAE 900496* (1990).
- [24] M. Misono, *Cattech* **2**, 183 (1998).
- [25] Iwamoto M., *Catal. Today* **29**, 29 (1996).
- [26] Parvulescu V.I., Grange P., Delmon B., *Catal Today* **46**, 233 (1998).
- [27] Traa Y., Burger B., Weitkamp J., *Micropor. Mesopor. Mater.* **30**, 3 (1999).
- [28] Hamada H., Kintashi Y., sasaki M., Ito T., Tabata M., *Appl. Catal.* **75** L1 (1991).
- [29] Yan Y.J., Kung H.H., Sachtler W.M.H., Kung M.C., *J. Catal.* **172**, 178 (1997).
- [30] Feeley J., Deeba M., Farrauto R., *SAE 950747* (1995).
- [31] Jacobs E., “Berichte zur Energie- und Verfahrenstechnik”, Heft 99.1, 541 (1999).
- [32] Koebel M., Elsener M., Kleemann M., *Catal. Today* **59**, 335 (2000).
- [33] Penetrante B.M., Brusasco R.M., Merritt B.T., Pitz W.J., Vogtlin G.E., Kung M.C., Kung H.H., Wan C.Z., Voss K.E., *SAE 982808* (1998).
- [34] Hoard J., Balmer M.L., *SAE 982429* (1998).
- [35] Hammer T., Bröer S., *SAE 982428* (1998).
- [36] Kato K., Nohira H., Nakanishi K., Iguchi S., Tihara T., Muraki H., *Eur. Pat. Appl.* EP0573672 A1 (1993).
- [37] Kateshima S., Iguchi S. Tanaka T., Araki Y., Hirota S., Kobashi K., *Eur. Pat. Appl.* EP0560991 A1 (1993).
- [38] Muraki H., Saiki M., Arachi M., Watsumoto S., Kanazawa T., Kobashi K., *Eur. Pat. Appl.* EP056516 A1 (1993).
- [39] Katoh K., Kihara T., Asanuma T., Gotoh M., Shibagaki N., *Toyota Techn. Review* **44**, 27 (1995).
- [40] Miyoshi N., Matsumoto S., Katoh K., Tanaka T., Harada J., Takahashi N., Yokota K., Sugiura M., Kasahara K., *SAE Paper* 950809 (1995).
- [41] Miyoshi N., Tanizawa T., Kasahara K., Tateishi S., *Eur. Pat. Appl.* EP0669147 A1 (1995).
- [42] Takahashi N., Miyoshi N., Matsumoto S., Tanaka T., Shinjoh H., Iijima T., Yokota K., Suzuki T., Suzuki H., Yamazaki K., Tanizawa T., Tateishi S., Kasahara K., *Catal. Today* **27**, 63 (1996).

- [43] Machida M., Yasuoka K., Eguchi K., Arai H., *J. Chem. Soc. Chem. Commun.*, 1165 (1990).
- [44] Eguchi K., Kondo T., Hayashi T., Arai H., *Appl. Catal. B* **16**, 69 (1998).
- [45] Fridell E., Skoglundh M., Westerberg B., Johansson S., Smelder G., *J. Catal.* **183**, 196 (1999).
- [46] Brogan M.S., Brisley R.J., Walker A.P., Webster D.E., Boegner W., Fekete N.P., Kramer M., Krutzsch B., Voigtlander D. *SAE* 952490 (1995).
- [47] Mahzoul H., Brillhac J. F., Gilot P., *Appl. Catal. B* **20**, 47 (1999).
- [48] Hodjati S., Bernhardt P., Petit C., Pitchon V., Kiennemann A., *Appl. Catal. B* **19**, 209 (1998).
- [49] Hodjati S., Bernhardt P., Petit C., Pitchon V., Kiennemann A., *Appl. Catal. B* **19**, 221 (1998).
- [50] Bögner W., Krämer M., Krutzsch B., Pischinger S., Voigtländer D., Wenninger G., Wirbeleit F., Brogan M.S., Brisley R.J., Webster D.E., *Appl. Catal. B* **7**, 153 (1995).
- [51] Coronado J. M., Anderson J. A., *J. Mol. Catal. A: Chem.* **138**, 83 (1999).
- [52] Cant N. W., Patterson M. J., *Catal. Today* **73**, 271 (2002).
- [53] Prinetto F., Ghiotti G., Nova I., Lietti L., Tronconi E., Forzatti P., *J. Phys. Chem. B* **105**, 12732 (2001).
- [54] Fridell E., Skoglundh M., Persson H., Olsson L., Amberntsson A., Westerberg B. *Topics in Catal.* **16/17**, 133 (2001).
- [55] Engström P., Amberntsson A., Skoglundh M., Fridell E., Smelder G., *Appl. Catal. B*, **22** L241 (1999).
- [56] Strehlau W., Leyrer J., Lox E.S., Kreuzer T., Hori M. and Hoffmann M., *SAE* 962047 (1996).

Chapter 2

Experimental

Abstract

In this chapter the experimental methods and techniques used for the preparation, characterization and testing of the catalysts are described in details.

2.1 Catalyst preparation

2.1.1 Alkali- and alkaline earth metal ion exchanged zeolites Y

For the alkali and alkaline earth metal exchanged Y zeolites, a commercial Na-H-Y zeolite (product no. CBV 400 obtained from Zeolyst International) was exchanged with sodium and barium acetates by a common liquid phase ion exchange procedure [1]. The modified zeolites were calcined in dry air (100 ml/min) at a heating rate of 2°C/min up to 500°C and kept at this temperature for 3h.

The elemental composition of these materials was analyzed by atomic absorption spectroscopy (AAS) and EDAX. Structural analysis was performed by X-ray diffraction. The morphology was probed by scanning electron microscopy (SEM).

2.1.2 Commercial NO_xSR catalyst

The catalyst investigated was a commercial NO_x NSR catalyst supplied in powdered form by Johnson Matthey, Royston, UK containing noble metals (Pt and Rh) as oxidation/reduction component and BaO/BaCO₃ as storage component deposited on an Al₂O₃ support. The specific surface area of the catalyst determined by N₂ sorption (BET method) was 110 m²/g.

2.2 Characterization techniques

2.2.1 Infrared spectroscopy

Infrared spectroscopy measurements were performed *in situ* in a BRUKER IFS 88 FTIR spectrometer equipped with a flow cell and a vacuum cell. The spectra were recorded in the transmission/absorption mode with a resolution of 4 cm⁻¹ using a MCT detector. The catalyst samples were pressed into self-supporting wafers (3-10

mg) and placed in a heatable golden sample holder and placed in the centre of a stainless steel chamber equipped with CaF_2 windows. In case of the vacuum cell the samples were activated under vacuum (below 10^{-6} mbar) at 450°C (zeolitic materials) and 500°C (metal oxides), respectively. Subsequently, the catalysts were cooled down to the required temperature and the reactant gases were brought in contact with the catalyst at defined and constant partial pressures *via* a gas dosing system.

The flow cell was equipped with a gas-mixing unit for the simultaneous and controlled admission of reaction gases (Fig.2.1). The samples were activated in a

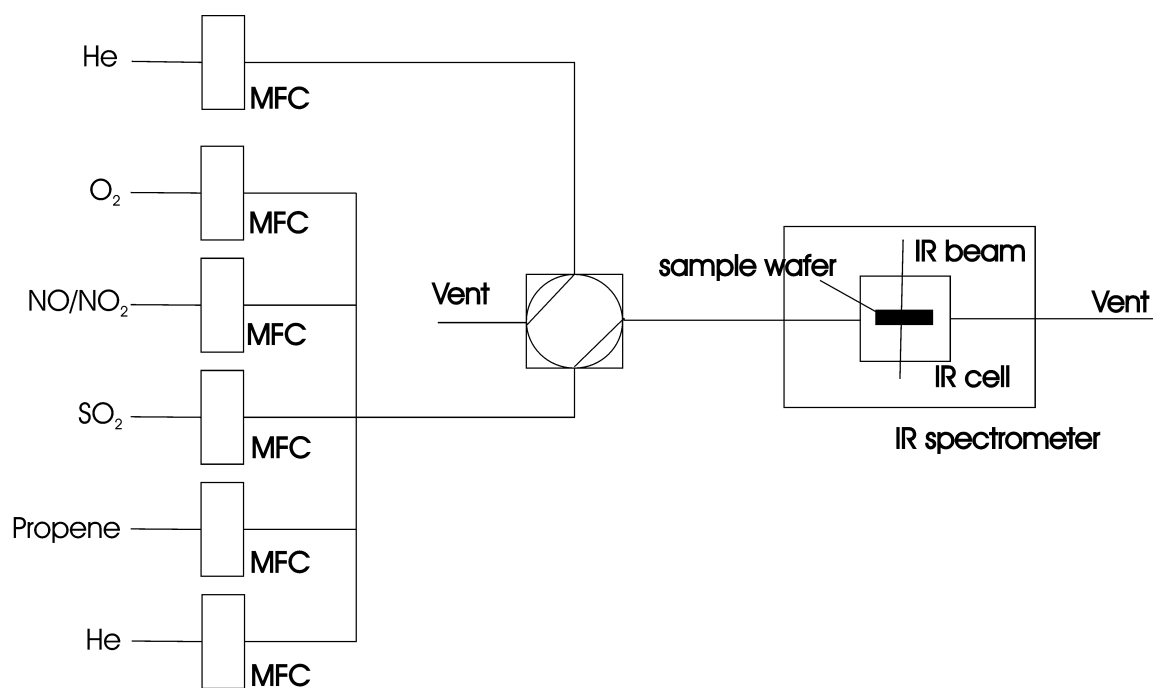


Fig 2.1: Schematic drawing of the flow cell IR system.

stream of He at 500°C for 1h. The adsorption experiments were carried out at temperatures between 50°C and 500°C with a total gas stream of 25 ml/min. Difference spectra were derived from the spectra in contact with sorbents and the spectra of the clean parent sample after activation.

2.2.2 Temperature programmed desorption

Temperature programmed desorption experiments were used to investigate stability, sorption capacity of NO_x and SO_x and their transformation on the surface species. A weighed amount of sample (around 100 mg) was placed in a quartz sample tube, connected to a vacuum system, activated by heating to a temperature of 450-600°C in vacuum at a rate of 10 °C/min and holding this temperature for 60 min. The sample was then exposed at a constant temperature to the desired gas at a pressure of approximately 10 mbar until the adsorption-desorption equilibrium was reached. The sample was then outgassed for 1 h to remove weakly physisorbed molecules. The TPD profile was recorded during a temperature increment of 10°C/min in the range of the desired temperatures (typically 50-600°C) with a Balzers QMG 420 mass spectrometer.

2.2.3 X-ray absorption spectroscopy

The structural and chemical properties of BaO and platinum were investigated by X-ray absorption spectroscopy (XAS) measured on beamline X1.1 and E4 at Hasylab, DESY, Hamburg, Germany. The measurements were carried out in transmission mode using a stepwise moving Si (111) monochromator. The intensity of incident and transmitted X-rays were recorded using ionization chambers. The monochromator was detuned to 60% of the maximum intensity to avoid contributions of high harmonics in the X-ray beam. For an accurate energy calibration of the position of the absorption edge a reference metal foil was simultaneously measured with the sample, located in-between the second and third ionization chamber. The samples were pressed into self-supporting wafers and placed in the sample holder equipped with a heating and cooling system, which allowed activation up to 450°C as well as cooling to liquid nitrogen temperature. The weight of the sample was chosen to achieve a total absorption of $\mu x = 2.5$. The

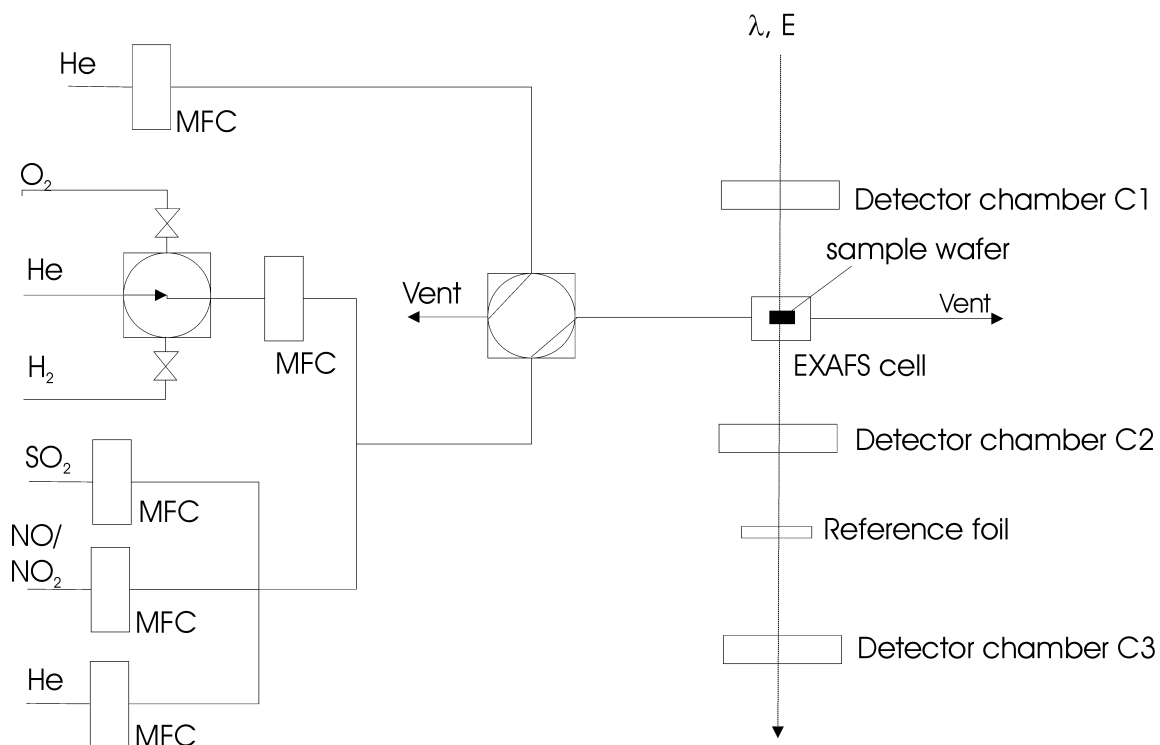


Figure 2.2: Experimental setup for EXAFS/XANES experiments.

sample holder was placed in a stainless steel reactor containing Kapton windows and a gas feeding system for the controlled admission of reaction gases. The activation and adsorption/reaction was performed *in situ* while recording the XAS. The data analysis was performed using Winxas (Version 2.0) [2]. The spectra were calibrated to the energy using the first inflection point of the edge from the simultaneously measured reference foil. For qualitative comparison of the EXAFS the oscillations were extracted from the background using a 3rd order polynomial function and after weighting with K^2 fourier transformed in the range 2.1 to 8 Å. For the XANES analysis the scattering contributions of the background were removed by fitting the pre-edge region with a 2nd order polynom and the region above the edge with a 3rd order polynomial function. For analysis, the area of the peak above the Pt-L_{III} edge (11564 eV), which can be related to the oxidation state of the Pt, was integrated by fitting the adsorption edge using an arctan function [3]. The fitted arctan function was subtracted from the XANES and the resulting peak was integrated numerically.

2.2.4 Flow reactor studies

Reaction studies were carried out in a furnace-heated horizontal quartz tube reactor. The catalyst particles were sealed in the middle of the heated zone with quartz wool. Mass flow controllers were used for the admission of NO, SO₂, O₂ and C₃H₆. As internal standard a constant flow of Ar was injected. A mass spectrometer continuously probes a fraction of the reactant and product gases.

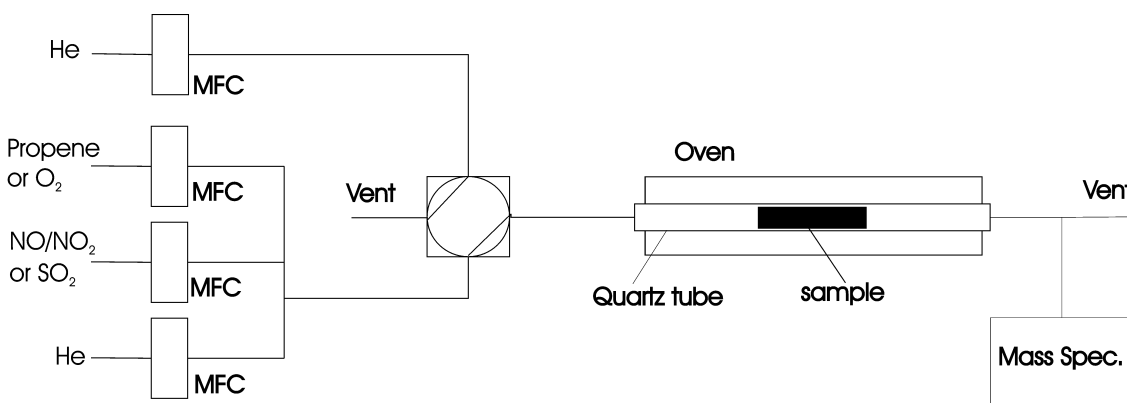


Figure 2.3: Schematic drawing of the setup used for flow reactor studies.

Typical catalyst testing conditions involved 400 mg of catalyst, activated in He (200 ml/min) for 60 min at 550°C, exposed to desired gas mixtures at 350°C, chosen as the reaction temperature. He gas was used as diluent in all experiments.

2.2.5 XRD experiments

XRD measurements were performed on a Rigaku powder diffractometer with Cu K α radiation. The tube voltage was 40 kV, and the current was 40 mA. The XRD diffraction patterns were taken in the 2θ range of 10-90° at a scan speed of 2° per min every 50°C from RT up to 700°C. The last pattern was taken after cooling down to ambient temperature.

References

- [1] Palomares A.E., Eder-Mirth G., Lercher J.A., *J. Catal.* **168**, 442 (1997).
- [2] Ressler, T.; *J. Synch. Rad.* **5**, 118 (1998).
- [3] D.A. Outka, J. Stöhr, *J. Chem. Phys.* **88**, 3539 (1988).

Chapter 3

An *in situ* IR study of the NO_x adsorption/reduction mechanism on modified Y zeolites

Abstract

The surface species formed during adsorption of NO, NO+O₂ and NO₂ on sodium and barium exchanged Y zeolites have been investigated by *in situ* IR spectroscopy. Ionically bound nitrates and nitrites on the exchanged metal cation sites are the main species formed during adsorption of NO and NO₂. Extra framework alumina was identified as additional sorption site forming small concentrations of bridging, chelating and monodentate nitrates. N₂O₄ and NO⁺ were found to be reaction intermediates during the NO_x adsorption process. The direct oxidation of NO₂ with reactive oxygen from the zeolite surface is facilitated by the formation of nitrates *via* the disproportionation reaction of N₂O₄ to NO⁺ and NO₃⁻. NO⁺ was found to act as precursor for the creation of nitrites. Decomposition of the nitrate species occurs between 150 and 450°C. During the temperature increase less stable nitrite/nitrate species are transformed into Ba-nitrates showing the highest thermal stability. The stability of surface nitrates/nitrites was found to be lower, if NO instead of NO₂ is present in the feed during temperature increase. For the interaction of surface NO_x species with propene two pathways are proposed. At low temperatures, NO⁺ was identified as the active NO_x surface species reacting with propene to nitriles. At higher temperatures the reduction of surface nitrates/nitrites occurred *via* organic nitro/nitrito species, carboxylic species and isocyanates.

3.1 Introduction

An effective method for the reduction of NO_x under excess oxygen conditions from lean-burn and diesel engines is based on the concept of NO_x storage-reduction (NSR), where the engine is operated in a mixed lean/rich operation mode [1, 2]. NSR catalysts generally contain noble metals providing oxidation/reduction functionality and NO₂ storage components, typically alkali or alkaline earth metals. During lean operation conditions (i.e., oxidizing atmosphere) NO is oxidized to NO₂ over the noble metal component and stored on the storage component. By changing periodically to short cycles of fuel rich operation conditions (i.e., reducing atmosphere) NO₂ is released from the storage component and converted to N₂ over the noble metal component.

For the design of efficient NSR catalysts, storage components are required which temporarily store high concentrations of NO_x between 100 and 450°C [3, 4] in the presence of the typical gas components of motor exhaust gases and release the NO_x stored during short regeneration cycles. In general a high basicity of the storage component increases the amount of adsorbed NO_x. A high surface area and, therefore, a small particle size is additionally important for an efficient NO_x storage, as the NO_x is mainly stored as surface species [5, 6].

Zeolites are known to have a well defined 3-dimensional structure, the capability for cation exchange at defined positions with a high level of dispersion and acid-base properties, which could easily be adjusted for the desired application [7]. Research on different zeolites exchanged with various metal cations for the removal of NO_x from engine exhaust gases is reported mainly on the field of NH₃- and HC-SCR [8, 9]. For the application of zeolites in the NSR process only a few studies were published [10, 11]. Monticelli *et al.* [10] studied the NO_x storage of alkali and alkaline earth exchanged Y zeolites for exhaust gas of lean burn engines. They found a correlation between the type of alkali and alkaline earth metal exchanged and the storage capacity (BaY > CsY > NaY > LiY). They proposed the

adsorption of NO_x as nitrates created by the reaction of NO_2 with water *via* nitric acid as intermediate and observed no influence of SO_2 on the NO_x adsorption capacity on NaY [12].

As alkali and alkaline earth metal exchanged Y zeolites are claimed to be promising materials to be applied as NO_x traps for lean burn and diesel engines an improved understanding of the reaction mechanism is required. The aim of this work is to elucidate the surface species and reaction intermediates as well as their thermal stability under conditions similar to the storage/catalysis cycle. Therefore, sodium and barium exchanged Y zeolites were exposed to different gas compositions typically for the NSR process (i.e. NO , NO/O_2 and NO_2) and the NO_x species formed were investigated by *in situ* IR spectroscopy. The intermediates during the reduction of the NO_x surface species by C_3H_6 were also identified.

3.2 Experimental

Materials

The sodium and barium exchanged Y-type zeolites were prepared by ion exchange of a commercial Na-H-Y zeolite obtained from Zeolyst International (CBV 400, $\text{Si}/\text{Al} = 2.5$). Ion exchange with Na-acetate and Ba-acetate was carried out in liquid phase [13]. After the ion exchange procedure the zeolites were calcined in dry air (100 ml/min) at a heating rate of $2^\circ\text{C}/\text{min}$ up to 500°C and kept at this temperature for 3h.

The elemental composition of the materials was analyzed by atomic absorption spectroscopy (AAS) and EDAX. The ion exchange degrees for the Na^+ and Ba^{2+} exchanged zeolites Y were around 40 %. The chemical composition of the three investigated materials is given in Table 1.

The Si/Al ratios are close to the value of the parent zeolite, which indicates that no significant variations in the chemical framework composition during the ion exchange took place. The structural integrity of the zeolite framework before and

after the ion exchange was verified by XRD, which did not show any significant differences between the diffractograms of the modified and the parent zeolites.

Table 1: Chemical composition and calculated unit cell of the zeolites investigated.

<i>Sample code</i>	<i>Si/Al</i>	<i>[M]/Al</i>	<i>Unit cell</i>
NaHY (CBV-400)	2.53	4.93	Na ₃ Al ₅₄ Si ₁₃₈ O ₃₈₄
NaY	2.59	42.86	Na ₂₃ Al ₅₄ Si ₁₃₈ O ₃₈₄
BaY	2.53	37.19	Ba ₂₀ Al ₅₄ Si ₁₃₈ O ₃₈₄

²⁷Al-MAS-NMR experiments were used to determine the ratio of framework and extra-framework alumina (EFAL) and for all materials a ratio of ~25% extra-framework alumina was obtained. In the following paper the parent material is identified as NaHY, the sodium exchanged material as NaY and the barium exchanged one as BaY.

IR spectroscopy

Infrared spectroscopy measurements were performed with a BRUKER IFS 88 FTIR spectrometer in an IR cell that allows to collect IR spectra *in situ*, while the sample is in contact with the reactant molecules [14]. The spectra were recorded in the transmission absorption mode with a resolution of 4 cm⁻¹ using a MCT detector. The catalyst samples were pressed into self-supporting wafers (~5 mg) and placed in a heatable sample holder in the center of the *in situ* IR cell equipped with CaF₂ windows. The flow of reactants through the cell was adjusted by electronic mass flow controllers. Further details of the experimental setup are described in ref. [14].

The samples were activated in a stream of He at 450°C for 1h. After activation, the samples were exposed to a gas stream containing 500 ppm NO, 500 ppm NO/ 5 % O₂ and 500 ppm NO₂ in helium (total flow 25 ml/min) at 50°C until further changes in the concentration of surface species were not observed. The thermal

stability of the NO_x surface species formed on the catalyst after exposure to NO , NO/O_2 or NO_2 were investigated at temperatures between 50 and 450°C with a temperature increment of 5°C/min in He flow and in the flow of 500 ppm NO , 500 ppm $\text{NO}/5\% \text{O}_2$ and 500 ppm NO_2 in helium. To study the interaction of the NO_x surface species with C_3H_6 , a flow of 2000 ppm C_3H_6 in He was fed over the catalysts pre-exposed to NO , NO/O_2 or NO_2 at 50°C for 10 min followed by an temperature increase to 450°C with a temperature increment of 5°C/min. Difference spectra were derived from the spectra in contact with sorbents and the spectra of the parent sample after activation.

3.3 Results and discussion

3.3.1 NO_2 adsorption on NaHY and NaY

IR spectra during adsorption of NO_2 at 50°C are shown for NaY in Figure 3.1 and for NaHY in Figure 3.2. Note, that the scaling of the absorption in the IR spectra of NaHY (Fig. 3.2) is 4 times smaller compared to NaY (see Fig. 3.1). Similar NO_x surface species between 2200 and 1300 cm^{-1} were observed for the parent and the sodium exchanged form of the zeolite. The differences in the intensity of the bands reflected the different concentration of the species as a function of the sodium contents. For NaY the main NO_x surface species formed were ionically bound nitrates evidenced by the doublet with the characteristic splitting of the asymmetric stretching vibration band at 1423 and 1374 cm^{-1} , which appeared after 2 min of adsorption [15, 16]. The splitting results from the lowered symmetry of the nitrate ion in the adsorbed state [17] caused by interaction of the nitrate with neighboring cations. These bands of the nitrates were also observed for NaHY, but with significantly lower intensity. The higher intensity for the nitrate doublet for NaY, which has a higher sodium content compared to NaHY, together with results reported by Chao *et al.* [16], who observed this doublet on a NaY zeolite doped

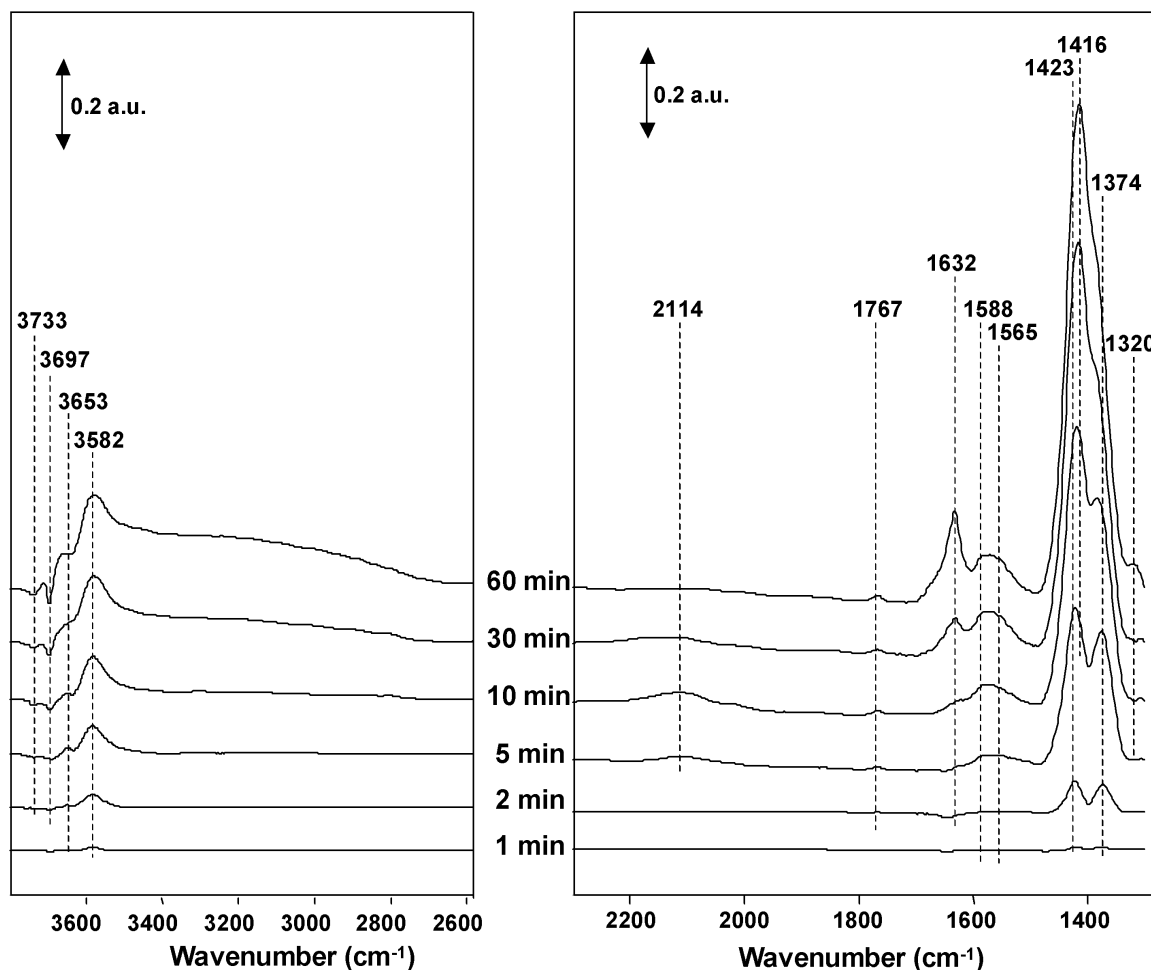


Figure 3.1: IR spectra during exposure of NaY to 500 ppm NO₂ at 50°C.

with NaNO₃, indicates that the ionically bound nitrates were located on the sodium cations.

With increasing time of NO₂ exposure the doublet disappeared and one band with a maximum at 1416 cm⁻¹ appeared. This could either indicate the additional formation of a Na-nitrito species exhibiting a stretching vibration at approximately 1420 cm⁻¹ [15, 16], and/or be caused by the broadening of the nitrate bands due to intermolecular interactions. The observed changes are in agreement with Chao *et al.* [16], who reported for high NO₂ loadings on NaY an increase in band intensity and the loss of the doublet structure. Note that for NaHY, the sample with a lower

concentration of Na cations per supercage and, therefore, a lower amount of NO_2 adsorbed, the disappearance of the doublet structure was not observed.

For NaHY the main surface NO_x species formed are bridging and chelating nitrates on extra-framework alumina species (EFAL). Already in the beginning of the NO_2 exposure two broad bands at 1634 and 1588 cm^{-1} , assigned to the asymmetric stretching mode of bridging surface nitrates and to chelating surface nitrates, were observed increasing in intensity with time. The bands for the corresponding symmetric stretching vibrations, expected between 1300 - 1200 cm^{-1} [15, 18] are

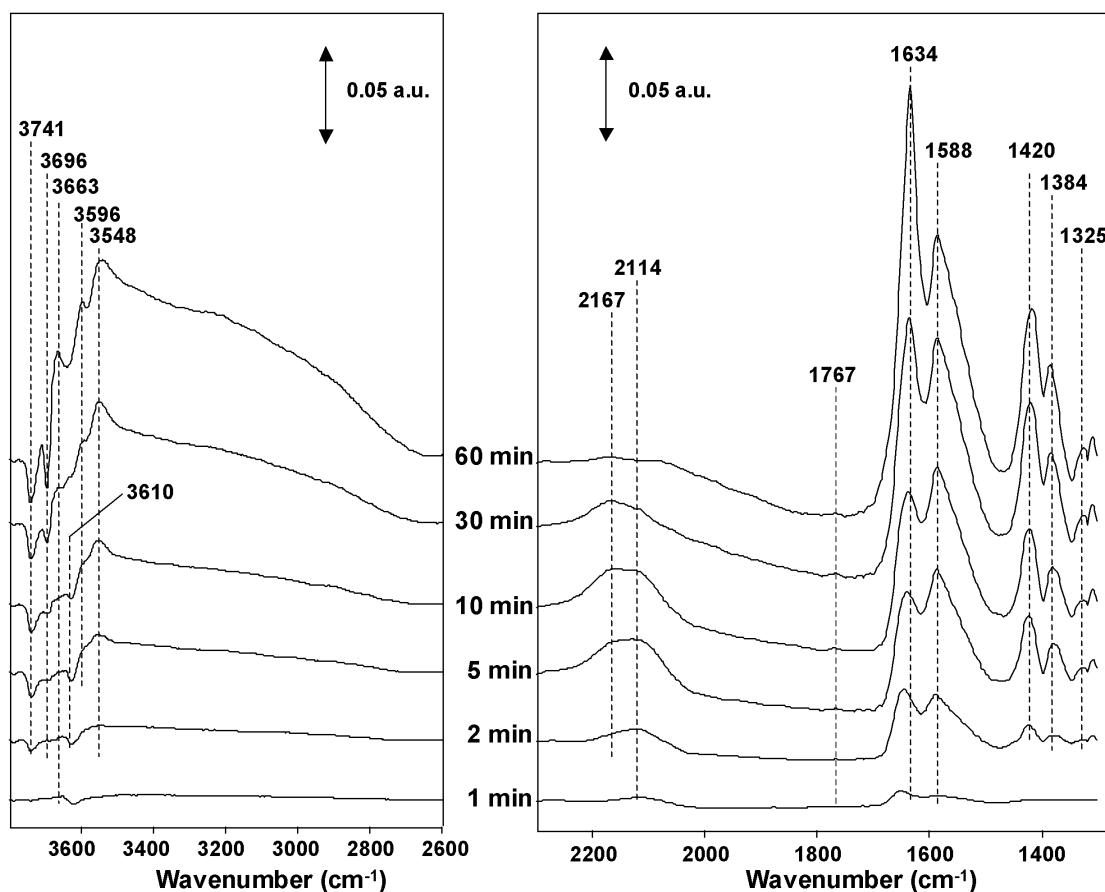


Figure 3.2: IR spectra during exposure of NaHY to 500 ppm NO_2 at 50°C .

masked by the high IR-absorption of the zeolitic framework in this spectral region. On NaY the formation of these surface nitrates starts after 5 min of NO exposure indicated by weak bands at 1632 and 1588 cm^{-1} and in addition a band at 1565 cm^{-1} , partially overlapped by the band at 1588 cm^{-1} , which is assigned to

monodentate nitrates [18]. The presence of monodentate nitrates on NaHY was not unequivocally confirmed due to the large contribution of the band at 1588 cm⁻¹, but the shape of the band suggests the presence of two overlapping contributions in this

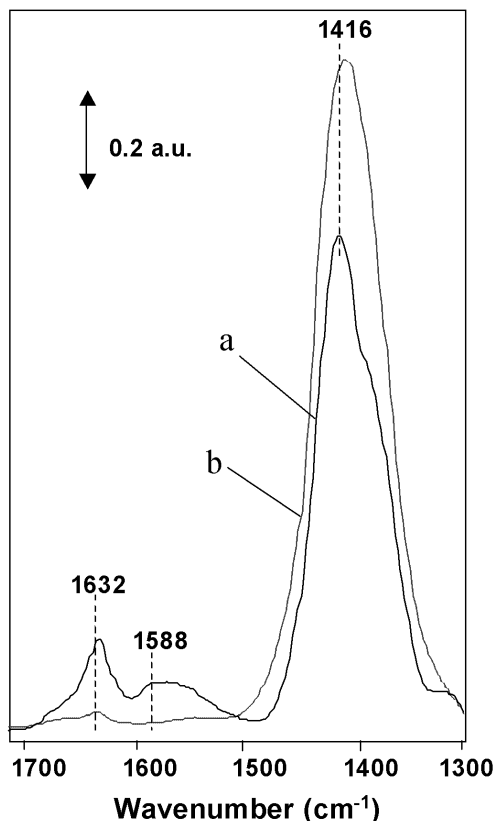


Fig. 3.3: IR spectra after exposure to 500 ppm NO₂ at 50°C. (a) NaY (with EFAL); (b) NaY (CBV100) without EFAL.

region. Due to the significant amount of extra-framework alumina present in the investigated zeolites and the fact, that these bands were absent during NO₂ adsorption on a Y type zeolite without extra-framework alumina (Fig. 3.3), these species are most likely being formed on extra-framework alumina sites.

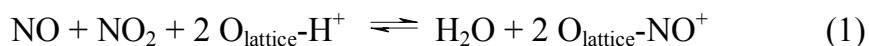
The band at around 1320 cm⁻¹ appearing after 10 min of NO₂ exposure is assigned to the symmetric stretching vibration of nitrites on Na⁺ sites [15, 19]. The corresponding band for the asymmetric stretching mode

expected at around 1260 cm⁻¹ is masked by the intense bands of zeolite lattice vibrations.

The very weak contribution at 1767 cm⁻¹ after 5 min of NO exposure is assigned to the asymmetric stretching mode of surface N₂O₄ species [15, 20], while the corresponding symmetric stretching mode at around 1360 cm⁻¹ is concluded to be masked by the contributions of the other nitrate/nitrite species.

For NaHY, a band at 2114 cm⁻¹ was observed in the region between 2000 and 2200 cm⁻¹ from the start of the NO₂ adsorption and a second band appeared with

further time on stream at 2167 cm^{-1} . Both reached a maximum after 30 min and decreased during further NO_2 exposure. For NaY a very weak band at 2114 cm^{-1} was observed after 10 min of NO_2 exposure, while the band around 2167 cm^{-1} was absent. These bands have been reported previously and were either assigned to coordinatively bound NO_2^+ , $\text{NO}_2^{\delta+}$ or NO^+ species [16, 20-24]. Recent studies by Hadjiivanov *et al.* [22] and Iwamoto *et al.* [23] confirmed the assignment of these bands between 2200 and 2100 cm^{-1} to NO^+ species. Hadjiivanov *et al.* [22] used isotope-labeled oxygen and showed that these NO_x species contain only one oxygen atom, whereas Iwamoto [23] found evidence for only one nitrogen atom by using isotope-labeled nitrogen and confirmed the assignment of these bands to the asymmetric stretching mode of NO^+ species. The existence of two different bands for NaHY could be explained by the formation of NO^+ on different cation vacancy sites [22, 24, 25]. It is known that the stretching frequency of NO^+ in nitrosonium salts depends on the degree of electron transfer of the corresponding anion in the π^* orbital of NO^+ [18]. Therefore, variation in acidity of different adsorption sites should result in a variation of the stretching frequency for NO^+ . Aylor *et al.* [24] and Hadjiivanov *et al.* [22] found indications for the additional formation of water, if these NO^+ species are created on bridging hydroxyl groups. Hadjiivanov proposed an exchange of protons from acidic OH-groups by NO^+ , which subsequently forms a water molecule hydrogen bonded to another zeolite hydroxyl group, as shown in scheme 1.



For NaHY a weak band at 1640 cm^{-1} characteristic for the δ (H_2O) mode of water was observed together with the increasing intensity of the band assigned to NO^+ at 2114 cm^{-1} . The simultaneous disappearance of the band at 3610 cm^{-1} characteristic for Brønsted acid sites located in the supercages of zeolite Y confirms the assignment of the band at 2114 cm^{-1} to NO^+ species located on acidic hydroxyl groups of the zeolite framework. With NaY the molecular adsorption of H_2O

characterized by the deformation vibration band at approximately 1640 cm⁻¹ was not clearly observed due to the contributions of bridging nitrates on EFAL in this region. The band at 2167 cm⁻¹ could be attributed to the N-O stretching mode from [NO⁺][N₂O₄] adducts [26].

Besides the disappearance of the band at 3610 cm⁻¹, related to bridging hydroxyl groups, the negative intensity of the band at 3741 cm⁻¹ was observed on NaHY, which could be assigned to silanol groups affected by the adsorption of NO₂ or H₂O. After 5 min of adsorption a third negative band at 3696 cm⁻¹ was observed, which is generally attributed to hydroxyl groups located on Na⁺ cations [27]. The consumption of the silanol groups and acidic hydroxyl groups on NaHY is explained by the replacement or the interaction of the hydroxyl groups with NO_x species. On NaY a similar interaction could be only observed for hydroxyl groups located on Na⁺ cations indicated by increase of the negative band at 3697 cm⁻¹.

Additional hydroxy bands appeared at 3653 and 3582 cm⁻¹ for NaY and at 3663, 3596 and 3548 cm⁻¹ for NaHY. The bands at 3653/3663 cm⁻¹ and 3582/3596 cm⁻¹ are attributed to perturbed hydroxyl groups on extra-framework alumina, which is in line with results reported in the literature [27-30]. The position of the band at 3548 cm⁻¹ is close to the position of the band for LF Brønsted acid sites resulting from protons in the sodalite cage [31]. Therefore, it is suggested that this band arises from perturbed LF Brønsted acidic hydroxyl sites interacting *via* the proton with NO₂ or surface NO_x species and forming nitric acid-like surface species.

3.3.2 Thermal stability of NO_x surface species on NaY and NaHY

After the flow of NO₂ was stopped and the samples were flushed with He at constant temperature for 10 min significant changes in the band intensities were not observed (Figure 3.4) indicating that a reorganization of NO_x surface species did not occur. The stability of the surface species was investigated by increasing the

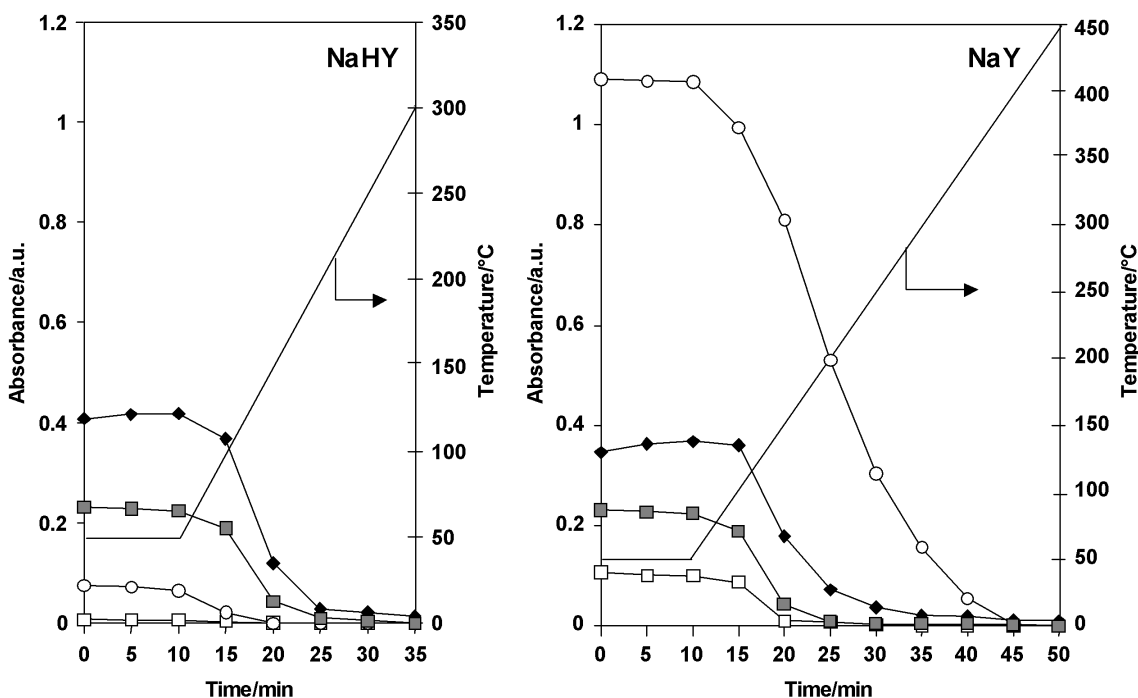


Fig. 3.4: Variation of IR band intensities of different types of NO_x surface species on NaHY and NaY after adsorption of 500 ppm NO_2 during TPD in He: bridged Al-nitrates (\blacklozenge), chelating Al-nitrates (\blacksquare), Ba-nitrates (\circ), nitrites (\square).

temperature during constant He flow. The less stable species on NaY and NaHY were nitrites, which were completely desorbed around 160°C followed by chelating and bridging Al-nitrates desorbed at around 200 and 250°C , respectively. Judged from the decreasing bands, the ionically bound Na-nitrates, which are the main surface species on NaY slowly decomposed between 150°C and 450°C . Small amounts were even observed at the final temperature of 450°C . From the viewpoint of designing suitable NO_x storage materials, the results indicate, that the exchanged metal cations are the responsible species to achieve stable NO_x surface species at temperatures above 250°C .

3.3.3 NO_2 adsorption on BaY

For the adsorption of NO_2 on BaY similar surface species was identified as for the adsorption of NO_2 on NaY and NaHY (Figure 3.5). Bridging and chelating nitrates on extra-framework alumina resulted in bands at 1632 and 1580 cm^{-1} . They were

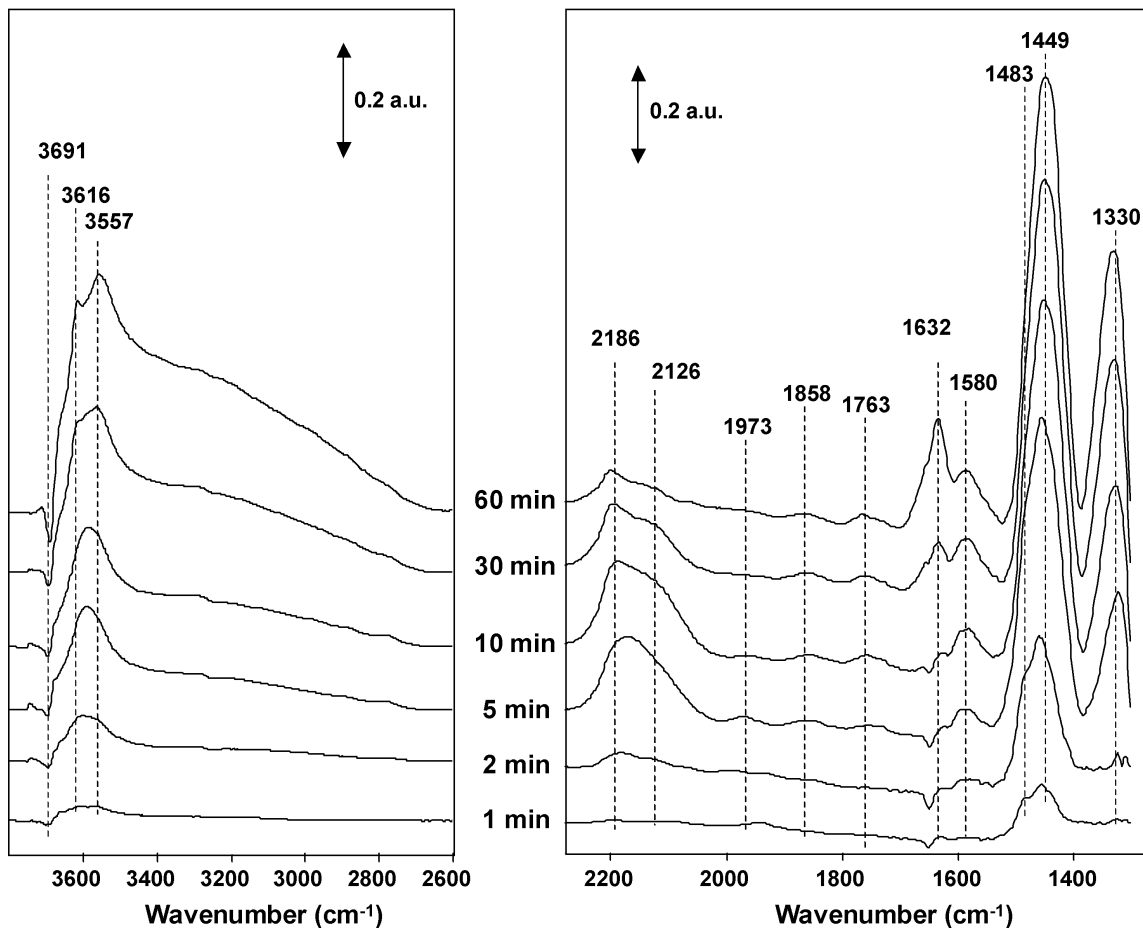


Fig. 3.5: IR spectra during exposure of BaY to 500 ppm NO₂ at 50°C.

formed from the beginning of the NO₂ exposure and increased with time. The doublet of bands attributed to the (splitted) asymmetric stretching mode of ionically bound nitrates formed on Ba²⁺ sites were observed at 1483 and 1455 cm⁻¹. The shift of this band to higher wavenumbers for the Ba-nitrates compared to the Na-nitrates indicates a more covalent character of the bonding, which is tentatively explained by the softer ionic character of the Ba cation [18]. Similar to NaY, the doublet structure disappeared with time of exposure and the maximum of the band shifted to 1449 cm⁻¹. As above, this is tentatively attributed to the dependence of the band splitting to the concentration of nitrates adsorbed on Ba sites in agreement with Chao *et al.* [16]. However, due to the unequal increase of the two

contributions of the doublet a partial attribution of the band at 1449 cm^{-1} to nitrito species formed on Ba^{2+} cations could not be completely ruled out.

After 5 min of adsorption nitrites identified by the symmetric stretching vibration at 1330 cm^{-1} were formed and accumulated until the end of the NO_2 exposure. Additionally, small amounts of N_2O_4 with a characteristic stretching band at 1763 cm^{-1} were present after 5 min of adsorption. Different to the results obtained for NaHY and NaY, a weak contribution at 1853 cm^{-1} was observed after 5 min of adsorption, which is attributed to the $\text{N}=\text{O}$ stretching mode of N_2O_3 . Additional bands for the asymmetric and symmetric NO_2 stretching mode of N_2O_3 are expected at 1590 and 1270 cm^{-1} [15, 16, 25]. The latter one was not observed due to the high absorbance of the zeolite, but the band at 1590 cm^{-1} was observed as a small shoulder of the band at 1580 cm^{-1} (assigned to chelating nitrates on extra-framework alumina). A formation of N_2O_3 was reported to occur mainly during adsorption of NO and NO_2 or NO/O_2 on zeolites, especially at ambient temperature and high partial pressures. [16, 32 -34]. The formation of N_2O_3 during adsorption of NO_2 indicates the disproportionation of NO_2 on the zeolite surface, most probably *via* N_2O_3 intermediates. The presence of coordinatively bound NO on Ba^{2+} cation sites, concluded from the appearance of the characteristic band at 1973 cm^{-1} [17, 35], confirmed this suggestion.

The bands at 2186 and 2126 cm^{-1} are attributed to NO^+ species on cation vacancy sites close to Ba^{2+} and on bridging hydroxyl groups, respectively. Similar to NaHY and NaY a steady increase in intensity was observed until a maximum at around 30 min of adsorption was reached. The main OH stretching band perturbed was that at 3691 cm^{-1} , assigned to hydroxyl groups on Ba^{2+} . The appearance of bands at 3616 and 3557 cm^{-1} indicated an interaction of NO_x species with hydroxyl groups by forming H-ONO species. In contrast to the sodium Y materials, a perturbation of silanol groups (3740 cm^{-1}) was not observed.

3.3.4 Thermal stability of NO_x surface species on BaY

When purging the sample exposed to NO₂ with He only, the NO⁺ band disappeared completely, whereas the doublet at around 1449 cm⁻¹ assigned to ionically bound

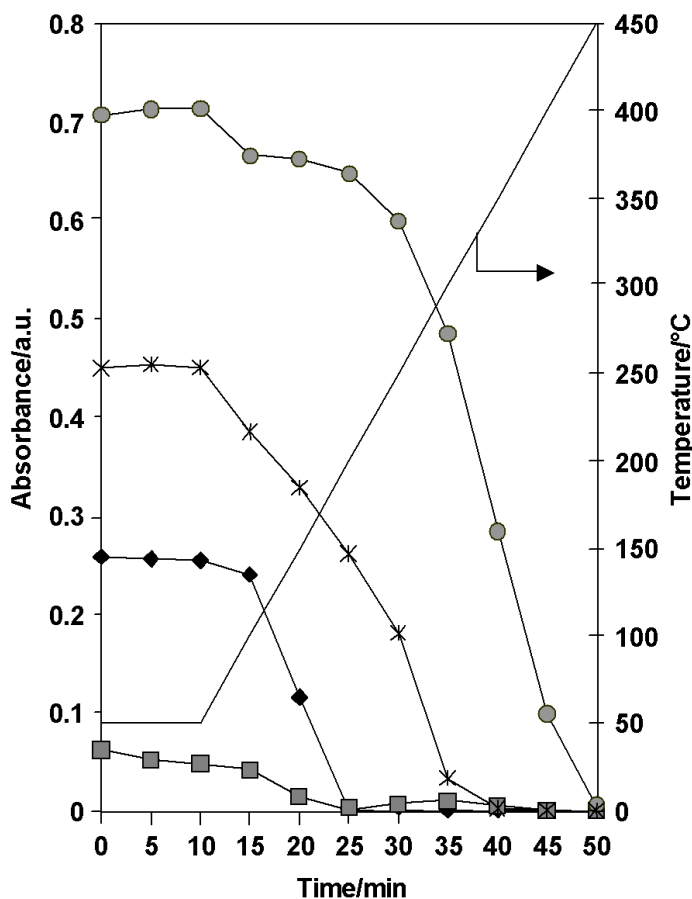


Fig. 3.6: Variation of IR band intensities of different types of NO_x surface species on BaY after adsorption of 500 ppm NO₂ during TPD in He: bridged Al-nitrates (◆), chelating Al-nitrates (■), Ba-nitrates (●), nitrites (✱).

nitrites desorbed continuously and were completely removed at around 280°C. For the band related to ionically bound nitrates a small decrease was observed between 50 and 100°C. From 100 to 250°C the intensity remained constant and decreased subsequently until the final temperature. The stable intensity of Ba-nitrates between 100 and 250°C could be observed simultaneously with the desorption of nitrates located on extra-framework alumina species, which

increased slightly (Figure 3.6). With increasing temperature bridging and chelating nitrates on extra-framework alumina were observed on the catalyst surface up to around 200°C, which is similar to the stability of these species observed for NaHY and NaY. The NO_x species on the Ba²⁺, however, showed a higher thermal stability compared to the Na⁺. Judged from the changing intensities of the bands at 1330 cm⁻¹, the

suggests a transformation or regrouping of the Al-nitrates onto Ba^{2+} sites. A similar transformation of Al-nitrates onto Na sites was not observed during TPD of NaY (Figure 3.4).

3.3.5 Effect of different gas mixtures NO, NO+O₂ and NO₂

The influence of different NO_x gas mixtures on the formation of the NO_x surface species was investigated by the adsorption of NO, NO + O₂ and NO₂ on BaY. The IR spectra for BaY after 60 min of exposure to the different gas mixtures are shown in Fig. 3.7. Only minor differences in the intensities of band assigned to the various NO_x surface species, described for Figs. 3.1, 3.2 and 3.5, during exposure

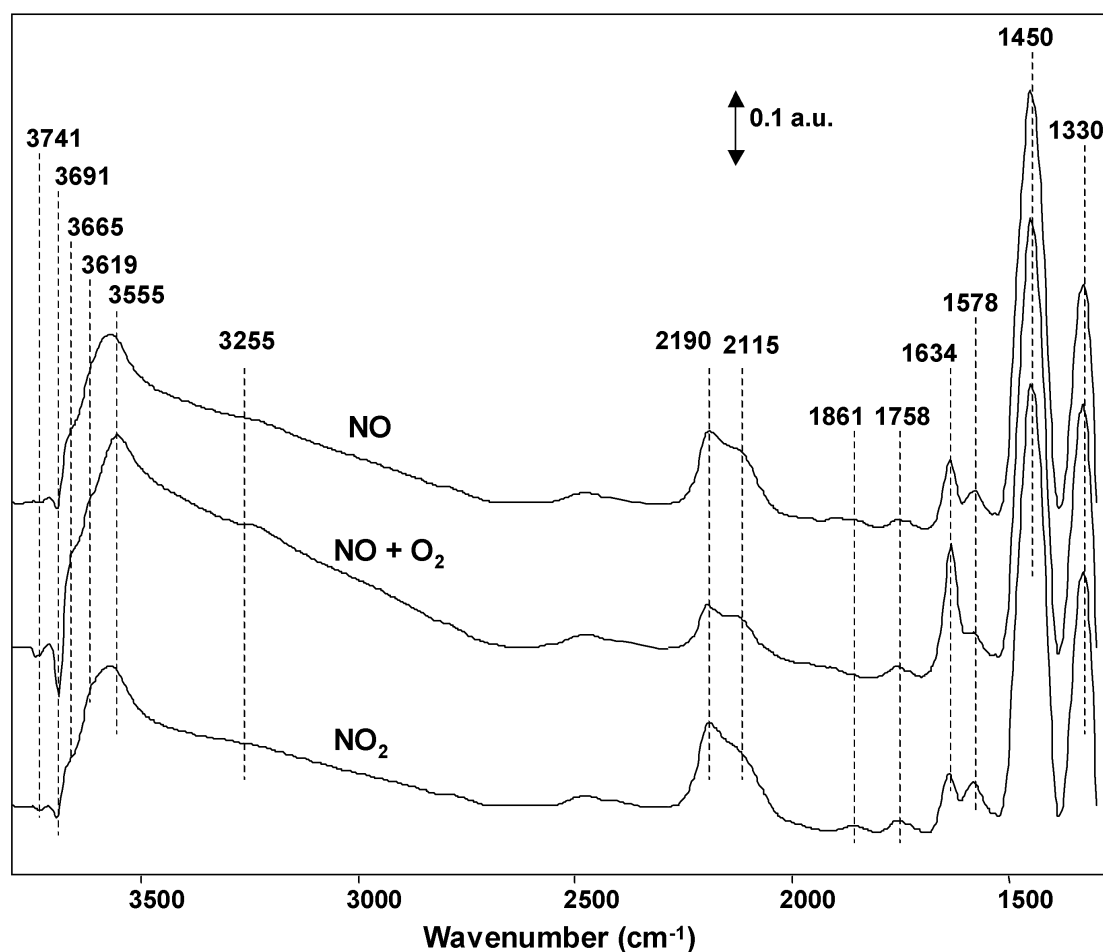


Fig. 3.7: IR spectra of BaY after exposure to 1000 ppm NO₂; 1000ppm NO and 5% O₂ and 1000 ppm NO at 50°C for 60 min.

to the different gas atmospheres were distinguished. The concentration of nitrate and nitrite species on barium cation sites after 60 min of adsorption is comparable for all three experiments. The variation of the intensity as function of exposure time for the ionically bound nitrate and nitrite IR bands is compared in Fig. 3.8. The surface concentration of nitrates and nitrites increased in a similar manner

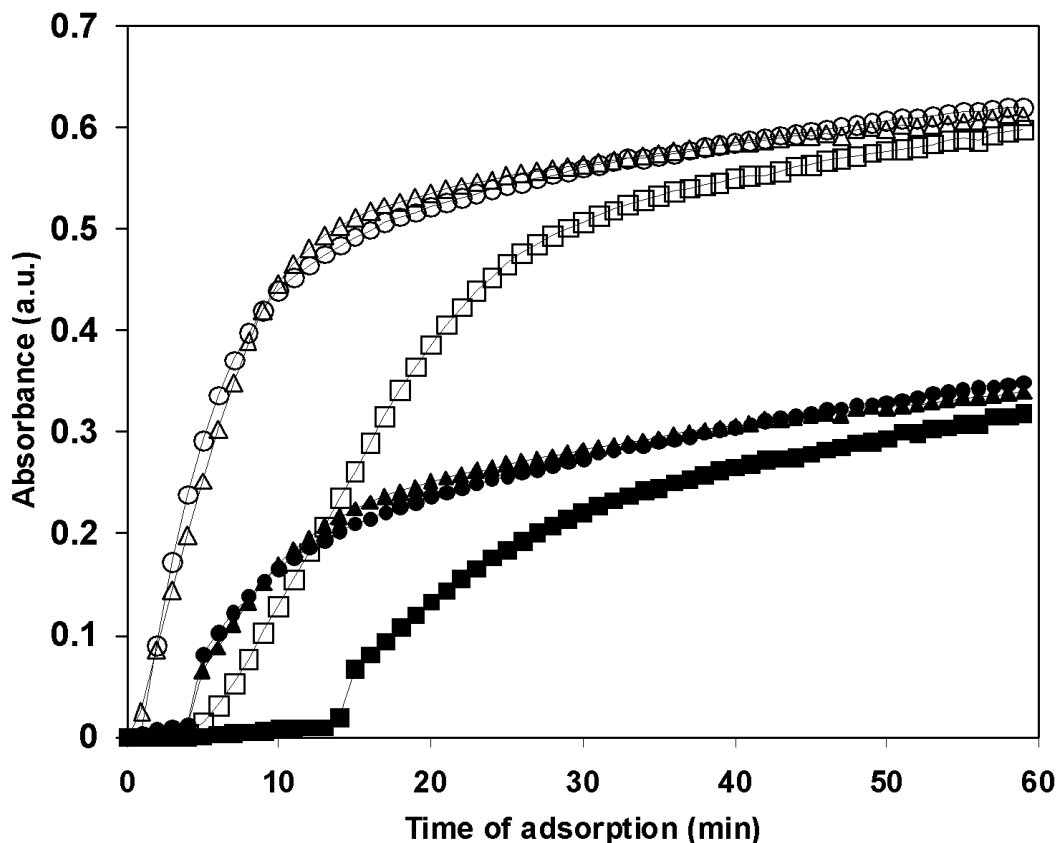


Fig. 3.8: Variation of the intensity of IR bands (1450 cm^{-1} , 1330 cm^{-1}) for nitrates (open symbols) and nitrites (solid symbols) over BaY during adsorption of 1000 ppm NO₂ (triangles); 1000 ppm NO and 5% O₂ (circles) and 1000 ppm NO (squares) at 50°C for 60 min.

during NO₂ and NO + O₂ exposure. However, a delay in the formation of nitrates and nitrites during exposure to NO was observed. Furthermore, the smaller slope of the increase of the uptake curve with exposure time indicates a slower formation of nitrates/nitrites during exposure to NO. After 60 min of adsorption the final amount of nitrate/nitrites coverage was also reached for the NO exposed material.

Comparing the formation of nitrates and of nitrite during the three experiments the relative amount of nitrates formed is higher than the amount for nitrites.

Furthermore, a threshold for the formation of nitrites was identified on all three investigated materials. This indicates a preferred formation of nitrates at the beginning of adsorption. After a certain surface coverage with nitrates the formation of nitrites starts. The delay for the formation of nitrites is similar for the exposure of the material to NO_2 or NO/O_2 , while for the exposure to NO the time delay was three times longer. This result together with the comparable relative amounts of nitrates/nitrites formed during NO exposure suggests an indirect formation of the nitrites *via* an intermediate NO_x species formed on the zeolite surface.

3.3.6 Adsorption of NO , $\text{NO}+\text{O}_2$ and NO_2 under non isothermal conditions

The variations in the intensities of the IR bands for the NO_x species formed during temperature increase under the different gas atmospheres are compared in Fig. 3.9. Under NO_2 atmosphere, the most stable species were ionically bound Ba-nitrates, which were observed until 450°C . The concentration of nitrites continuously decreased up to 300°C , with the main decline around 200°C . The nitrates formed on extra-framework alumina were less stable and completely removed at 200°C . The same experiments performed under NO and NO/O_2 atmosphere gave similar stabilities for nitrates on extra-framework alumina and nitrite species up to 200°C . The Ba-nitrates were already completely removed at 320°C . This indicates a dependence of the stability of Ba-nitrates on the partial pressure of NO_2 in the gas phase. At high NO_2 partial pressure the Ba-nitrates were stable up to more than 450°C , whereas under low partial pressure of NO_2 the stability was lowered below 350°C . This difference could be of importance for the design of an industrially applicable NSR catalyst, as it indicates an enhanced ease of Ba in a zeolitic environment for reducing the nitrates.

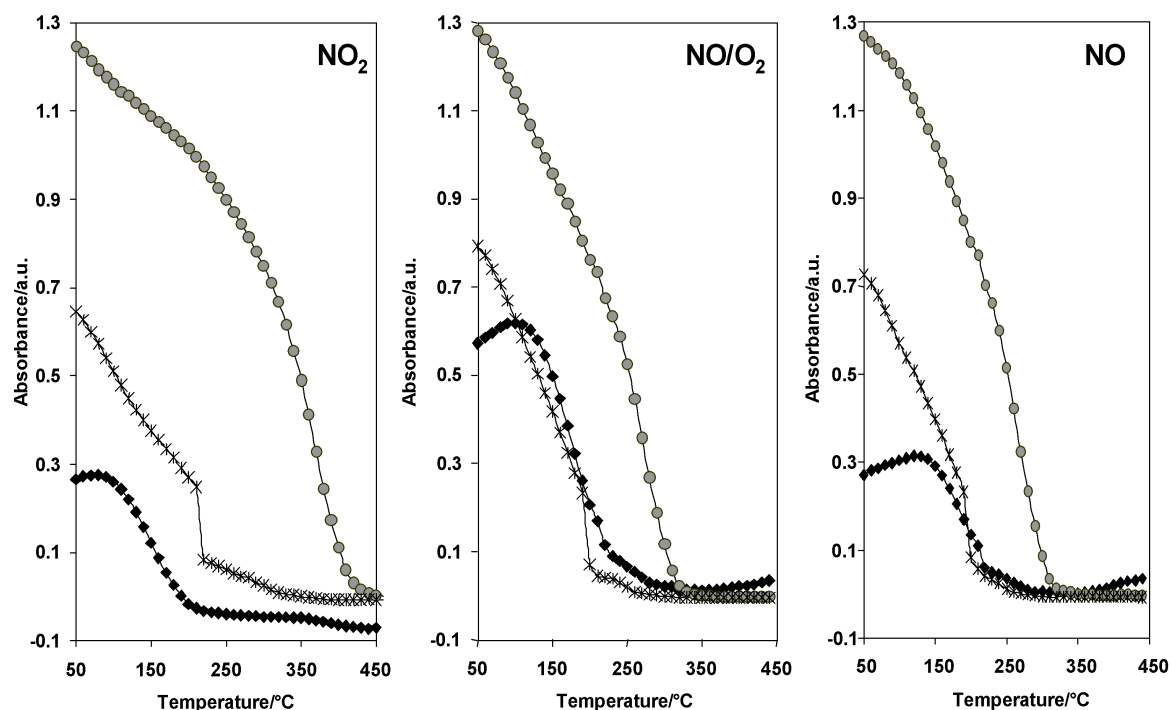
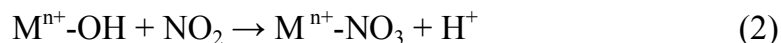


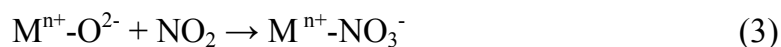
Fig. 3.9: Variation of the intensity of IR bands for the main NO_x surface species: Al-nitrates (◆), Ba-nitrates (●), nitrites (✱) on BaY during TPReaction of 1000 ppm NO₂ from 50 to 450°C.

3.3.7 Mechanistic model for NO_x adsorption

The adsorption of NO_x on sodium and barium exchanged Y zeolites occurred preferentially *via* surface nitrates on the exchangeable metal cation sites and partly on cationic sites of extra-framework alumina. As the hydroxyl groups located on Ba and Na sites decreased with the increase of nitrates one pathway for the formation of nitrates from NO₂ could be proposed as following:



The H⁺ is bonded to zeolite lattice oxygen [36] or interacts with the nitrates to form nitric acid-like species. The identical mechanism could also be operative on cation defect sites such as extra-framework alumina.



The comparable nitrate formation during the exposure to NO and O₂ could be related to reactive oxygen species created on the metal cation sites by a dissociative or molecular adsorption of oxygen [37, 38] and the subsequent reaction of the nucleophilic oxygen adsorbed with a NO molecule.



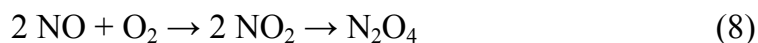
During exposure to NO (without O₂ in the feed) a similar final concentration of surface nitrates, formed with a smaller rate compared to the exposure to NO+O₂ was observed, which indicates the formation of nitrates by a different pathway in absence of O₂. In principle it can be assumed, that small amounts of nitrates are formed *via* the oxidation of NO to NO₂ by reactive oxygen species present on the catalyst surface, most likely from defect sites of the zeolite framework, which was also proposed by other authors [16, 11].



Chao *et al.* [16] as well as Kanno *et al.* [39] observed the formation of nitrates during NO adsorption on CaY zeolites and proposed a formation *via* N₂O₃ adsorbed on the metal sites with a subsequent disproportionation of N₂O₃ to N₂O and NO₂.



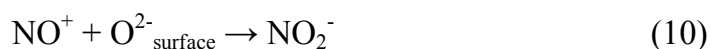
As only on BaY small contributions of N₂O₃ during NO exposure were observed, we suggest a very low contribution of this reaction pathway among the main routes for the formation of nitrates. With further time of exposure, the amount of adsorbed NO₂ is sufficiently high for the formation of N₂O₄ *via* dimerization of two NO₂ molecules.



Note that NO⁺ and nitrites were formed simultaneously on the surface indicating a disproportionation reaction of N₂O₄ [40].



NO₃⁻ formed is an additional source for subsequent nitrate formation on metal cations, whereas the NO⁺ could either be coordinatively bound or interact with surface oxygen atoms to form nitrites.



Besides the direct formation of nitrates *via* NO₂, the reaction *via* the intermediate N₂O₄ with a subsequent disproportionation is proposed to be the main pathway for the creation of nitrates and nitrites on Y zeolites during adsorption of NO₂ and NO+O₂ at low reaction temperatures.

3.3.8 Reduction of surface NO_x species by propene

The reduction of NO_x surface species by hydrocarbons is one of the main reactions during the regeneration process of NO_x storage reduction catalysts. Thus, the interaction of surface NO_x species on BaY with propene was investigated at the adsorption temperature and during temperature increase to 450°C. After exposure of the catalyst to NO₂ (Fig. 3.10, spectrum (a)) 2000 ppm C₃H₆ in He were added for 10 min at 50°C (Fig 3.10, spectrum (b)).

In the region for CH stretching vibrations three bands were observed characteristic for -CH₃ antisymmetric stretching vibrations (2993 cm⁻¹), -CH₂ antisymmetric stretching (2947 cm⁻¹) and -CH₃ symmetric stretching at 2883 cm⁻¹ [41]. Simultaneously, a decrease of the bridging hydroxyl groups located in the supercage leading to a band at 3624 cm⁻¹ was observed indicating that propene

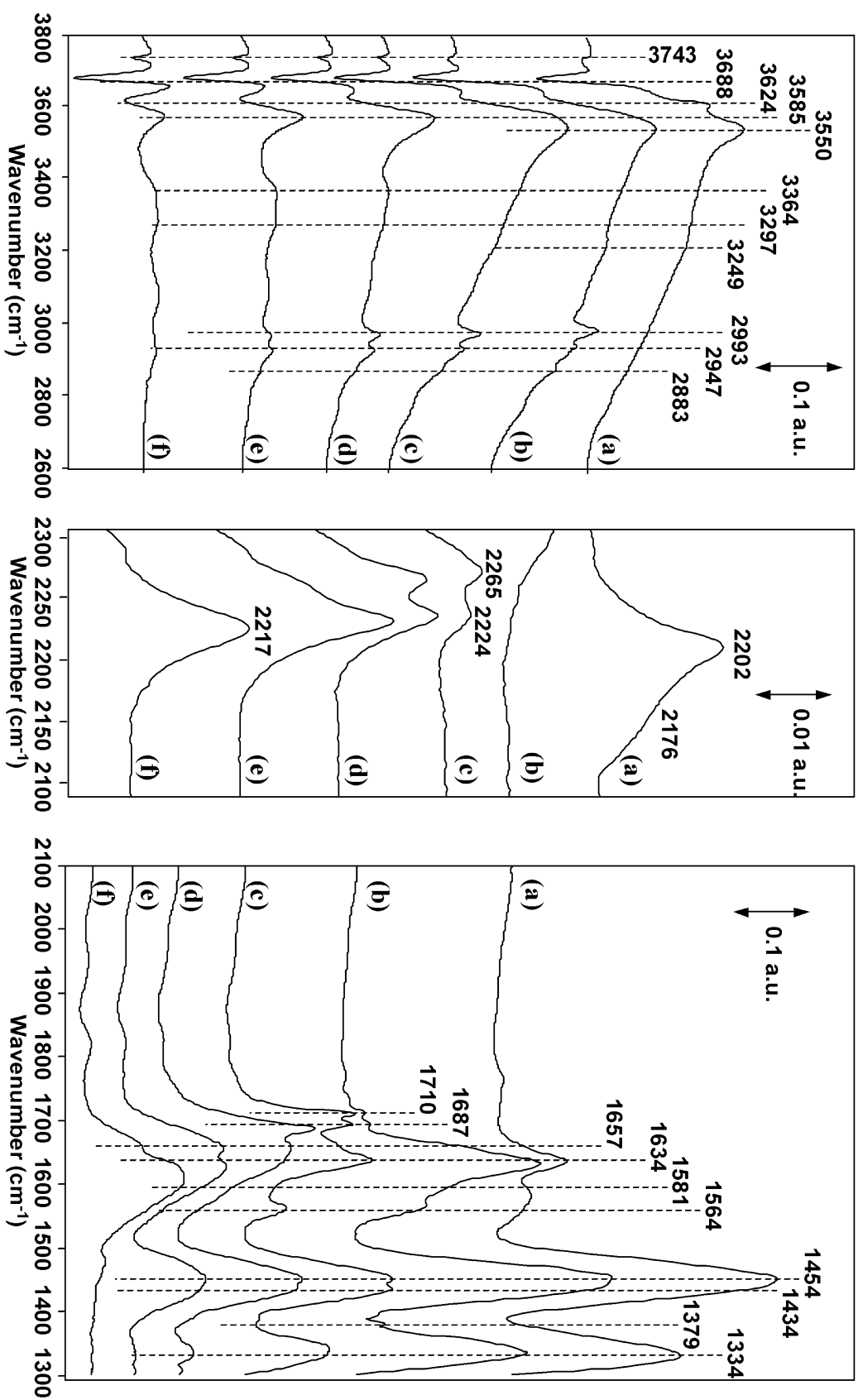


Fig 3.10: IR spectra of BaY after adsorption of 500 ppm NO_2 for 60 min at 50°C (a), after subsequent exposure to 2000 ppm C_3H_6 for 10 min at 50°C (b). During TPRReduction in 2000 ppm C_3H_6 at 150°C (c), 250°C (d), 350°C (e) and at 450°C (f).

were adsorbed preferably on these sites. The increase of the band at 3550 cm⁻¹ is attributed to the perturbed bridging hydroxyl groups coordinated to C₃H₆. An increase of the negative band at 3688 cm⁻¹ indicates an additional interaction of propene with hydroxyls located on Ba²⁺ cation sites. A broad contribution between 3550 and 2600 cm⁻¹ was observed, which is typically for stretching vibrations of OH groups and molecularly adsorbed water strongly bonded *via* hydrogen to acid sites [42]. The remarkable increase of the band at 1634 cm⁻¹ attributed to bridging nitrates on extra-framework alumina is tentatively attributed to the overlapping contributions of the -C=C stretching mode and of the δ (H₂O) mode of molecularly adsorbed water.

In the region between 2300 and 2100 cm⁻¹ the disappearance of the bands assigned to NO⁺ at 2202 and 2176 cm⁻¹ was observed, which indicate a fast reaction of NO⁺ with C₃H₆. Gerlach *et al.* [43] proposed an acid catalyzed reaction of propene with NO⁺ *via* propenal oxime (11) to acrylonitrile and water (12) on acidic mordenite:



They attributed the broad band between 3500-2600 cm⁻¹ and bands at 1458 and 1414 cm⁻¹ to stretching and deformation vibrations of propenal oximes. The existence of the latter ones could not be confirmed in our experiments due to the intense Ba-nitrate band in this region. Furthermore, the authors postulated a hydrolysis of the nitriles to ammonia indicated by the symmetric stretching band at 3255 cm⁻¹ characteristics for adsorbed ammonium ions. This band was also observed in our experiments as a weak band at 3249 cm⁻¹.

The small contributions at 1710 cm⁻¹ and 1687 cm⁻¹ was assigned to -C=O vibrations of carboxylic groups [44, 45]. However, the latter one could also be attributed to the -ONO mode of organic nitrito compounds (R-ONO) [46]. The shoulder at 1564 cm⁻¹ could be attributed to the -NO₂ stretching vibration of organic nitro species (R-NO₂) adsorbed on the surface [47]. The small contribution

at 1434 cm^{-1} visible as a shoulder of the Ba-nitrate band at 1454 cm^{-1} could be attributed to the CO_2 mode of surface carboxylates [44, 48]. The formation of carboxylic species and organic –nitro/nitrito compounds suggests the direct (partial) oxidation of sorbed C_3H_6 by NO_x surface species.

Significant changes were observed during temperature increase up to 450°C . At 150°C (Fig 3.10, spectrum (c)) two bands appeared at 2265 and 2224 cm^{-1} , which could be assigned to isocyanate species located on two different sites. The former is assigned to $-\text{NCO}$ vibrations of isocyanate located on alumina sites, most likely on extra-framework alumina [49], the latter one to isocyanate coordinated to Ba^{2+} [50]. It should be noted, however, that the frequency region is also characteristic for $-\text{C}-\text{N}$ vibrations of nitriles, which cannot be ruled out completely [15]. With increasing temperature a shift of the band at 2224 cm^{-1} assigned to Ba-isocyanate to lower wavenumbers was observed, which could probably related to a contribution of nitriles most likely formed *via* the abstraction of the oxygen atom of isocyanate species by hydrocarbons [51].

With increasing temperatures a significant decrease of the bands assigned to Ba-nitrates and nitrites occurred, whereas the bands related to carboxylic groups, organic nitrito and organic nitro species at 1710 and 1687 cm^{-1} and 1564 cm^{-1} increased markedly in intensity. The bands between 3500 and 2600 cm^{-1} and at approximately 1640 cm^{-1} related to molecularly adsorbed water decreased in intensity. At 250°C (Fig 3.10, spectrum (d)) $-\text{C}=\text{O}$ related bands disappeared or were at least masked by a broad band between 1750 and 1550 cm^{-1} with an overlapping band at 1682 cm^{-1} . The broad band indicates the formation of coke like deposits, whereas the contribution at 1682 cm^{-1} is assigned to organic nitrito compounds [46]. The increase of the isocyanate bands combined with the simultaneous decrease of the bands attributed to carboxylic species suggests a conversion of carboxylic species to isocyanates, most likely by the participation of surface nitrates. Similar results were reported by Weingand *et al.* [44], who investigated the interaction of propene with surface NO_x species on $\text{WO}_3\text{-ZrO}_2$.

Two weak bands are assigned to the antisymmetric (3364 cm⁻¹) and symmetric (3297 cm⁻¹) –NH stretching band, which suggests a partial hydrolysis of the isocyanate to –NH containing species (amines) and CO₂.

At 350°C (Fig 3.10, spectrum (e)) the band at 1334 cm⁻¹ attributed to nitrite surface species completely disappeared. Bands for Ba-nitrates (1454 cm⁻¹), carboxylates (1434 cm⁻¹/1620 cm⁻¹) and coke like deposits (1650-1500 cm⁻¹) were observed. The weak band at 3093 cm⁻¹ corresponds to the C-H stretching mode of π -bonded propene complexes on Ba²⁺ [52]. The band assigned to isocyanates on Ba-sites markedly increased in intensity, whereas the band of isocyanates located on Al sites decreased. Besides weak contributions of -NH species, hydrocarbons and nitriles the coke like species are the dominating surface compounds at 450°C (Fig 10, spectrum (f)).

In conclusion, two main pathways for reaction of C₃H₆ with NO_x surface species on BaY are proposed. At low temperatures and in the presence of nitrosonium ions the conversion of NO⁺ with C₃H₆ *via* propenal oximes to nitriles with a subsequent hydrolysis to ammonia seems to be the main reaction pathway. With increasing temperatures, the reduction of NO_x surface species with C₃H₆ *via* carboxylic species and isocyanates are proposed to be the predominant reaction route.

3.4 Conclusions

In situ IR spectroscopy was used to investigate the surface species formed during adsorption of NO, NO+O₂ and NO₂ on sodium and barium exchanged Y zeolites. It was found that NO_x was mainly adsorbed as nitrates and nitrites formed on the exchangeable metal cation sites. Small amounts of bridging, chelating and monodentate nitrates on extra-framework alumina were also identified. As reaction intermediate N₂O₄ species were observed. Besides the direct oxidation reaction of NO₂ with reactive oxygen from the surface, the disproportionation reaction of N₂O₄ to NO⁺ and NO₃⁻ was proposed to be a significant reaction pathway for the formation of nitrates. NO⁺ was assumed to act as precursor for the creation of

nitrites. Small amounts of N_2O_3 surface species were detected only on BaY, which indicates that N_2O_3 plays only a minor role in the adsorption reactions during the NSR process of NO_x on NaY and BaY.

The same type and concentration of surface species were formed during the exposure of the samples to NO, NO + O₂ and NO₂. However, a slower formation of surface nitrate/nitrite species was observed during exposure to NO and related to the additionally required oxidation of NO to NO₂, which appears to be slow in the absence of O₂. The nitrate and nitrite species showed similar temperature stability between 200 and 450°C on all materials investigated. Decomposition of the nitrate species occurred between 150 and 450°C. During the temperature increase a transformation of less stable nitrite/nitrate species into Ba-nitrates, which showed the highest thermal stability, was observed. The stability of surface nitrates/nitrites was found to be lowered if NO is present in the feed during temperature increase.

For the interaction of C₃H₆ with NO_x surface species on BaY two different pathways are proposed. At low temperatures and in the presence of nitrosonium ions the conversion of NO⁺ with C₃H₆ *via* propenal oximes to nitriles with a subsequent hydrolysis to ammonia is concluded to be the main reaction. The interaction of surface nitrate/nitrites with C₃H₆ at low temperature seems to be negligible. With increasing temperatures, the reduction of surface nitrates/nitrites with C₃H₆ *via* carboxylic species and isocyanates could be proposed to be the predominant reaction route.

Acknowledgements

The author is grateful to the European Union for partial funding of this project in the Brite/EuRam program (STORECAT; BRPR-CT98-0613). Thanks also to B.Gil for doing part of the IR experiments. F.X. Hecht is kindly acknowledged for the BET measurements, M. Neukamm for AAS analysis, Dr. S. Joergens for EDAX measurements and J. O. Barth for the NMR measurements.

References

- [1] Katoh K., Kihara T., Asanuma T., Gotoh M., Shibagaki N., *Toyota Techn. Review* **44**, 27 (1995).
- [2] N. Miyoshi, S. Matsumoto, K. Katoh, T. Tanaka, J. Harada, N. Takahashi, K. Yokota, M. Sugiura, K. Kasahara, *SAE Paper* 950809 (1995).
- [3] Zelenka P., Cartellieri W., Herzog P., *Appl. Catal. B* **10**, 3 (1996).
- [4] Adams K.M., Cavataio J.V., Hammerle R.H., *Appl. Catal. B* **10**, 157 (1996).
- [5] Sedlmair Ch., Seshan K., Jentys A., Lercher J.A., submitted to *J. Catal.*
- [6] Westerberg B., Fridell E., *J. Mol. Catal. A: Chem.* **165**, 249 (2001).
- [7] Armor J.N., *Micropor. Mesopor. Mater.* **22**, 451 (1998).
- [8] Traa Y., Burger B., Weitkamp J., *Micropor. Mesopor. Mater.* **30**, 3 (1999).
- [9] Busca G., Lietti L., Ramis G., Berti F., *Appl. Catal. B* **18**, 1 (1998).
- [10] Monticelli O., Loenders R., Jacobs P.A., Martens J.A., *Appl. Catal. B* **21**, 215 (1999).
- [11] Bentrup U., Brückner A., Richter M., Fricke R., *Appl. Catal. B* **32**, 229 (2001).
- [12] Sultana A., Loenders R., Monticelli O., Kirschhock C., Jacobs P.A., Martens J.A., *Angew. Chem. Int. Ed.* **39**, 2934 (2000).
- [13] Palomares A.E., Eder-Mirth G., Lercher J.A., *J. Catal.* **168**, 442 (1997).
- [14] Mirth G., Lercher J. A., *Appl. Spectroscopy* **48**, 194 (1994).
- [15] Hadjiivanov K. I., *Catal. Rev.-Sci. Eng.* **42**, 71 (2000).
- [16] Chao C.C., Lunsford J.H., *J. Am. Chem. Soc.*, **93**, 71 (1971).
- [17] Pozdnyakov D.V., Filimonov V.N., *Kinet. Katal.* **14**, 655 (1973).
- [18] Davydov A. A., "Infrared Spectroscopy of Adsorbed Species on the Surface of Transition Metal Oxides" Wiley, New York, 1990.
- [19] Laane J., Ohlsen J. R., *Prog. Inorg. Chem.* **27**, 465 (1980).
- [20] Hoost T.E., Laframboise K.A., Otto K. *Catal. Lett.* **33**, 105 (1995).
- [21] Beutel T., Adelman B., Sachtler W.M.H, *Appl. Catal. B* **9**, L1 (1996).
- [22] Hadjiivanov K., Saussey J., Freysz J. L., Lavalley J. C., *Catal. Lett.*, **52**, 103 (1998).
- [23] Iwamoto M., Furukawa H., Kagawa S., "New Developments in Zeolite Science and Technology" Elsevier, Amsterdam 1986.
- [24] Aylor A.W., Lobree L.J., Reimer J.A., Bell A.T., *J. Catal.* **170**, 390 (1997).
- [25] Szanyi J., Paffett M.T., *J. Catal.* **164**, 232 (1996).
- [26] Hadjiivanov K., Tsyntsarski B., Nikolova T., *Phys. Chem. Chem. Phys.* **1**, 4521 (1999).

- [27] Fritz P.O., Lunsford J.H., *J. Catal.* **118**, 85 (1989).
- [28] Shannon R.D., Gardner K.H., Staley R.H., Bergeret G., Gallezot P, Auroux A.J., *J. Phys. Chem.* **89**, 4778 (1985).
- [29] Lohse U., Löffler E., Hunger M., Stöckner J., Patzelová, *Zeolites* **7**, 11 (1987).
- [30] Khabtou S., Chevreau T., Lavalley J.C., *Mic. Mat.* **3**, 133 (1994).
- [31] Morin S., Ayrault P., Gnep N.S., Guisnet M., *Appl. Catal. A* **166**, 281 (1998).
- [32] Hadjiivanov K., Klissurski D., Ramis G., Busca G., *Appl. Catal. B* **7**, 251 (1996).
- [33] Lobree L.J., Aylor A.W., Reimer A.J., Bell A.T., *J. Catal.* **181**, 189 (1999).
- [34] Adelman B.J., Lei G.-D., Sachtler W.M.H., *Catal. Lett.* **28**, 119 (1994).
- [35] Nakamoto K., “Infrared and Raman Spectra of Inorganic and Coordination Compounds”, 4th ed.; Wiley; New York, 1986.
- [36] Wada Y., Otsuka K., Morikawa A., *J. Catal.* **71**, 136 (1981).
- [37] Chi Y., Chuang S.C., *J. Phys. Chem.* **104**, 4673 (2000).
- [38] Borchert H., Baerns M.J., *J. Catal.* **168**, 315 (1997).
- [39] Kanno Y., Matsui Y., Imai H., *J. Inclusion Phenomena* **3**, 461 (1985).
- [40] Ito E., Mergler Y.J., Niewenhuys B.E., van Bekkum H., van den Bleek C.M., *Micropor. Mater.* **4**, 455 (1995).
- [41] Coltup N.B., Daly L.H., Wiberley S.E., „Introduction to infrared and raman spectroscopy“ 3rd ed., Academic Press, San Diego, 1990.
- [42] Angell C.L., Schaffer P.C., *J. Phys. Chem.* **69**, 3463 (1965).
- [43] Gerlach T., Schütze F.-W., Baerns M., *J. Catal.* **185**, 131 (1999).
- [44] Lercher J.A., *Z. Phys. Chem.* **129**, 209 (1982).
- [45] Weignand T., Kuba S., Hadjiivanov K., Knözinger H., *J. Catal.* **209**, 539 (2002).
- [46] Okuhara T., Hasada Y., Misono M., *Catal. Today* **35**, 83 (1997).
- [47] Haneda M., Kintaichi Y., Inaba M., Hamada H., *Catal. Today*, **42**, 127 (1998).
- [48] Hoost T.E., Laframboise K.A., Otto K. *Appl. Catal. B* **7**, 79 (1995).
- [49] Solymosi F., Bánsági T., *J. Catal.* **156**, 75 (1995).
- [50] Bamwenda G.R., Ogata A., Obuchi A., Oi J., Mizuno K., Skrzypek J., *Appl. Catal. B* **6**, 311 (1995).
- [51] Schießer W., Vinek H., Jentys A., *Appl. Catal. B* **33**, 263 (2001).
- [52] Davydov A., *Mater. Chem. Phys.* **13**, 243 (1985).

Chapter 4

Elementary steps of NO_x adsorption and surface reaction on a commercial storage-reduction catalyst

Abstract

The surface species formed during adsorption of NO_x on a commercial NSR catalyst (containing barium oxide, Pt and alumina as the main components) were investigated by *in situ* IR spectroscopy. During adsorption of NO mainly linear and bridged bonded nitrites of Ba-O-N-O-Ba type were formed on Al- and Ba-oxide components. Nitrites were detected during the initial phase of the NO/O₂ and NO₂ adsorption, whereas with further exposure nitrates were the dominant surface species. Using the different surface species and reaction intermediates identified by IR spectroscopy a series of sequential reaction steps during the sorption of NO_x on a NSR catalyst was derived. Initially, NO is stored in the form of nitrites on the storage component (Ba-oxide). NO₂ formed by oxidation on the noble metal component (Pt) either sorbs molecularly by forming nitrate species or dissociatively by forming nitrites. After a certain concentration of NO_x is adsorbed, the transformation and further oxidation of the surface nitrites into surface nitrates by NO₂ occurs. The stability of the NO_x surface species was found to increase in the order: Al-nitrites < Ba-nitrites < Al-nitrates < Ba-nitrates.

4.1 Introduction

Conventional Pt-Rh based three-way catalysts (TWCs) are very efficient in reducing nitrogen oxide (NO_x), CO and unburned hydrocarbon (HC) emissions from gasoline engines. However, the general demand for lower CO₂ emissions and, thus, the requirement of more fuel efficient gasoline engines led to the development of lean-burn engines operating at significantly higher air-to-fuel ratios compared to traditional engines [1]. Under these oxygen rich exhaust gas conditions three way catalysts cannot efficiently reduce NO_x. The most promising approach for the reduction of NO_x under lean-burn conditions is based on the concept of NO_x storage-reduction (NSR), where the engine is operated in a mixed lean/rich operation mode [2,3]. NSR catalysts contain storage components, typically alkali or alkaline earth metals, such as barium, and noble metal components providing oxidation/reduction functionality. During lean operation conditions (i.e., oxidizing atmosphere) NO is oxidized to NO₂ over the noble metal component and stored on the storage component. By changing periodically to short cycles of rich operation conditions (i.e., reducing atmosphere) NO₂ is released from the storage component and converted to N₂ over the metal component. The major drawback of this process at present is their high susceptibility of the NSR catalysts to sulfur poisoning, which lowers the NO_x storage capacity [4,5].

A detailed understanding of the overall NO_x storage mechanism is one of the basic steps required to improve the efficiency, as well as the sulfur resistance of the catalysts. Several studies have focused recently on the mechanism of NO_x storage on model NSR catalysts [5-11]. In an early study, Takahashi *et al.* [5] investigated commercial NSR catalysts and found indications for oxidation of NO on metal sites and a subsequent storage on adjacent storage site in form of nitrates. Mahzoul *et al.* [8] suggested that two different Pt sites are involved in the storage process, one close to BaO related to the nitrate formation and another (further away) acting as

oxidation catalysts for NO. The authors also reported the formation of nitrates in the absence of gas phase oxygen and in the absence of Pt.

Fridell *et al.* [10] suggested two possible reaction pathways for NO_x storage with NO₂ as primary oxidizing agent during NO_x storage. The first proposed reaction path includes the oxidation of BaO to BaO₂ by NO₂, whereas the second pathway proposed involves the initial formation of nitrites with a subsequent oxidation to nitrates by NO₂. In more detail, Prinetto *et al.* [11] as well as Westerberg *et al.* [6] studied the interaction of NO and NO₂ in presence of O₂ with model storage catalysts such as Pt/BaO/Al₂O₃ by IR spectroscopy. The main surface species observed were hyponitrites, nitrites and nitrates on alumina and Ba-oxide. Furthermore, Westerberg *et al.* [6] proposed that Al₂O₃ could play an important role as storage site at temperatures below 300°C.

As most of the studies were performed on model systems, detailed investigations of the NO_x storage mechanism on commercial NSR catalyst are required. The purpose of the present study is to obtain an improved understanding of the NO_x storage mechanism by identifying the surface species and reaction intermediates on such a catalyst under reaction conditions closely related to the practical application conditions. The catalyst was exposed to different gas compositions typically for the NSR process (i.e., NO, NO/O₂ and NO₂) and the NO_x species formed on the catalyst surface were investigated by *in situ* IR spectroscopy, leading to a sequence of reaction steps for the NO_x storage process.

4.2 Experimental

The catalyst studied in this work was a commercial NO_x storage reduction catalyst containing ~ 1 wt% noble metals (Pt and Rh) as oxidation/reduction component and BaO/BaCO₃ (~8 wt%) as storage component deposited on an Al₂O₃ support. From EXAFS analysis of the fresh sample the dispersion of the Pt particles was

estimated to be 95%. The specific surface area of the catalyst determined by N₂ sorption (BET method) was 110 m²/g.

XRD measurements were performed on a Rigaku powder diffractometer with Cu K α radiation. The tube voltage was 40 kV, and the current was 40 mA. The XRD diffraction patterns were taken in the 2 θ range of 10-90° at a scan speed of 2° per min at RT before and after heating the sample up to 700°C in He.

The sorption experiments of the reactants were carried out in an IR flow cell (CaF₂ windows) using a gas-mixing unit controlled by electronic flow controllers used for the simultaneous admission of NO₂, NO and O₂. The catalyst powder was pressed into thin self supporting wafers and analyzed *in situ* during all treatments by IR spectroscopy in the transmission absorption mode (resolution 4 cm⁻¹). The wafer was fixed in a heatable sample holder made of Au in the middle of the IR cell. For temperature control, a thermocouple was in direct contact with the sample holder. Further details of the experimental setup are described in ref. [12].

Prior to each adsorption experiment the fresh catalyst was activated in He (flow 25 ml/min) at 550°C for 60 min. After activation the catalysts were exposed to a gas stream containing 500 ppm NO, 500 ppm NO/ 5 % O₂ and 500 ppm NO₂ in helium (total flow 25 ml/min) at 50°C.

The thermal stability of the NO_x surface species formed on the catalyst after exposure to NO, NO/O₂ or NO₂ were investigated at temperatures between 50 and 550°C with a temperature increment of 5°C/min under constant He flow.

All spectra shown are difference spectra derived from the spectra of the catalyst in contact with the sorbents subtracted by the spectra of the catalyst after activation.

4.3 Results

4.3.1 Catalyst characterization

XRD pattern of the fresh and activated catalyst are given in Fig. 4.1. Besides the reflections typical for the support [13], the XRD pattern of the catalyst before activation exhibited reflections characteristic for BaCO_3 at 2Θ values of 24° , $24,3^\circ$, $34,1^\circ$, $34,7^\circ$, $42,1^\circ$ and $44,8^\circ$ (indicated by \star) and for BaO at $46,2^\circ$ (indicated by \circ). In the XRD pattern recorded after thermal treatment up to 700°C the presence of BaCO_3 was observed in a much lower concentration. Characteristic peaks for additional Ba-oxide species formed during the decomposition of the carbonates were not observed. This suggests that the Ba-carbonates are transformed into highly dispersed or amorphous barium oxide species, which are not detectable by XRD. A crystalline phase of Pt was not observed, which indicates the presence of highly dispersed platinum particles.

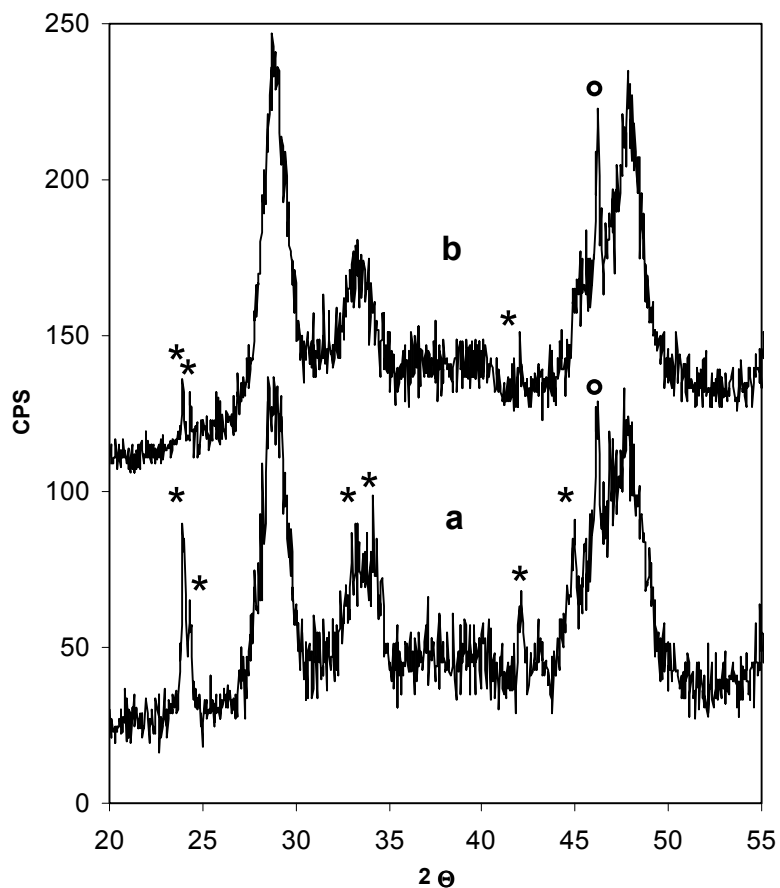


Fig. 4.1: XRD diffraction pattern for the catalyst: (a) before and (b) after activation up to 700°C in He. Both patterns were recorded at 50°C . (\star) BaCO_3 ; (\circ) BaO .

IR spectra recorded during activation of the catalyst to 500°C (not shown here) confirmed these observations. A broad band at 1450 cm^{-1} with shoulders at 1500 , 1420 and 1367 cm^{-1} was observed on the fresh catalyst, which is assigned to

Ba-carbonates [14,15]. During activation the decrease of the intensity of this band indicated a partial decomposition of BaCO₃ at temperatures up to 500°C. It should be noted, however, that the temperature observed for carbonate decomposition in these experiments was far below that typically required for the decomposition of bulk BaCO₃ (> 1000°C) [16].

4.3.2 IR spectroscopic study of the NO_x storage process

Exposure to NO

IR spectra during exposure of the catalyst to 500 ppm NO at 50 °C are shown in Fig. 4.2. The sorbed species are attributed predominantly to nitrites affiliated with Ba- and Al-oxide. After 5 min of exposure a broad band at 1206 cm⁻¹ was observed, together with weak bands at 1627 and 1569 cm⁻¹ and two negative bands at 1456 and 1297 cm⁻¹. The negative bands result from the decomposition of Ba-carbonates during NO sorption [14]. The weak bands at 1627 and 1569 cm⁻¹ are assigned to nitrates on Al-oxide sites forming bridging bidentate and chelating bidentate type

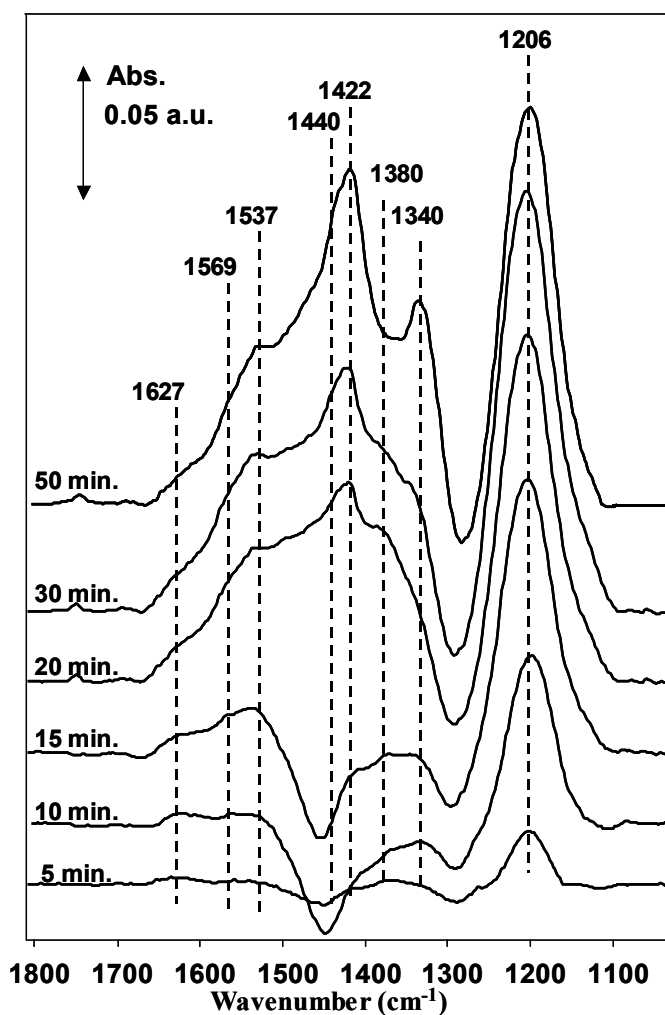
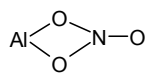
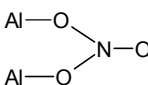
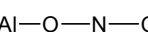
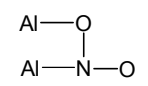
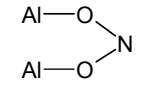
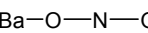
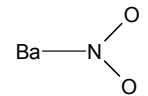
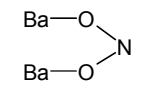



Fig.4.2: IR spectra during exposure of the catalyst to 500 ppm NO at 50°C.

species, respectively [6,11]. These species are expected to have further vibrational modes in the range 1300 to 1200 cm^{-1} [17,18], which were overlapped by the negative band at 1297 cm^{-1} (carbonates decomposition) and the broad band at 1206 cm^{-1} , arising from the contributions of several NO_x species. Note that the formation of nitrates during NO exposure requires the oxidation of adsorbed NO with reactive oxygen species that are present on the catalyst surface. Besides the contribution assigned to bridged and chelating nitrates, the main component of the broad band at 1206 cm^{-1} is assigned to bridged bidentate nitrites, which are expected to have also band at approximately 1300 cm^{-1} [11]. This band could not be clearly distinguished, which is attributed to its masking by the negative carbonate band in this region.

With further NO exposure, bands at 1340, 1380, 1422, 1440 and 1537 cm^{-1} were observed. The broad band at 1537 cm^{-1} together the increase of the intensity of the band at 1206 cm^{-1} is assigned to bridged N-coordinated nitrites on Al-oxide [6,17]. The assignment of the bands at 1340, 1422 and 1440 cm^{-1} is controversial, because various NO_x species show vibrational modes in the region between 1500 and 1300 cm^{-1} . Prinetto *et al.* [11] assigned bands at 1375 and 1310 cm^{-1} , detected during NO adsorption, to hyponitrites (NO^- , $\text{N}_2\text{O}_2^{2-}$) formed on sites with high basicity, such as BaO. Monodentate nitrites have bands between 1450 and 1300 cm^{-1} [17,18], whereas linear nitrites affiliated with Ba are reported to exhibit a band around 1420 cm^{-1} [18,19]. All these species could in principal contribute to the broad band observed. Tentatively, these bands are assigned to monodentate nitrites (1340 and 1440 cm^{-1}) and linear nitrites on Ba (1422 cm^{-1}) and hyponitrites (1380 cm^{-1}). The assignments of the various bands to NO_x surface species of adsorbed NO are summarized in Table 1.

Table 1: Assignment of IR bands to surface species formed during adsorption of NO

		NO _x species	Frequency / cm ⁻¹	Vibration
Al		Chelating bidentate nitrate	1569	v (N=O)
			1180-1260	v (NO _{2,as})
		Bridging bidentate nitrate	1627	v (N=O)
			1180-1260	v (NO _{2,as})
		Linear nitrite	~1480*	v (N=O)
Ba		Bridged N-coordinated nitrite	1537	v (N=O)
			~ 1160	
		Bridged bidentate nitrite	~1300*	v (NO _{2,as})
			~ 1230	v (NO _{2,s})
Ba		Linear nitrite	ca. 1422	v (N=O)
		Monodentate nitrite	1440	v (N=O)
			1340	v (N-O)
		Bridged bidentate nitrite	~ 1300*	v (NO _{2,as})
			~ 1230	v (NO _{2,s})
	Hyponitrite	1380/1306	v (N-N)	

* possibly masked by bands of decomposing CO₃²⁻

Exposure to NO₂

The IR spectra during exposure of the catalyst to 500 ppm NO₂ at 50°C are shown in Fig.4.3. At the start of the NO₂ admission, bands at 1203, 1332 and 1419 cm⁻¹ together with a very weak band at around 1621 cm⁻¹ were observed. The bands at 1203 and 1332 cm⁻¹ are assigned to bidentate nitrites on BaO. The formation of linear Ba-nitrites, characterized by the weak band at 1419 cm⁻¹, was observed after 5 min of NO₂ adsorption. The weak band at 1621 cm⁻¹ is assigned to bidentate nitrates on Al-oxide. After 10 min of NO₂ adsorption the band at 1203 cm⁻¹ reached

its highest intensity and slowly decreased with further exposure. Simultaneously, a new band at 1429 cm^{-1} gradually appeared, while the bands at 1564 , 1479 cm^{-1} increased in intensity with further NO_2 exposure. The band at 1564 cm^{-1} is assigned to chelating bidentate surface nitrates on Al-oxide. The corresponding band for the asymmetric vibration, expected between 1200 and 1300 cm^{-1} , was masked by bands of other surface nitrate/nitrite species. The band at 1479 cm^{-1} is assigned to linear nitrites on Al-oxide.

The bands at 1429 cm^{-1} and the main contribution of the band at 1332 cm^{-1} arise from monodentate nitrates on BaO [13]. Small shoulders, observed at 1439

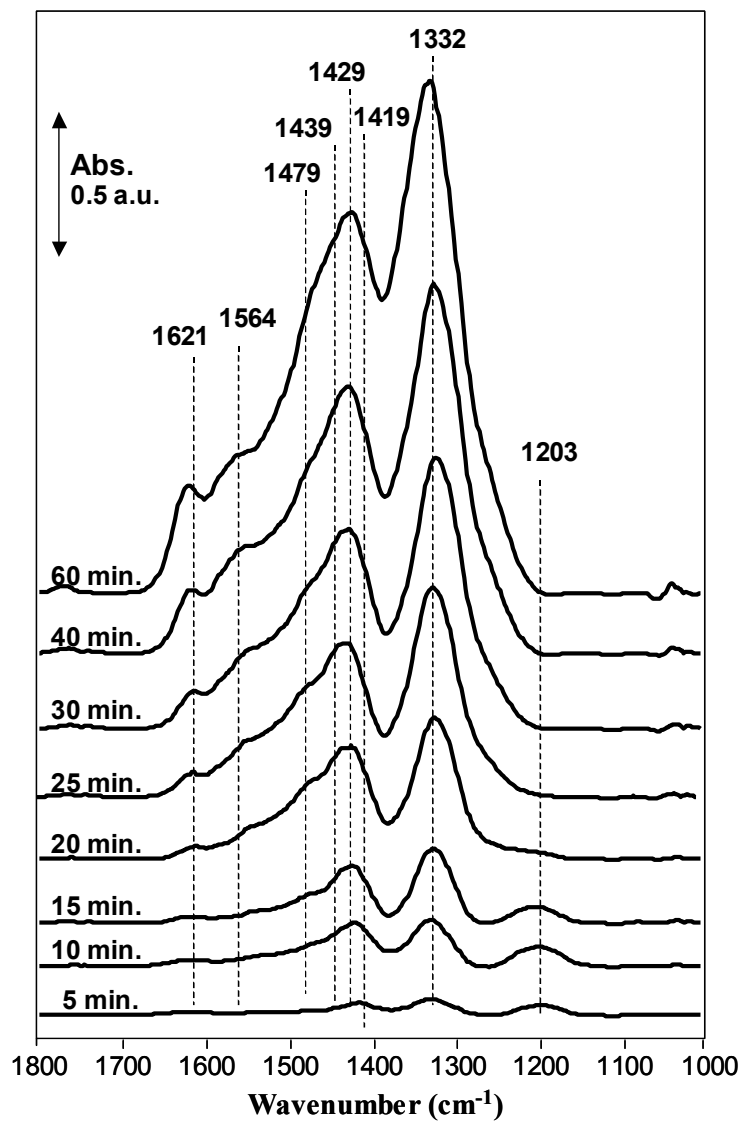


Fig.4.3: IR spectra during exposure of the catalyst to 500 ppm NO_2 at 50°C .

and 1340 cm^{-1} could indicate the formation of monodentate nitrites on Ba. The formation of bulk nitrates, with a characteristic band at around 1370 cm^{-1} [6], was not observed. The band assignment for the NO_x surface species during adsorption of NO_2 is summarized in Table 2.

Simultaneous exposure to NO and O₂

The IR spectra during exposure of the catalyst to 500 ppm NO and 5% O₂ at 50°C are shown in Fig. 4.4. At the start of the adsorption, a band assigned to surface nitrite species was present at around 1200 cm⁻¹, which reached a maximum in intensity after 18 min adsorption, similar to situation observed during NO₂

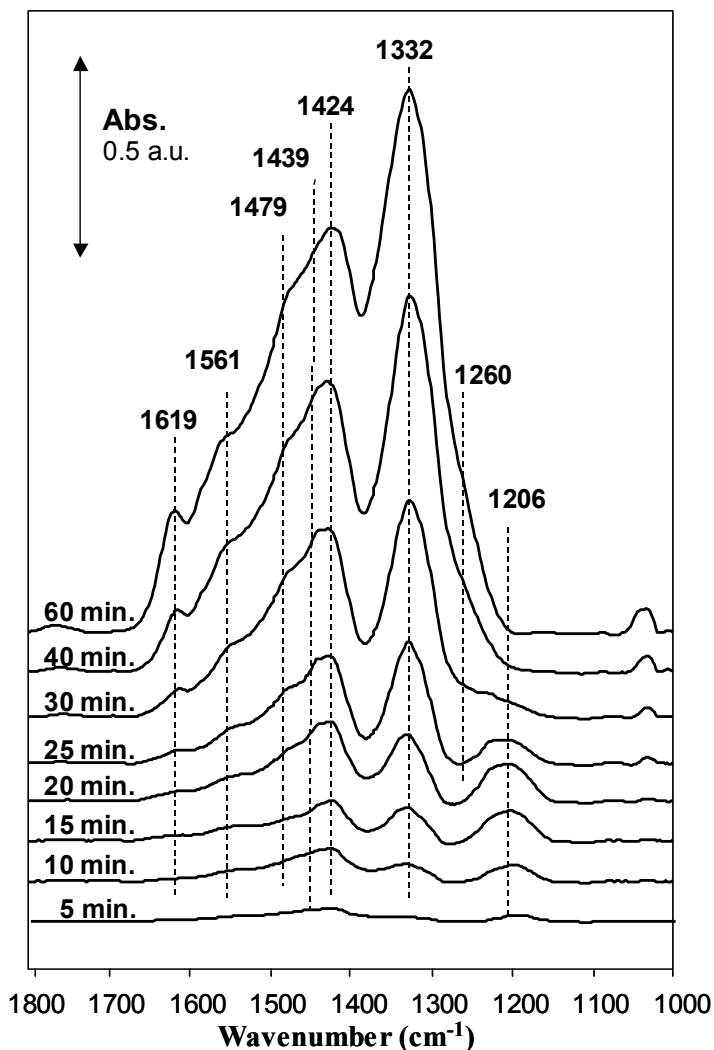


Fig. 4: IR spectra during exposure of the catalyst to 500 ppm NO and 5% O₂ at 50°C.

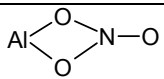
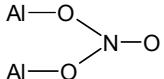
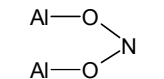
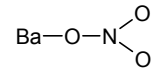
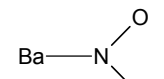
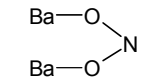
adsorption (Fig. 4.3). It decreased in intensity with further NO/O₂ exposure. The weak band at 1419 cm⁻¹ observed in the beginning of the NO/O₂ adsorption procedure is assigned to linearly bound Ba-nitrites. After 10 min of exposure additional bands at 1424 and 1332 cm⁻¹ were observed and with further exposure (15 min) overlapping bands at 1619, 1561, 1479, 1439 cm⁻¹ and a weak shoulder at 1260 cm⁻¹ were observed.

Bridging bidentate nitrates on Al-oxide show a characteristic N=O

band at 1479 cm^{-1} . The bands at 1424 and 1332 cm^{-1} are attributed to the presence of monodentate nitrates on Ba-oxide sites.

The presence of monodentate nitrates on Al could not be unequivocally confirmed because of the unresolved broad bands in the $1500\text{-}1300\text{ cm}^{-1}$ region. As also observed for the adsorption of NO_2 the formation of bulk nitrates is negligible, indicated by the absence of the characteristic absorption band for free ionic nitrates around 1370 cm^{-1} . The band assignments for NO/O_2 adsorption are summarized together with the assignments for NO_2 adsorption in Table 2.

Table 2: Assignment of IR bands to surface species formed during adsorption of NO_2 and NO/O_2

	NO_x species	Frequency / cm^{-1}	Vibration	
Al		Chelating bidentate nitrate	1564/61 ~1290	$\nu(\text{N}=\text{O})$ $\nu(\text{NO}_{2,\text{as}})$
		Bridging bidentate nitrate	1621/19 1260	$\nu(\text{N}=\text{O})$ $\nu(\text{NO}_{2,\text{as}})$
	$\text{Al}-\text{O}-\text{N}-\text{O}$	Linear nitrite	1479	$\nu(\text{N}=\text{O})$
		Bridged bidentate nitrite	1200-1230 ~1330	$\nu(\text{NO}_{2,\text{s}})$ $\nu(\text{NO}_{2,\text{as}})$
Ba		Monodentate nitrate	1429/24 1332	$\nu(\text{NO}_{2,\text{as}})$ $\nu(\text{NO}_{2,\text{s}})$
	$\text{Ba}-\text{O}-\text{N}-\text{O}$	Linear nitrite	1419	$\nu(\text{N}=\text{O})$
		Monodentate nitrite	1439 1340	$\nu(\text{N}=\text{O})$ $\nu(\text{N}-\text{O})$
		Bridged bidentate nitrite	~1330 1200-1230	$\nu(\text{NO}_{2,\text{as}})$ $\nu(\text{NO}_{2,\text{s}})$

4.3.3 Thermal stability of NO_x surface species

The IR spectra during a controlled temperature rise from 50 to 550 °C of the catalysts after exposure to NO, NO₂ and NO/O₂ in an inert gas stream are shown in Fig. 4.5.

For the catalyst pre-exposed to 500 ppm NO (Fig. 4.5a), bridged and bidentate nitrates on Al-oxide sites with characteristic bands at 1627 and 1574 cm⁻¹ and bridged N-coordinated nitrites with characteristic bands at 1536 and 1154 cm⁻¹ remained on the surface until 200°C. The band at 1206 cm⁻¹, attributed mainly to bridged bidentate nitrites, continuously decreased and vanished at around 250°C. The bands at 1438 and 1342 cm⁻¹ (monodentate nitrites) also decreased with increasing temperature. At 200°C a new band at 1306 cm⁻¹ was observed growing in intensity until 400°C. During further temperature increase the intensity of this band decreased again, but a small contribution was visible up to 550°C. This band can be assigned to hyponitrites on Ba-oxide, which are reported to be formed during decomposition of NO_x species from highly basic metal oxides pre-exposed to NO. The high thermal stability observed for these species is in agreement with the literature [20,21]. The negative bands at 1460 and 1370 cm⁻¹ result from the further decomposition of residual carbonates during temperature increase.

After pre-exposure of the catalyst to NO₂ (Fig. 4.5b) the linear bonded nitrites on Al-oxide desorbed at temperatures around 150 °C shown by a decrease of the band at 1478 cm⁻¹. It was shown that the thermal stability of chelating bidentate nitrates on Al-oxide (up to 350°C) is higher compared to bridged bidentate nitrates on Al-oxide (up to 250°C) [22]. The bands at 1429 and 1332 cm⁻¹ can be assigned to monodentate nitrates on Ba, which were thermally stable to temperatures higher than 550°C. At temperatures above 250°C the band at 1332 cm⁻¹ was broadened and shifted to lower wavenumbers indicating an increasing ionic character of the monodentate nitrates. These bands were partly present up to 550°C.

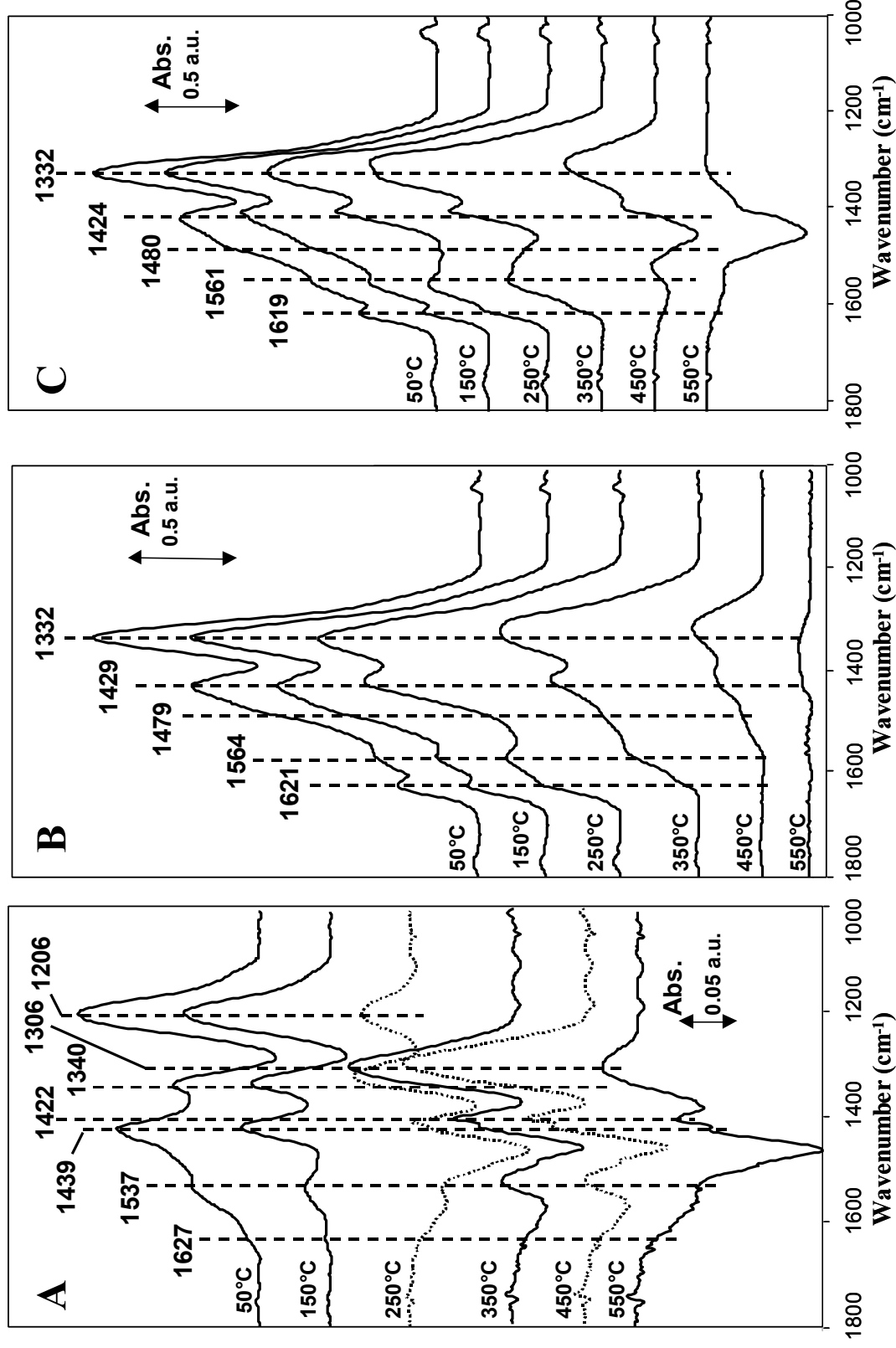
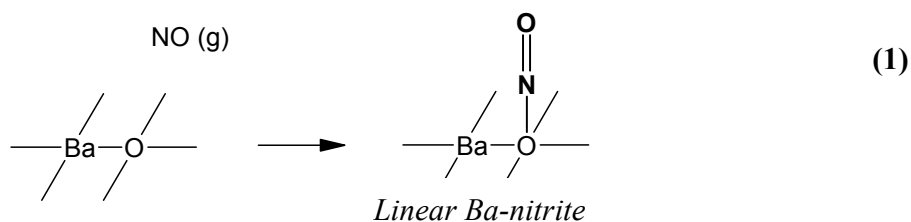


Fig. 4.5. IR spectra during temperature increase from 50 to 550°C of the pre-exposed catalyst in an inert gas stream: (a) after exposure of the catalyst to 500 ppm NO at 50°C; (b) after exposure to 500 ppm NO₂ at 50°C and (c) after exposure to 500 ppm NO and 5% O₂ at 50°C.

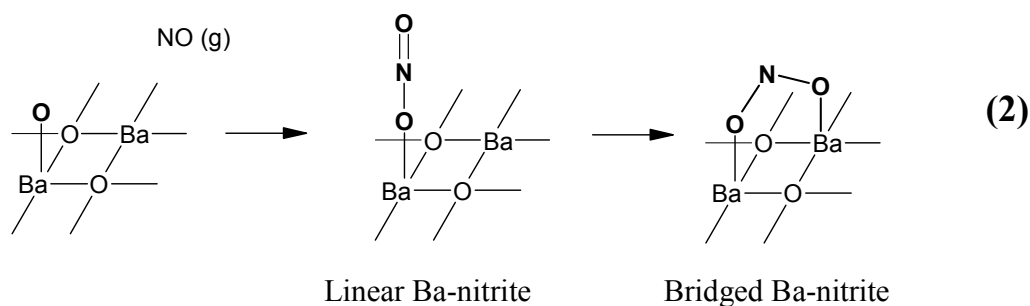
The thermal stability of the NO_x species formed after exposure of the catalyst to NO and O₂ (Fig. 4.5c) was similar than that of the species formed upon NO₂ exposure. Among the different nitrite/nitrate species on Ba-oxide and Al-oxide, the linear and monodentate Ba-nitrites had the lowest thermal stability, followed by the bridged and chelating bidentate nitrates on aluminum oxide. At 350°C, the band assigned to monodentate Ba-nitrate (1332 cm⁻¹) shifted to lower wavenumber was observed. The asymmetric stretching vibration of monodentate Ba-nitrate around 1425 cm⁻¹ was partly masked by the appearance of the negative band at 1450 cm⁻¹ assigned together with a band at 1380 cm⁻¹ to the decomposition or replacement of carbonates.

4.4 Discussion

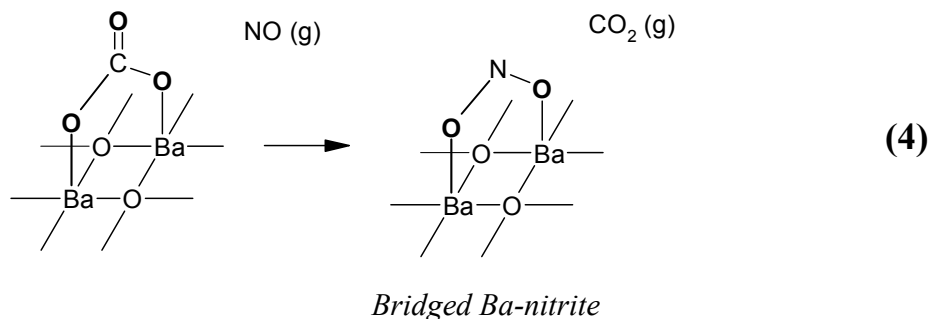
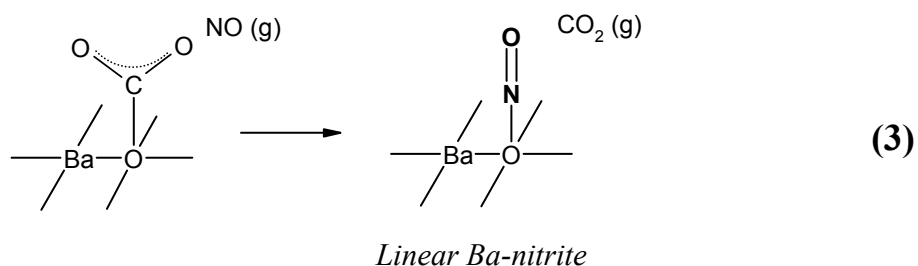
During the exposure of the catalyst to NO predominantly nitrite surface species are formed on Ba -oxide and Al-oxide sites. Initially, linear and bridged nitrites are formed, which were preferably located on Ba -oxide surface sites, due to their higher basicity [23]. It is likely that the nitrite first interacts *via* the positively charged N atom with the negatively charged oxygen atom next to Ba creating a linear nitrite species [24] as shown in Scheme 1.



If linear Ba-nitrites are formed on less coordinated surface oxygen site they could subsequently interact *via* the oxygen of NO with an adjacent Ba-atom and lead to the formation of bridged Ba-nitrites as shown in Scheme 2.



Simultaneously with the formation of nitrites, the amount of Ba-carbonates species decreased which indicates the partial replacement of carbonates by the nitrites formed on BaO. The decomposition of surface carbonates, however, was only detected during the exposure of the catalyst to NO and NO/O₂, but not during the exposure of the catalyst to NO₂. Therefore, NO appears to be the active species during the replacement of barium carbonates on the surface of the catalyst. On metal oxide surfaces carbonates exist in monodentate, chelating and bridged carbonates form [25,26]. The reaction steps for the replacement of monodentate and bidentate carbonates by forming linear and bridged nitrites could be proposed according to Schemes 3 and 4:



With further exposure of the catalysts to NO, also Al-oxide sites are concluded to be involved in the storage process. The main species being formed are linear N-coordinated nitrites.

It is interesting to note that bands characteristic for bridged and chelating nitrates on Al-sites were observed in the absence of gas phase O₂.

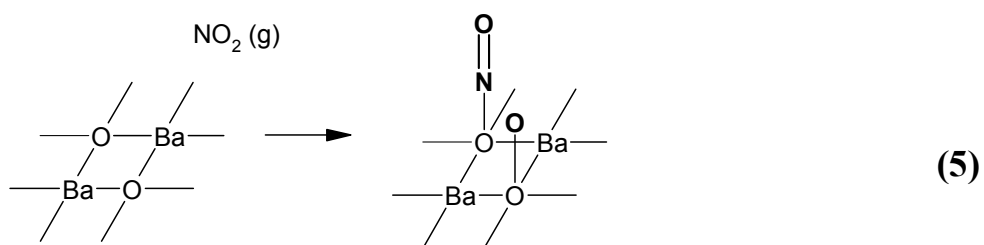
For nitrate formation from NO different pathways are plausible. One possibility is the presence of reactive oxygen species on the catalyst surface, such as peroxides or defect metal sites on the surface of Ba-oxide or Al-oxide. As the formation of peroxides on Al-oxide is negligible, even when O₂ is present in the feed [6], Ba-peroxides are the only plausible source for highly reactive oxygen. However, because of the higher basicity of BaO, the spill over of the NO_x species to Al-oxide sites after oxidation does not seem to be likely. Therefore, linear N-coordinated nitrites and linear nitrites on Al-oxide sites are expected to act as intermediates during the nitrate formation *via* coordinatively unsaturated metal cations. Bands for linear nitrites could not be clearly identified, due to the negative band in this region arising from the carbonates replaced, however N-coordinated nitrites were observed. Thus, the bridging and chelating bidentate Al-nitrates are speculated to be formed on cation vacancy sites on the alumina surface.

Summarizing these observations, four parallel reaction steps for the adsorption of NO were identified:

- (i) Molecular adsorption of NO by formation of nitrites on BaO sites
- (ii) (Partial) replacement of Ba-carbonates by NO, resulting in the formation of Ba-nitrites
- (iii) Formation of hyponitrites on BaO sites
- (iv) Formation of bridging and chelating bidentate nitrates on Al-oxide *via* the formation on cation vacancy sites on the Al-oxide surface

It should be noted, however, that the amount of adsorbed NO_x species during the exposure of the catalyst to NO is much lower compared to the exposure to NO/O_2 and NO_2 .

The main surface species formed during exposure of the catalyst to 500 ppm NO_2 are nitrates formed on alumina and barium-oxide sites. Surface nitrites seem to play, however, an important role as an initial step in the storage process. Similar to the exposure of the catalyst to NO bridged and linear nitrites on Ba-oxide and Al-oxide were observed at the beginning of the NO_2 exposure. Bridged nitrites could be generated via a molecular adsorption of NO_2 on two neighboring BaO sites, whereas for the formation of linear nitrites the presence of NO is necessary. Broqvist *et al.* [27] investigated NO_2 adsorption at a BaO (100) surface by density functional theory calculations and proposed a mechanism in which nitrites are generated during pairwise NO_2 chemisorption on Ba and O sites with a subsequent redox-reaction of both with adsorbed NO_2 species forming a nitrite-nitrate pair. Schneider *et al.* [28] proposed a similar adsorption – oxidation mechanism for two NO_2 molecules for the formation of nitrates on MgO. Dissociative adsorption of NO_2 was proposed by Schmitz *et al.* [21], who investigated NO_2 adsorption at BaO films with XPS. They postulated an adsorption of NO_2 on the BaO surface *via* a dissociation of the NO_2 creating linear Ba-nitrites and BaO_2 . As in our experiments only insignificant amounts of Ba-nitrates were detected during the initial formation of linear Ba-nitrites a dissociative adsorption of NO_2 (Scheme 5) seems to be more likely.



The decreasing concentration of bridged nitrites with increasing time of exposure could result from an oxidation of Ba-nitrites with gas phase NO₂ creating bridged bidentate nitrates or by a direct replacement of nitrites by nitrates formed on adjacent sites and a subsequent surface transport. Monodentate nitrites and nitrates on Ba are formed by the molecular adsorption of NO₂ at a Ba and an O site, respectively [21].

The reaction steps derived from the sorption of NO₂ on the NSR catalyst could be summarized as follow:

- (i) Formation of bridged nitrites *via* adsorption of NO₂ on two adjacent metal sites
- (ii) Formation of linear nitrites *via* a dissociative adsorption of NO₂
- (iii) Oxidation of nitrites by gas phase NO₂ or direct replacement by nitrates after extended exposure
- (iv) Nitrates are the main species after an extended NO₂ exposure

As mentioned above, the decomposition or replacement of remaining Ba-carbonates, indicated by negative bands in the difference IR spectra, did not occur during exposure of the catalysts to NO₂. The replacement of carbonates was only observed when NO was present in the feed. In this context, it should be mentioned that Balcon *et al.* [29] and Amberntsson *et al.* [30] investigated the influence of CO₂ on the release of NO_x stored on a barium-containing NSR catalyst at temperatures between 250 and 550°C and observed a promoting effect of CO₂ on the release of NO_x. Balcon *et al.* [29] suggested a competitive storage of CO₂ and NO₂ for the same barium site and interpreted this in terms of the existence of the equilibrium: $\text{CO}_{2(\text{g})} + \text{Ba-nitrates} \rightleftharpoons \text{NO}_{2(\text{g})} + \text{Ba-carbonates}$, which would explain the inactivity of NO₂ for Ba-carbonate replacement observed during the exposure of the catalyst to NO₂. However, based on our observation, that a replacement of carbonates was observed during exposure to NO or NO/O₂ it could be speculated, that a comparable equilibrium for NO ↔ CO₂ storage on Ba sites does not exist or

that under the reaction conditions used the equilibrium is shifted towards the formation of Ba-nitrites and the release of CO₂.

Exposure of the catalysts to NO and O₂ led to similar results than the exposure to NO₂. The main differences observed are that bridged nitrites were observed for a longer period and that nitrate species are formed in lower concentration (around 80% of the amount of nitrates formed during exposure to NO₂), while the concentration of nitrite species formed was equal to the concentration formed during NO₂ exposure. Compared to the NO exposure, the amount of Al-nitrates is much higher and additional Ba-nitrates are present on the catalyst surface after NO/O₂ exposure.

As NO₂ formation *via* NO oxidation on Pt is known to occur at temperatures above 150°C, this reaction can be neglected to be the main source for NO₂ formation [6]. Therefore, the similarity of the surface species observed during exposure to NO₂ and NO/O₂ is unexpected. As the thermodynamic equilibrium for the reversible gas phase reaction of NO with O₂ forming NO₂ at low temperatures is on the side of NO₂ [31], a minor contribution of NO₂ forming surface nitrates could arise from the gas phase reaction of NO with O₂. Additionally, a small amount of nitrates is speculated to be formed *via* defect sites on Al-oxides and Ba-oxides, as already postulated for the Al-nitrates formed during exposure to NO. A third pathway for nitrate formation could be related to reactive oxygen species present on the metal surface. Several research groups investigated the interaction of O₂ with metal oxide surfaces (e.g. BaO, MgO, La₂O₃, Tb₄O₇) and proposed a molecular and a dissociative adsorption mechanism for O₂ [22, 32]. Thus, the formation of nitrates on Ba-oxide and Al-oxide could occur *via* the reaction of nucleophilic oxygen adsorbed on the surface with a NO molecule. A molecular and dissociative adsorption of O₂ on BaO and Al₂O₃ is also confirmed by results reported by Sedlmair *et al.* [33] for the adsorption of NO and O₂ on Ba exchanged Y zeolites containing no Pt. They observed similar amounts of surface nitrates formed during the exposure to NO/O₂ and NO₂ at 50°C and explained this by a molecular and

dissociative adsorption of O₂ on the metal surface sites forming reactive oxygen surface species. As small amounts of La-oxides and Ce-oxides are present in the NSR catalysts these species could also be assumed to act as a source for reactive oxygen species. Among all three possible pathways for nitrate formation the last one, which involves reactive oxygen species is speculated to be the most important. The longer presence of bridged nitrites during NO/O₂ exposure compared to NO₂ exposure indicates the slow oxidation of NO to nitrates. This observation and the lower concentration of nitrates formed during NO/O₂ adsorption suggest that the oxidation with NO₂ as oxidation agent is more important than the oxidation with gas phase oxygen.

The thermal stability of the NO_x species formed on the catalyst upon the exposure to NO, NO₂ and to NO/O₂ is comparable. In all cases nitrates show a higher thermal stability than nitrites. In general, nitrites and nitrates formed on Ba-oxide were more stable than those formed on Al-oxide. Hyponitrites, only detected after the exposure of the catalyst to NO, show in contrast a high thermal stability. The shift of the monodentate Ba-nitrate bands to lower wavenumbers during temperature increase indicates a change in the covalent – ionic bonding character of the nitrates. For covalently bound nitrates an IR band around 1470 cm⁻¹ is expected, whereas for ionically bound nitrates a IR band is located at around 1370 cm⁻¹ [34]. Therefore we conclude that the ionic bonding character of Ba-nitrates increases with increasing temperature. The presence of ionic bulk-like nitrates after heating to 550°C suggests a partial migration of surface Ba-nitrates into the bulk.

4.5 Conclusions

Surface species and reaction intermediates on a commercial NO_x storage reduction catalyst during exposure to NO, NO₂ and NO/O₂ have been identified by *in situ* IR spectroscopy. During exposure of the catalyst with NO mainly linear and bridged nitrites were formed by molecular adsorption of NO. After longer exposure small

concentrations of bridged and chelating nitrates on Al-oxide sites were seen, which were formed *via* the oxidation of NO by reactive oxygen and *via* oxidation of adsorbed nitrites.

The main surface species formed during the exposure of the catalyst to NO₂ and NO/O₂ are nitrates on the Al-oxide and Ba-oxide catalyst components. A higher concentration of adsorbed nitrates species was found for NO₂ exposure compared to NO/O₂ exposure. Nitrites were identified as intermediates during the formation of nitrates. For the formation of linear nitrites a dissociative adsorption mechanism of NO₂ on Ba-oxide sites is proposed. After longer exposure, nitrites are either oxidized by NO₂ to nitrates or directly replaced by nitrates. In particular, chelating, bridging and monodentate nitrates are the main NO_x species formed on the Ba-oxide and Al-oxide sites during exposure to NO/O₂ or NO₂. The total amount of NO_x species adsorbed is the lowest for NO exposure followed by NO/O₂ and NO₂ exposure. NO was found to be the active species for replacement of Ba-carbonates by Ba-NO_x species.

The thermal stability of the NO_x species formed on the catalyst increases in the order: Al-nitrites (linear, N-coordinated) < Ba-nitrites (linear, monodentate) < Al-nitrates (bridging bidentate, chelating bidentate) < Ba-hyponitrites < Ba-nitrates (monodentate).

The results clearly indicate the presence of a series of subsequent reaction steps during the adsorption of NO_x on a NSR catalyst. The proposed key elementary steps are summarized in a general scheme shown in Fig. 6. Initially NO is stored in the form of nitrites on the storage component either by a molecular adsorption on Al-oxides and Ba-oxides **(1)** or by the replacement of Ba-carbonates **(2)**. NO₂ formed by oxidation on the noble metal either sorbs molecularly and forms nitrates **(3)** or dissociatively and forms nitrites **(4)**. After a certain concentration of NO_x is adsorbed, the transformation and further oxidation of the surface nitrites into

surface nitrates by NO₂ (5) is the predominant reaction step during the storage of NO_x on the catalysts.

Acknowledgements

The authors would like to thank the European Union for funding of this project STORECAT; Brite/EuRam BRPR-CT98-0613. F.X. Hecht is gratefully acknowledged for the BET measurement.

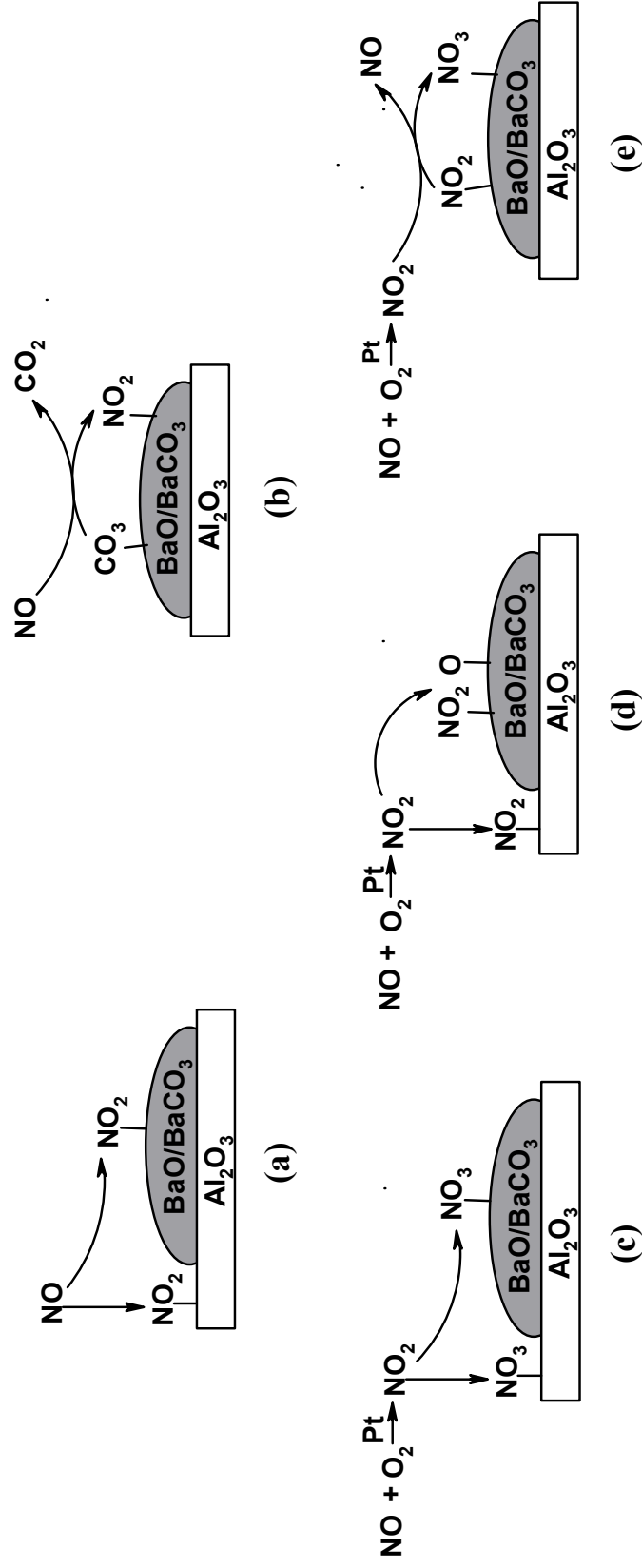


Fig. 6: General molecular scheme of the main elementary steps for the NO_x storage on a commercial storage reduction catalyst. (a) Formation of nitrates by molecular adsorption of NO ; (b) Replacement of Ba-carbonates with Ba-nitrites formed by NO ; (c) Formation of nitrates by molecular adsorption of NO_2 ; (d) Formation of Ba-nitrites and Ba-peroxides by dissociative adsorption of NO_2 ; (e) Transformation of surface nitrites to surface nitrates with NO_2 as oxidizing agent. Note, that in all schematic structures of surface species shown one oxygen arise from the Al-oxide or Ba-oxide surface.

References

- [1] Kreuzer T., Lox S. E., Lindner D., Leyrer J., *Catal. Today* **29**, 17 (1996).
- [2] Katoh K., Kihara T., Asanuma T., Gotoh M., Shibagaki N., *Toyota Techn. Review* **44**, 27 (1995).
- [3] N. Miyoshi, S. Matsumoto, K. Katoh, T. Tanaka, J. Harada, N. Takahashi, K. Yokota, M. Sugiura, K. Kasahara, *SAE Paper* 950809 (1995).
- [4] Sedlmair Ch., Seshan K., Jentys A., Lercher J. A. *Catal. Today* **75**, 413 (2002).
- [5] Takahashi N., Miyoshi N., Matsumoto S., Tanaka T., Shinjoh H., Iijima T., Yokota K., Suzuki T., Suzuki H., Yamazaki K., Tanizawa T., Tateishi S., Kasahara K., *Catal. Today* **27**, 63 (1996).
- [6] Westerberg B., Fridell E., *J. Mol. Catal. A: Chem.* **165**, 249 (2001).
- [7] Coronado J. M., Anderson J. A., *J. Mol. Catal. A: Chem.* **138**, 83 (1999).
- [8] Mahzoul H., Brilhac J. F., Gilot P., *Appl. Catal. B* **20**, 47 (1999).
- [9] Cant N. W., Patterson M. J., *Catal. Today* **73**, 271 (2002).
- [10] Fridell E., Skoglundh M., Persson H., Olsson L., Amberntsson A., Westerberg B. *Topics in Catalysis* **16/17**, 133 (2001).
- [11] Prinetto F., Ghiotti G., Nova I., Lietti L., Tronconi E., Forzatti P., *J. Phys. Chem. B* **105**; 12732 (2001).
- [12] Mirth G., Lercher J. A., *Appl. Spectroscopy* **48**, 194 (1994).
- [13] Anderson J. A., Fernandez-Garcia M., *Trans IChemE* **78**, 935 (2000).
- [14] Nakamoto K., "Infrared and Raman Spectra of Inorganic and Coordination Compounds", 4th ed.; Wiley; New York, 1986.
- [15] Little L. H., "Infrared Spectra of Adsorbed Species" Academic Press, London, 1966.
- [16] Weast R. C., "Handbook of Chemistry and Physics" Chemical Rubber Publishing Company, Ohio, 1970.
- [17] Davydov A. A., "Infrared Spectroscopy of Adsorbed Species on the Surface of Transition Metal Oxides" Wiley, New York, 1990.
- [18] Hadjiivanov K. I., *Catal. Rev.-Sci. Eng.* **42**, 71 (2000).
- [19] Fridell E., Skoglundh M., Olsson L., Westerberg B., Persson H., *Catal. Letters* **66**, 71 (2000).
- [20] Huang S.-J., Walters A. B., Vannice M. A., *J. Catal.* **192**, 29 (2000).
- [21] Davydov A. A., Lkhov Y. A., Shchekochikhin Y. M., *Kinet. Katal.* **19**, 673 (1978).
- [22] Chi Y., Chuang S. C., *J. Phys. Chem.* **104**, 4673 (2000).
- [23] Lietti L., Forzatti P., Nova I., Tronconi E., *J. Catal.* **204**, 175 (2001).
- [24] Schmitz P. J., Baird R. J., *J. Phys. Chem. B* **106**, 4172 (2002).
- [25] Lavalley J. C., *Catal. Today* **27**, 377 (1996).
- [26] Hattori H., *Chem. Rev.* **95**, 537 (1995).

-
- [27] Broqvist P., Panas I., Fridell E., Persson H., *J. Phys. Chem. B* **106**, 137 (2002).
- [28] Schneider W. F., Hass K. C., Miletic M., Gland J. L., *J. Phys. Chem. B* **106**, 7405 (2002).
- [29] Balcon S., Potvin C., Salin L., Tempère J. F., Djéga-Mariadassou G., *Catal. Letters* **60**, 39 (1999).
- [30] Amberntsson A., Persson H., Engström P., Kasemo B., *Appl. Catal. B* **31**, 27 (2001).
- [31] Laane J., Ohlsen J. R., *Prog. Inorg. Chem.* **27**, 465 (1980).
- [32] Borchert H., Baerns M. J., *J. Catal.* **168**, 315 (1997).
- [33] Sedlmair Ch., K.Seshan, A. Jentys, J.A. Lercher, submitted to *Phys. Chem. Chem. Phys.* (2002).
- [34] Pozdnyakov D. V., Filimonov V. N., *Kinet. Katal.* **14**, 655 (1973).

Chapter 5

Influence of sulfur dioxide on the catalytic performance of a commercial NO_x storage reduction catalyst

Abstract

The influence of SO₂ exposure under lean (oxygen-rich) and rich (reducing) reaction conditions on the storage and oxidation/reduction function of a commercial NO_x storage-reduction catalyst was investigated by (temperature programmed) uptake experiments and high temperature XRD. Both, the storage capacity and the oxidation/reduction function of the catalyst were deactivated by SO₂ exposure under lean and rich reaction conditions. The deactivation of the storage component, i.e., the loss of the NO_x storage capacity, resulted mainly from the formation of Ba-sulfates accumulating in the bulk phase. They possess a high thermal stability (>800°C) and could not be removed under the typical operation conditions of a NSR catalyst. For the oxidation function only a temporarily deactivation during lean reaction conditions was observed. Besides the formation of SO_x species on the storage component at the beginning of the SO₂ exposure under rich conditions, an adsorption of SO₂ on the noble metal component was observed resulting in the formation of sulfur deposits. The oxidation of these sulfur species with a subsequent spillover to the storage component during lean conditions could accelerate the deactivation of the storage capacity.

5.1 Introduction

Lean burn and diesel engines, which are effectively improving the efficiency compare to traditional gasoline engines [1], produce oxygen rich exhaust gas streams. Due to the surplus of oxygen the NO_x emissions can not be reduced applying a conventional three way catalytic converters. This drawback has lead to an intensive research in industrial and academic laboratories to develop catalysts for the reduction of NO_x in excess of oxygen. Among the strategies proposed [2], one of the most promising approaches is based on the concept of NO_x storage-reduction (NSR) using cyclic changes between lean and rich operation conditions of the engine [3, 4]. NSR catalysts contain storage components, typically alkali or alkaline earth metals, commonly barium, and oxidation/reduction components, typically provided by noble metal components. During lean operation conditions (i.e., oxidizing atmosphere) NO is oxidized to NO_2 over the noble metal component and stored on the storage component as nitrate [5, 6]. By changing periodically to short cycles of rich operation conditions (i.e., reducing atmosphere) NO_2 is released from the storage component and converted to N_2 over the metal component [7]. The major limitation for an immediate application of NSR catalysts derives from the rapid decrease of the storage capacity in presence of SO_x , which results from the use of sulfur containing fuels [8, 9].

Numerous studies have been focused on the influence of SO_x on the NO_x storage capacity [9-12], on sufficient regeneration procedures [13-15] and on improving the sulfur tolerance of NSR catalysts [16-18]. Engström *et al.* [9] found a correlation between the deactivation of the NO_x storage function and the total amount of SO_2 that the catalysts has been exposed to. An influence of SO_2 on the oxidation and reduction activity was also suggested. Mahzoul *et al.* [10] studied the sulfatization process by IR and adsorption/desorption experiments. Sulfate formation on barium and on the support was observed during oxygen rich conditions. In a recent study [12] it was proposed, that SO_2 first interacts with Ba

forming surface sulfates, which subsequently migrate into the bulk phase of the storage component. The sulfates are reported to show a high thermal stability up to 1000°C [10] and even under hydrocarbon rich conditions a removal at suitable temperatures (up to 550°C) was not observed [12]. However, Erkfeldt *et al.* [13] reported the partial removal of sulfates under strong reducing conditions using H₂ and CO during extended regeneration periods. Recent studies included also the possibility of a deactivation of the noble metal component during fuel rich reaction conditions [12, 15].

The aim of this study was to investigate in detail the deactivation of a commercial NSR catalyst by SO₂, mainly focussing on the influence of SO₂ on the storage capacity and on the oxidation/reduction function under lean and rich operation conditions. Uptake experiments were carried out using SO₂, NO, O₂ and C₃H₆ in an inert carrier gas monitoring the gas composition at the reactor outlet by mass spectrometry. The structural and chemical composition of the catalyst after the different exposure to the reactant gases was investigated by high temperature XRD to study the temperature dependency of the decomposition or migration of surface and bulk sulfur species.

5.2 Experimental

Material

The catalyst investigated was a typical NO_xSR material supplied in powdered form by Johnson Matthey, Royston, UK, and contained Pt and Rh as part of the oxidation/reduction components, BaO/BaCO₃ as storage component and Al₂O₃ as support. The specific surface area of the catalyst determined by N₂ sorption (BET method) was 110 m²/g. The material was crushed and sieved and the fraction with particle diameters in the range of 200 – 450 μm was used for kinetic experiments.

SO₂ uptake experiments

The SO₂ uptake under typical reaction conditions was studied in a horizontal quartz tube reactor containing the catalyst particles in the middle of the heated zone sealed by quartz wool. Electronic mass flow controllers were used for the admission of NO, SO₂, O₂ and C₃H₆ using He as carrier gas and Ar as internal standard. The partial pressure of the reactant and product molecules at the outlet of the reactor was continuously probed using a mass spectrometer.

Typically, 400 mg of the catalyst were activated in He (200 ml/min) for 60 min at 550°C and exposed to desired gas mixtures at a total flow of 200 ml/min at 350°C containing 310 ppm SO₂ and 5% O₂ (lean conditions) or 2000 ppm C₃H₆ (fuel-rich conditions). The storage capacity was determined by adding 1000 ppm NO and 5% O₂ into the gas stream. During regeneration, the catalyst was exposed to 2000 ppm C₃H₆ in He at 600°C for 60 min. Temperature programmed desorption (TPD) experiments were carried out in 200 ml He with a temperature increase of 10°C/min up to 850°C.

High-temperature XRD

XRD measurements were performed on a Rigaku powder diffractometer with Cu K α radiation at a tube voltage of 40 kV and a current of 40 mA. The XRD diffraction patterns were collected in the 2 θ range between 10 and 90° at a scan speed of 2° per min at RT before and after heating the sample up to 700°C in He. Prior to the XRD measurements one sample was exposed to 400 ppm SO₂ and 5%O₂ and another one to 400 ppm SO₂ / 500 ppm NO under cyclic lean and rich conditions at 350°C. Gas concentrations and reaction conditions are summarized in Tab. 5.1. The complete pretreatment was carried out for 5 h. The high temperature XRD patterns were recorded every 50°C up to 700°C under continuous He flow. After cooling down the last pattern was taken at ambient temperature.

Table 5.1: Reaction conditions of sample pretreatment for high temperature XRD.

Exp. Conditions	Lean	Cyclic	
SO ₂	400 ppm	400 ppm	400 ppm
NO	-	500 ppm	500 ppm
O ₂	5%	5%	-
C ₃ H ₆	-	-	2000 ppm
Cycle time (lean/rich)	-	100sec.	20sec.
Total flow (diluant: He)	100 ml/min	100 ml/min	

5.3 Results and discussion

5.3.1 XRD study of the interaction of SO₂ with the NSR catalyst

The XRD during the exposure of the catalyst to SO₂ for the pretreated materials before and after heating to 700 °C are shown in Figs 5.1a and 5.1b, respectively. Diffraction patterns were recorded for the fresh material, for a sample pretreated in a feed of 400 ppm SO₂ and 5 % O₂ and for a sample pretreated with 400 ppm SO₂ and 500 ppm NO during consecutive cycles of 5% O₂ (lean cycle) and 2000 ppm C₃H₆ (fuel-rich cycle) at 350°C. Besides reflections for the Al₂O₃ support, the fresh material before temperature treatment exhibited reflections characteristic for BaCO₃ at 24°, 24,3°; 34,1°; 34,7°, 42,1°, 44,8° and for BaO at 46,2°. After exposure to SO₂ and O₂ additionally peaks characteristic for BaSO₄ at 42,6° and 43,0° were observed, indicating the formation of bulk BaSO₄. The lower intensity of the reflections for Ba-carbonates observed on this sample indicates their partial replacement by Ba-sulfates. For the material treated under cyclic lean/rich reaction conditions only traces of BaCO₃ could be detected by XRD, while the majority of crystalline phases was Ba-sulfate. Reflections assigned to crystalline Ba-nitrates phases could not be identified, which either indicates that their formation is

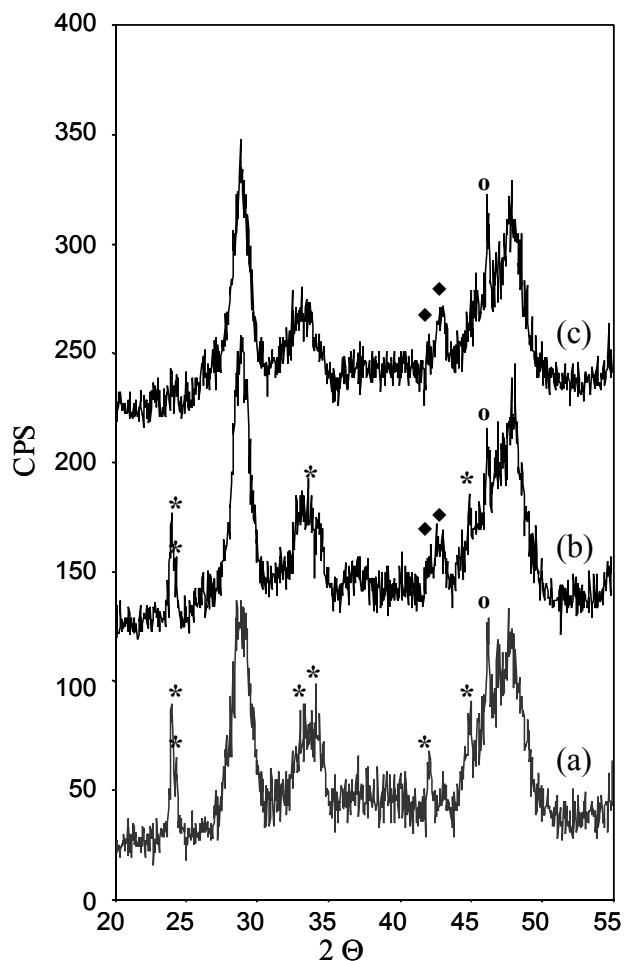


Fig. 5.1a: XRD diffraction pattern for the catalyst before thermal treatment: (a) fresh (b) exposed to 400 ppm SO₂/ 5% O₂ at 350°C (c) exposed to 400 ppm SO₂/ 1000ppm NO during cycling between 5% O₂ (100 sec.) and 2000 ppm C₃H₆ (20sec.) at 350°C. (*) BaCO₃; (o) BaO; (◆) BaSO₄.

suppressed by the formation of Ba-sulfates or they were only formed as highly dispersed clusters on the surface of the catalysts and were, therefore, not detectable by XRD.

After heating the material to 700°C in He (Fig. 5.1b) small amounts of residual BaCO₃ were observed for the fresh catalyst, while the majority of carbonates decomposed between 400 and 700°C. It should be noted that the temperature of 700 °C is far below the temperatures required for the decomposition of bulk BaCO₃ (>1000°C) [19]. On the material pre-exposed to SO₂ and O₂ BaCO₃ was completely decomposed already at 650°C, which revealed that the replacement of Ba-

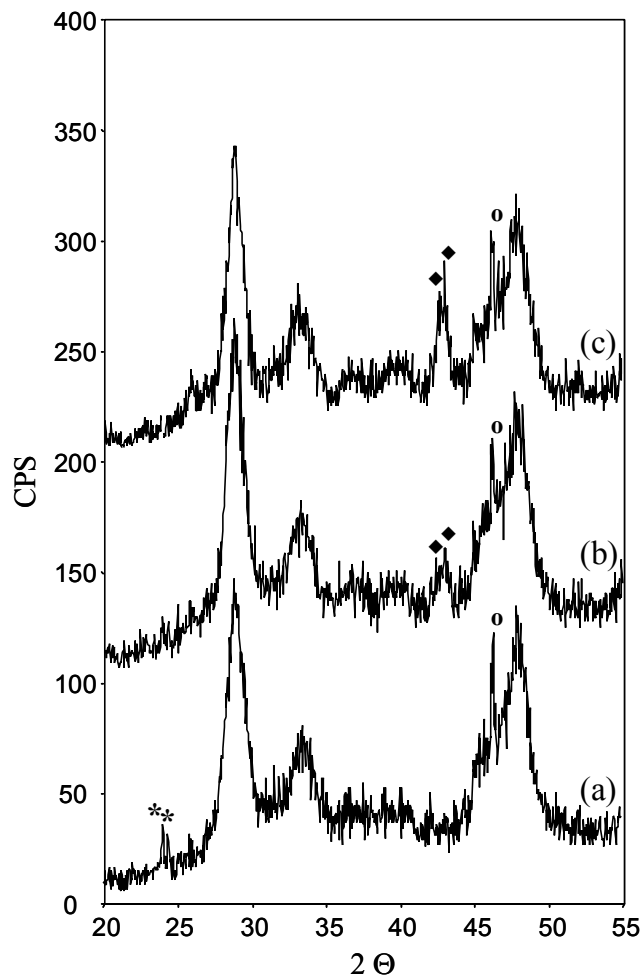


Fig. 5.1b: XRD diffraction pattern for the catalyst after heating to 700°C in He: (a) fresh (b) exposed to 400 ppm SO₂/ 5% O₂ at 350°C (c) exposed to 400 ppm SO₂/ 1000ppm NO during cycling between 5% O₂ (100 sec.) and 2000 ppm C₃H₆ (20sec.) at 350°C. (*) BaCO₃; (○) BaO; (◆) BaSO₄.

carbonates with Ba-sulfates accelerated the decomposition of carbonates. Reflections attributed to BaSO₄ species increased in intensity compared to the fresh material, which indicated an accelerated accumulation of BaSO₄ in the bulk during the thermal treatment at 700 °C.

The formation of crystalline Al-sulfate phases was not observed during exposure of the materials to SO₂. Jang et al. [20] investigated the thermal stability of Pt/Ba-Al₂O₃ and observed an interaction of Ba with alumina forming Ba-Al alloys (mainly BaAl₂O₄) above 600°C. However, on all materials investigated indications

for the formation of BaAl_2O_4 or other further substantial structural changes, caused either during pretreatment or during heating to 700°C , were not observed by XRD.

5.3.2 Sorption and retention of SO_2 under varying reaction conditions

5.3.2.1 Adsorption of SO_2 under lean and fuel-rich conditions

The concentration of SO_2 at the reactor outlet during exposure of the catalyst to SO_2 and O_2 at 350°C is shown in Figure 5.2. At the beginning of the SO_2/O_2 exposure more than 90% of SO_2 was adsorbed. After 90 min the SO_2 concentration increased markedly and reached a concentration of 260 ppm. The concentration of CO_2 at the reactor outlet continuously increased from the beginning of SO_2/O_2 exposure and reached the highest level prior to the SO_2 breakthrough, which clearly

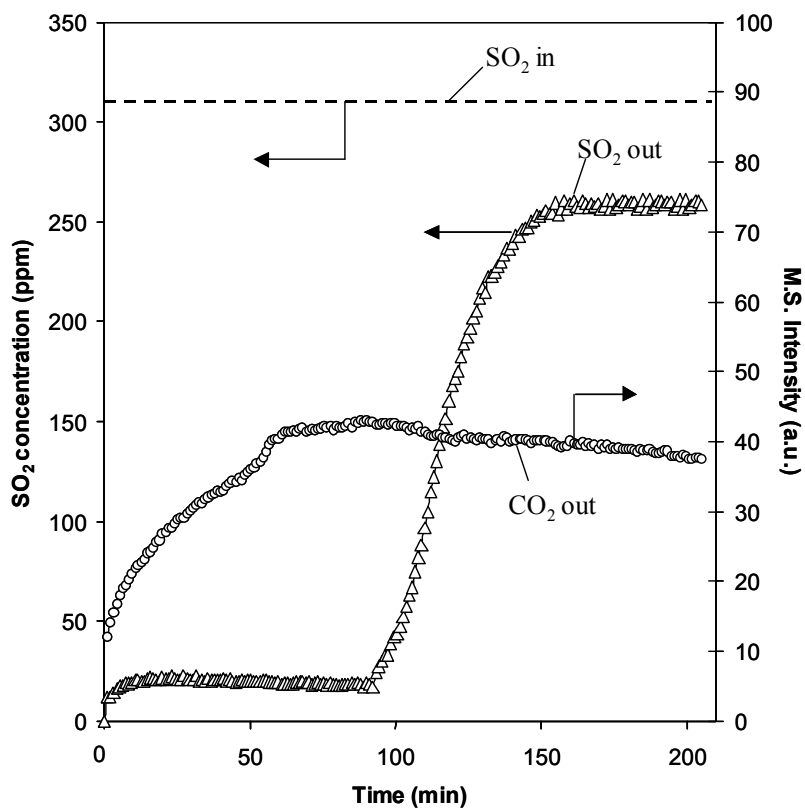


Fig. 5.2: SO_2 adsorption profile ($m/e = 64$) and CO_2 outlet signal ($m/e = 44$) during exposure to 310 ppm SO_2 and 5% O_2 (lean conditions) at 350°C .

indicated the partial replacement of Ba-carbonates by Ba-SO_x. The main source for CO₂ formation on this catalyst is the replacement of Ba-carbonates by the Ba-sulfate, which is also confirmed by the lower intensities of the XRD reflections for BaCO₃ after exposure to SO₂ and O₂. The formation of crystalline BaSO₄ phases, identified by XRD, indicated the oxidation of SO₂ to SO₃ on the noble metal and the subsequent replacement of BaCO₃ besides the reaction with BaO forming BaSO₄. The formation of Ba-sulfates occurring under lean conditions could therefore be summarized by equation (1) and (2):



Breen *et al* [21] reported a similar replacement process of BaCO₃ by BaSO₄ on a NSR catalyst consisting of Pt and Ba supported on ceria-zirconia. They observed an accelerate replacement of carbonates by sulfates during a temperature increase. This would explain the lower decomposition temperatures of BaCO₃ observed in the XRD for the sample pre-exposed to SO₂ and O₂ compared to the BaCO₃ decomposition on the fresh material. This indicates that the temperature increase accelerates the migration of surface SO_x species into the bulk phase of the storage component, which resulted in a faster replacement of Ba-carbonates by Ba-sulfates, followed by an enhanced decomposition of BaCO₃.

The difference between SO₂ inlet concentration at the reactor inlet (310 ppm) and at the outlet after saturation of the storage component (260 ppm), could be related to the oxidation of SO₂ to SO₃, which is hardly detectable by mass spectrometry, or to the migration of surface sulfates in to the bulk, which is considerably slower than the replacement of surface carbonates. The latter is supported by the slight decrease of the CO₂ concentration at the reactor outlet after the breakthrough of SO₂ was observed.

As for the sample pretreated with $\text{SO}_2/\text{NO}/\text{O}_2$ crystalline carbonate phases could not be identified by XRD (see Fig. 5.1a, pattern (c)), we would like to speculate that a promoting effect of NO on the replacement of carbonates by sulfates, probably by an additional oxidation of SO_2 by NO_2 , exists. The replacement of BaCO_3 by NO_x , reported for the adsorption of NO_x on a commercial NSR catalyst [5] furthermore indicates a faster removal of carbonates due to the additional replacement of carbonates by nitrites and nitrates. However, the absence of crystalline Ba-nitrate phases after the pre-treatment indicates, that subsequently to the replacement of carbonates by nitrites/nitrates the formation of sulfates occurs.

The concentration of SO_2 , H_2S and CO_2 at the reactor outlet during the exposure of the catalyst to SO_2 and C_3H_6 (rich reaction conditions) is shown in Fig. 5.3. At the beginning of the experiment an adsorption or consumption of SO_2 could

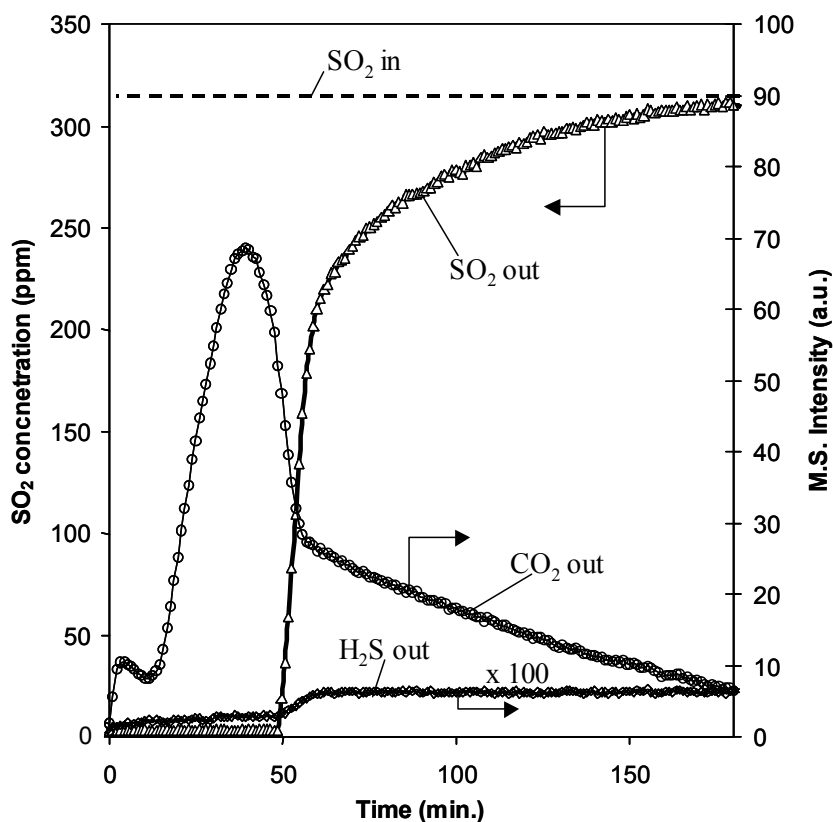


Fig. 5.3: SO_2 adsorption profile ($m/e = 64$) and CO_2 outlet signal ($m/e = 44$) during exposure to 310 ppm SO_2 and 5% O_2 (lean conditions) at 350°C . H_2S outlet signal ($m/e = 34$) is multiplied by 100.

also be observed during rich reaction conditions. The formation of sulfates on peroxide or oxygen-rich defect sites on the barium particles could be speculated to be one possible adsorption pathway for SO₂ storage. This reaction appears to be most relevant at the beginning of the SO₂ under rich reaction conditions, i.e., when reactive oxygen sites are present on the catalyst surface as the reduction of the surface sites by C₃H₆ is not finished.

Engström et al [9] observed an increasing amount of N₂O formed during the rich regeneration cycle in presence of SO₂ and attributed this to the deactivation of the noble metal, i.e., the reduction function, by sulfur species. Thus, an adsorption of SO₂ could occur on the noble metal sites. Wilson *et al.* [22] studied the interaction of SO₂ with Pt (111) and observed a dissociative adsorption of SO₂ on clean Pt at low temperatures, whereas on pre-oxidized Pt surfaces sulfates are formed even at high temperature. The sulfates adsorbed are reported to be highly reactive towards reduction reactions with hydrocarbon species (C₃H₆) leading to the formation of S deposits on the noble metal and to the oxidation of the hydrocarbons to CO₂.

The strong increase of the CO₂ partial pressure and the maximum observed before the breakthrough of the SO₂ signal in combination with the low concentrations of H₂S and higher thiols (which were close to the detection limit) indicate a reaction of C₃H₆ with SO_x species on Pt, resulting in the formation of S deposits on the noble metal after the reaction. Due to the presence of an oxidizing atmosphere during the lean reaction cycle, we would like to speculate that the sulfur deposits remaining on the surface of Pt are oxidized to sulfates and subsequently spill over to the storage sites, which would be the reason for an accelerated deactivation of the NO_x storage ability of the catalyst. This speculation is confirmed by the results of Fridell *et al.* [7], who observed a rapid deactivation of the NO_x storage capacity when SO₂ was injected during rich reaction conditions and proposed an adsorption of sulfur on Pt and the subsequent oxidation to sulfates that are trapped in the vicinity of the Pt particles when switching to lean reaction conditions.

5.3.2.3 Stability of SO_x species formed

The SO₂ partial pressure during temperature programmed desorption experiments after the pre-adsorption of SO₂/O₂ and SO₂/C₃H₆ is shown in Fig. 5.4. SO_x species formed on the storage component and on the noble metal component should show a different thermal stability due to their different bond strength to the surface sites and should, therefore, desorb at different temperatures during TPD experiments. For the catalyst pretreated with SO₂/O₂ (lean reaction conditions) two desorption maxima of SO₂ were observed at 740 and 830°C, while the material pretreated with

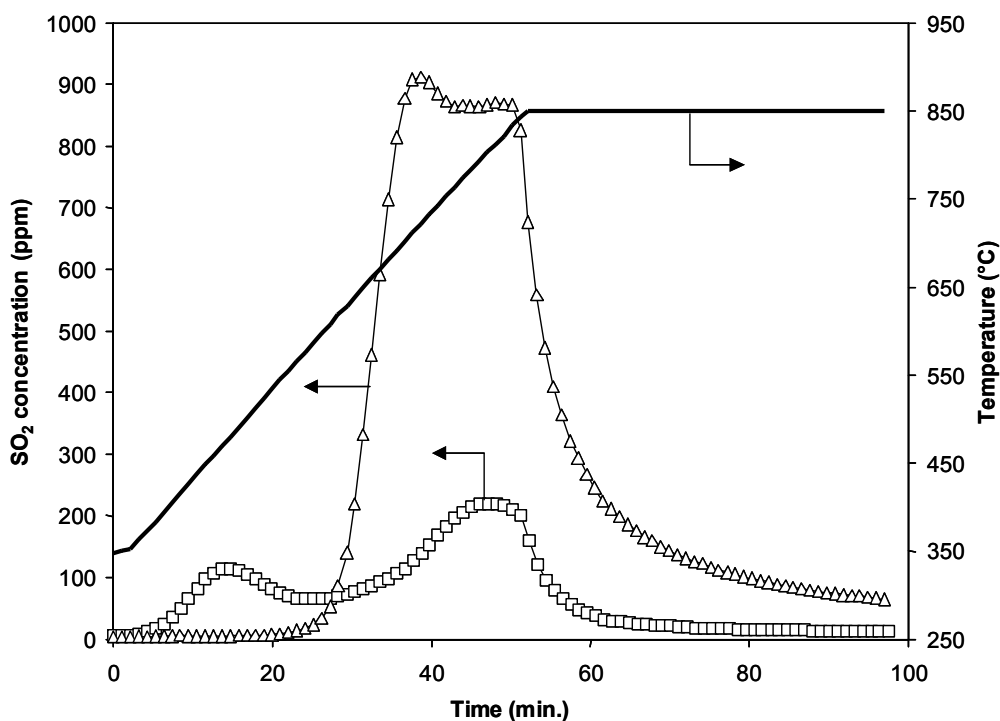


Fig. 5.4: SO₂ desorption profiles ($m/e = 64$) during TPD (350 to 850°C) in He after exposure to SO₂ and O₂ (Δ) and after exposure to SO₂ and C₃H₆ (\square) at 350°C.

SO₂/C₃H₆ (rich reaction conditions) exhibited a less intense maximum at 830°C and an additional desorption maximum at 450°C. In general this indicates the existence of weaker bonded SO_x species on the materials pretreated with SO₂/C₃H₆. The desorption maximum of SO₂ around 740°C for the material pretreated with SO₂/O₂ resulted most probably from sulfates located on the surface of the Ba

particles or on the Al_2O_3 support, while the peak at 830°C (with a broad shoulder still present at the final temperature of 850°C) could most likely be related to Ba-sulfates located in the bulk. After 850°C were reached in the TPD the temperature was kept constant for 60 min. During this time the concentration of SO_2 decreased only slowly and stabilized at a level of around 100 ppm, which indicates that even at 850°C the migration of the bulk sulfates to the surface is a relatively slow process. For the material preexposed to $\text{SO}_2/\text{C}_3\text{H}_6$ the desorption peak with a maximum around 830°C could be attributed to the formation of bulk BaSO_4 during the pre-treatment. As already described, these species were probably formed during the exposure to SO_2 under rich reaction conditions by the reaction of SO_2 and reactive surface oxygen on Ba particles [5] especially at the beginning of adsorption. The absence of a desorption peak for surfaces sulfates confirms their formation only at the beginning of the adsorption and their subsequent migration into the bulk, while the weaker bonded SO_2 species desorbing at around 440°C could be attributed to SO_x species formed on the Pt sites. This desorption peak was only observed for the catalyst pretreated under rich reaction conditions, which indicates the adsorption of SO_2 on the Pt metal particles.

Assuming, that the major fraction of SO_2 adsorbed during lean conditions is stored on the catalyst in form of sulfates and released during TPD (in the form of SO_2) the amount of SO_x remaining on the catalyst after TPD could be estimated by the difference between the SO_2 uptake area and the desorption area of SO_2 during TPD, which is given in Table 5.2.

Table 5.2: Difference of the uptake and desorption areas for SO_2 after lean and rich exposure.

<i>Treatment</i>	<i>Gas composition</i>	<i>Difference uptake area and desorption area in %</i>
lean	SO_2/O_2	29%
rich	$\text{SO}_2/\text{C}_3\text{H}_6$	68%

About 29 % of SO₂ adsorbed during lean conditions remained on the material after a high temperature treatment at 850°C for 40 min. This indicates that the thermal treatment of a deactivated NSR catalyst is not a successful strategy for the regeneration. Furthermore, it should be noted, that an extended high temperature treatment of NSR catalysts containing barium and alumina at temperatures above 600°C could cause a reaction between Ba-oxide and the Al₂O₃ support by forming Ba-Al mixed oxide phases, which lower the NO_x storage capacity [20].

For the catalyst pretreated under rich reaction conditions only 32% of the adsorbed SO₂ were removed after TPD. The difference in the amount of SO_x desorbing is in good agreement with the oxidation of C₃H₆ by SO₂ (sorbed on Pt) and the proposed formation of sulfur deposits on the noble metal particles. However, it could be not excluded, that a minor amount of SO₂ was consumed by the formation of H₂S and thiols, which are both known to deactivate the noble metals [15]. Nevertheless, H₂S and COS could be proposed to play only a minor role, as they are mainly formed when H₂ is used as reducing agent instead of C₃H₆ [13].

5.3.2.4 Effect of sulfation on the NO_x adsorption capacity

The influence of SO_x exposure on the NO oxidation and storage ability of the catalyst was investigated by comparing the NO/NO₂ response curves before and after sulfation by SO₂ under lean conditions and after exposure to 2000 ppm C₃H₆ at 600°C. The NO adsorption profiles are given in Figure 5.5. The fresh catalyst completely adsorbs NO for over 30 min, whereas after sulfation the NO (m/e = 30) breakthrough was detected immediately after the retention time. This indicates that NO_x was not stored on the catalyst after the storage sites were deactivated by sulfation. After exposure of the material to C₃H₆ at 600°C the NO concentration profile at the reactor outlet did not indicate a significant improvement of the NO_x storage ability of the catalyst. Thus, it could be concluded, that a regeneration at elevated temperatures under rich reaction conditions using hydrocarbons as

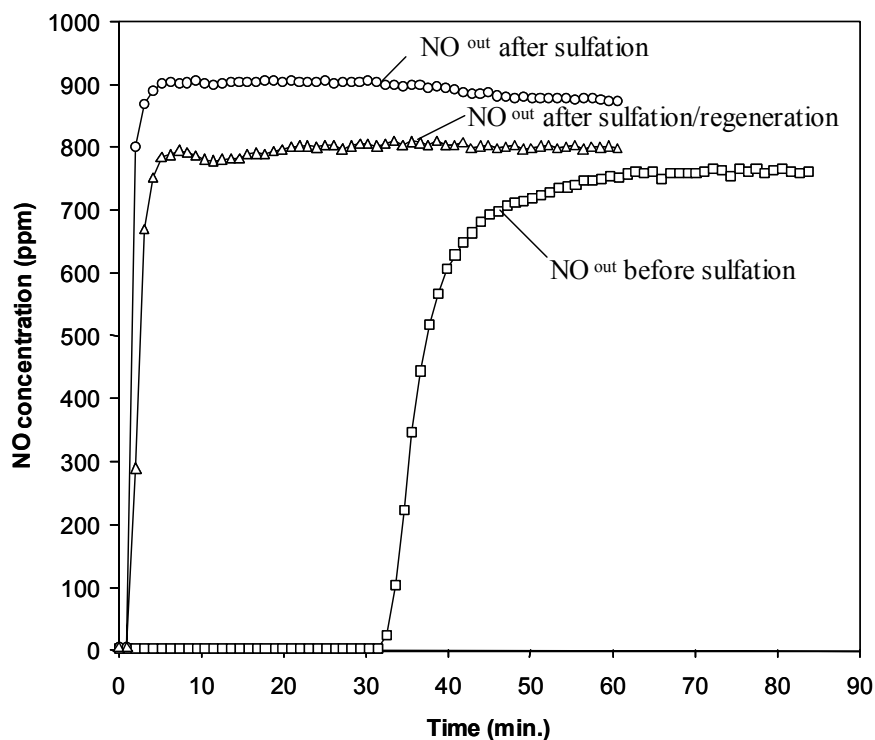


Fig. 5.5: NO adsorption profiles ($m/e = 30$) during exposure to 1000 ppm NO and 5%O₂ at 350°C before sulfation (□), after sulfation with 310 ppm SO₂ and 5% O₂ (O) and after sulfation and regeneration with 2000 ppm C₃H₆ for 60 min at 600°C (Δ).

reducing agents seem to be ineffective to regenerate the NO_x storage capacity of the NSR-catalyst.

For the catalysts after sulfation a higher fraction of NO in the total NO_x concentration was observed. Assuming, that NO₂ is mainly formed by the oxidation of NO on the noble metal, the lower concentration of NO₂ after sulfation of the catalysts (shown in Fig. 5.6) clearly indicates the deactivation of the noble metal function by SO_x-species. After the exposure of the catalyst to C₃H₆ at 600 °C the NO₂ and NO outlet concentrations reached levels similar to the fresh catalyst, which is a clear sign that in contrast to the deactivation of the NO_x storage functionality, the deactivation of the oxidation function of the noble metal is reversible under the regeneration conditions applied.

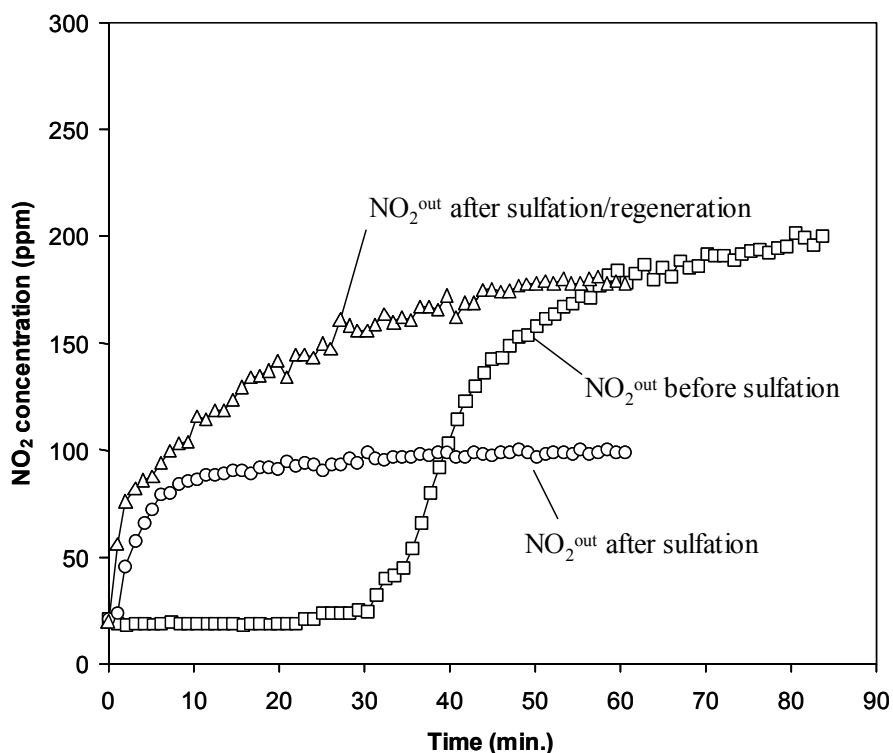


Fig. 5.6: NO₂ adsorption profiles ($m/e = 46$) during exposure to 1000 ppm NO and 5% O₂ at 350°C before sulfation (\square), after sulfation with 310 ppm SO₂ and 5% O₂ (O) and after sulfation and regeneration with 2000 ppm C₃H₆ for 60 min at 600°C (\triangle).

5.4 Conclusions

The influence of SO₂ exposure under lean and rich reaction conditions on the NO_x storage and the oxidation/reduction function of a commercial storage-reduction catalyst was investigated by uptake studies and high temperature XRD. A deactivation of the catalyst by SO₂ was observed under lean (oxygen-rich) as well as under rich (reducing) reaction conditions. Under lean conditions the formation of sulfates on the storage component (barium) was the main reason for the decrease in the NO_x storage capacity. These sulfates were found to accumulate in the bulk, where they replaced BaCO₃ and showed a high thermal stability at temperatures above 800°C. The oxidation function of noble metal was also lowered after the

exposure to SO₂ and O₂, in contrast to the storage capacity the oxidation function could be recovered by an exposure to propene at 600°C.

An adsorption of SO₂ was also observed during rich reaction conditions, which was attributed to the formation of SO_x species on the storage component at the beginning of the exposure and to the adsorption of SO₂ on the noble metal, which subsequently reacted with C₃H₆ to sulphur species on the noble metal. These sulfur species could be oxidized during the lean reaction conditions and a spillover to the storage component was proposed, which accelerates the deactivation of the storage capacity.

Therefore, both the storage capacity and the oxidation/reduction function of NSR catalysts are affected by the presence SO₂ under lean and rich exposure. The main and permanent deactivation of the NSR catalysts by SO₂ occurs on the storage component, whereas the oxidation/reduction component is only reversibly deactivated, as regeneration under conditions typical for the NSR process is possible. However, the regeneration process of the noble metal seems to accelerate the irreversible deactivation of the storage component.

Acknowledgements

The authors would like to thank the European Union for funding of this project in the framework of the Brite/EuRam program (BRPR-CT98-0613, STORECAT).

References

- [1] Kreuzer T., Lox S. E., Lindner D., Leyrer J., *Catal. Today* **29**, 17 (1996).
- [2] Fritz A., Pitchon V., *Appl. Catal. B* **13**, 1 (1997).
- [3] Katoh K., Kihara T., Asanuma T., Gotoh M., Shibagaki N., *Toyota Techn. Review* **44**, 27 (1995).
- [4] Miyoshi N., Matsumoto S., Katoh K., Tanaka T., Harada J., Takahashi N., Yokota K., Sugiura M., Kasahara K., *SAE Paper* 950809 (1995).
- [5] Sedlmair Ch., Seshan K., Jentys A., Lercher J.A., submitted to *J.Catal.*
- [6] Mahzoul H., Brilhac J. F., Gilot P., *Appl. Catal. B* **20**, 47 (1999).
- [7] Fridell E., Persson H., Olsson L., Westerberg B., Amberntsson A., Skoglundh M., *Topics in Catalysis* **16/17**, 133 (2001).

- [8] Takahashi N., Miyoshi N., Matsumoto S., Tanaka T., Shinjoh H., Iijima T., Yokota K., Suzuki T., Suzuki H., Yamazaki K., Tanizawa T., Tateishi S., Kasahara K., *Catal. Today* **27**, 63 (1996).
- [9] Engström P., Amberntsson A., Skoglundh M., Fridell E., Smelder G., *Appl. Catal. B*, **22** L241 (1999).
- [10] Mahzoul H., Limousy L., Brillhac J.F., Gilot P., *J. Anal. Appl. Pyrolysis* **56**, 179 (2000).
- [11] Amberntsson A., Westerberg B., Engström P., Fridell E., Skoglundh M., *Stud. Surf. Sci. Catal.* **126**, 317 (1999).
- [12] Sedlmair Ch., Seshan K., Jentys A., Lercher J. A. *Catal. Today* **75**, 413 (2002).
- [13] Erkfeldt S., Skoglundh M., Larsson M., *Stud. Surf. Sci. Catal.* **126**, 211 (1999).
- [14] Mahzoul H., Gilot P., Brillhac J.F., Stanmore B.R., *Topics Catal.* **16/17**, 293 (2001).
- [15] Amberntsson A., Jonsson M., Skoglundh M., Fridell E., *Catal. Today*, in press (2002).
- [16] Matsumoto S., Ikeda Y., Susuki H., Ogai M., Miyoshi N., *Appl. Catal. B* **25**, 115 (2000).
- [17] Nakatsuji T., Yasukawa R., Tabata K., Ueda K., Niwa M., *Appl. Catal. B* **21**, 121 (1999).
- [18] Huang H.Y., Long R.Q., Yang R.T., *Appl Catal. B* **33**, 127 (2001).
- [19] Weast R. C., "Handbook of Chemistry and Physics" Chemical Rubber Publishing Company, Ohio, 1970.
- [20] Jang B.-H., Yeon T.-H., Han H.-S., Park Y.-K., Yie J.-E., *Catal. Lett.* **77**, 21 (2001).
- [21] Breen J.P., Marella M., Pistarino C., Ross J.R.H. *Catal. Lett.* **80**, 123 (2002).
- [22] Wilson K., Hardacre C., Baddeley C.J., Lüdecke J., Woodruff D.P., Lambert R.M., *Surf. Sci.* **372**, 279 (1997).

Chapter 6

Mechanistic aspects on the deactivation by sulfur dioxide

Abstract

The interaction of sulfur dioxide with a commercial NO_x storage-reduction catalyst (NSR) has been investigated using in situ IR and X-ray absorption spectroscopy. Two pathways of catalyst deactivation by SO₂ were identified. Under lean conditions (exposure to SO₂ and O₂) at 350°C the storage component forms barium sulfates, which transform from surface to hardly reducible bulk sulfate species. The irreversible blocking of the Ba sites led to a decrease in NO_x storage capacity. Under fuel rich (SO₂/C₃H₆) conditions at 350 to 500 °C evidence for the formation of sulfides on the oxidation/reduction component (Pt) of the catalyst was found, which block the metal surface and thus hinder the further reduction of the sulfides.

6.1 Introduction

Lean-burn gasoline and diesel engines offer substantial reductions in fuel consumption and, hence, lead to lower CO₂ emissions compared to traditional gasoline engines. The crucial difference between these engines and traditional gasoline engines is the high concentration of O₂ ($\lambda > 1$) in the exhaust gas [1], which does not allow the use of conventional three-way catalysts (TWC) for the removal of NO_x.

A promising strategy in developing catalytic devices to convert NO_x under oxidizing conditions for lean-burn and diesel engines is based on the concept of NO_x storage-reduction (NSR) [2, 3]. This concept utilizes a catalyst with dual functionality: (i) a storage function, typically Ba-oxides and (ii) a NO_x reduction/oxidation component, typically Pt. During lean operation conditions (i.e., oxidizing atmosphere) NO is oxidized to NO₂ and stored on the barium component as nitrate. When a switch is made to fuel-rich conditions (i.e., reducing atmosphere) NO₂ is released from the storage component and converted to N₂ over the noble metal component of the catalyst. The major drawback of these catalysts at present is their high susceptibility to sulfur poisoning by competitive sorption of SO₂/SO₃, which lowers the capacity of the catalyst to store and reduce NO_x [4, 5].

In the present study the deactivation processes of a commercial NSR catalyst by sulfur components under lean and rich periods was investigated by *in situ* IR and X-ray absorption spectroscopy. The interaction of SO_x with barium (storage component) and Pt (oxidation/reduction component) was examined in detail regarding the formation and stability/reducibility of the sulfur species formed.

6.2. Experimental

The catalyst investigated was a typical NO_xSR material supplied in powdered form by Johnson Matthey, Royston, UK, containing Pt as part of the oxidation/reduction components and BaO/BaCO₃ as storage component on Al₂O₃

as support. The reference materials used for XAS experiments were obtained by Aldrich Chem. (BaO 97%; BaCO₃ 99,98% and BaSO₄ 99%).

The nature of sulfur species was investigated by sorption experiments carried out in an *in situ* IR-cell, which allows the simultaneous and controlled admission of reaction gases. The catalyst powder was pressed into self-supporting wafers and analyzed *in situ* during all treatments by transmission IR-spectroscopy (resolution 4 cm⁻¹). The adsorption experiments were carried out at temperatures between 350 °C and 500°C. Activated catalysts were investigated using a gas stream (25 ml/min) containing 400 ppm SO₂ in helium, 5 % O₂ or 2000 ppm C₃H₆ in helium.

The structural and chemical properties of barium and platinum were investigated by X-ray absorption spectroscopy (XAS). The materials were activated at 450°C in He for 60 min. To investigate the sulfur poisoning of barium under lean conditions, the activated catalyst was treated with 400 ppm SO₂ and 5% O₂ at 350°C in a total gas flow of 100 ml/min for 2h. X-ray absorption spectra were recorded at the Ba-L_{III} edge (5247 eV) *in situ* before and after the treatment.

To study the oxidation state of platinum, the catalyst was pre-treated (a) under lean (400 ppm SO₂/ 5% O₂), (b) under rich conditions (400 ppm SO₂/ 2000 ppm C₃H₆) and (c) cycling lean (100 sec.) and rich (20 sec.) conditions at 350°C and 500°C. All samples were pretreated for 5 h under the conditions described. XANES was used to probe the reducibility of Pt on the pretreated catalysts. Spectra were recorded every 50°C during TPR in H₂ with a temperature increment of 10°C/min up to 450°C. For analysis of the XANES, the scattering background was subtracted using a second order polynomial function and the position of the edge was calibrated using the spectra of a simultaneously measured Pt foil. The area of the peak above the Pt-L_{III} edge (11564 eV), which can be related to the oxidation state of the Pt, was integrated numerically. For qualitative comparison of the EXAFS, the oscillations were extracted from the background using a third order polynomial function and after weighting with k^2 , Fourier transformed in the range between 2.1

to 8 \AA^{-1} . The program WINXAS 97 (version 1.3) was used to extract the EXAFS from the measured absorption and to analyze the data.

6.3. Results

6.3.1 Interaction of SO_x with the storage component (Ba)

Time resolved *in situ* IR spectra during adsorption of 400 ppm SO_2 and 5% O_2 on the catalyst at 350°C are presented in Fig. 6.1. In the activated sample a broad absorption band at 1460 cm^{-1} was observed before SO_2 exposure, which is attributed to barium carbonate species [6]. During contact with SO_2 and O_2 this band decreased indicating the progressive removal and partial substitution of the carbonate by sulfates. After 1 min of adsorption two small bands appeared at 1120 cm^{-1} and 1060 cm^{-1} , which increased in intensity with exposure time. Bands at 1248 cm^{-1} , 1155 cm^{-1} and in the region of $1060\text{--}1000 \text{ cm}^{-1}$ appeared after 5 min of SO_2/O_2 adsorption. The bands at 1120 and 1060 cm^{-1} are characteristic for the S-O stretching vibrations of bidentate sulfates located on the surface of an alkaline earth

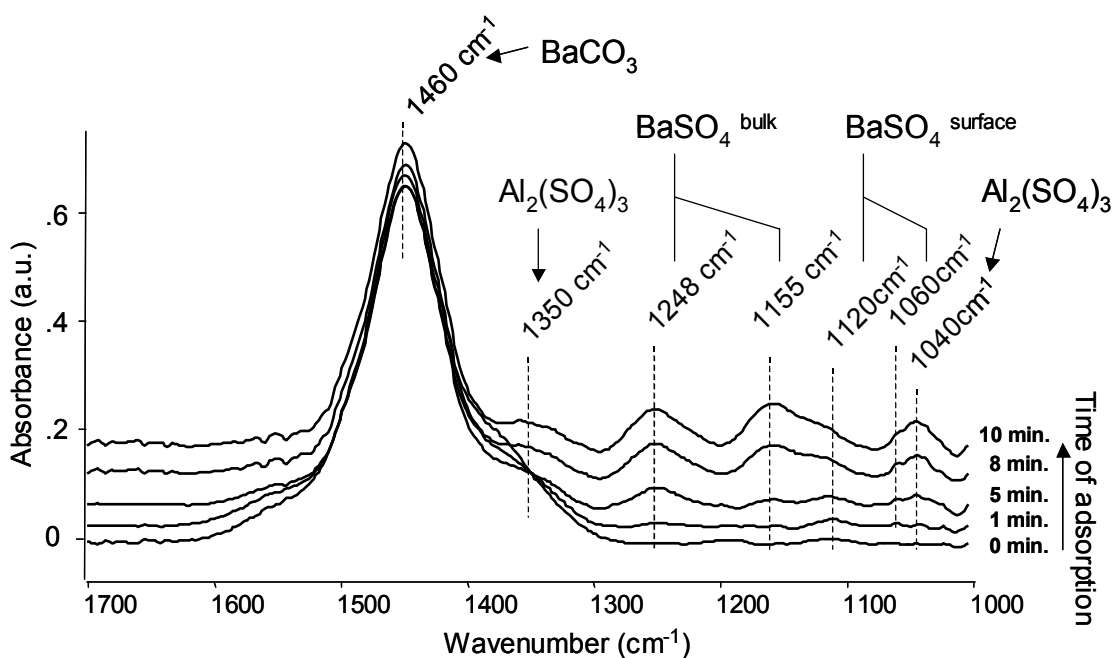


Figure 6.1: IR-spectra during adsorption of 400 ppm SO_2 and 5% O_2 at 350°C for 10 min.

metal [7, 8], while the bands at 1248 and 1155 cm^{-1} were attributed to bulk barium sulfate species [9]. Additionally bands at 1350 cm^{-1} and 1040 cm^{-1} were observed, which correspond to the $\nu(\text{S}=\text{O})$ vibration and to the $\nu(\text{S}-\text{O})$ vibration of tri-coordinated sulfate species on the Al_2O_3 support [10]. The IR spectrum remained almost unchanged when the SO_2/O_2 exposure was stopped and the catalyst was treated in He flow only at 350°C. After exposing the catalyst for 20 min at 350°C to 2000 ppm C_3H_6 in He (simulate a reducing/rich atmosphere) significant differences in the band intensities were not observed also confirming the high stability of the sulfates formed on barium.

To investigate the SO_x formation on the material under reducing conditions the fresh catalyst was activated and subsequently exposed to 400 ppm SO_2 and 2000 ppm C_3H_6 in He at 350°C. The corresponding IR spectra are shown in Fig. 6.2. Besides the already described disappearance of the carbonate species (band at 1460 cm^{-1}), no additional bands were observed between 1350 and 1000 cm^{-1} , the region characteristic for the formation of sulfate species on the storage function.

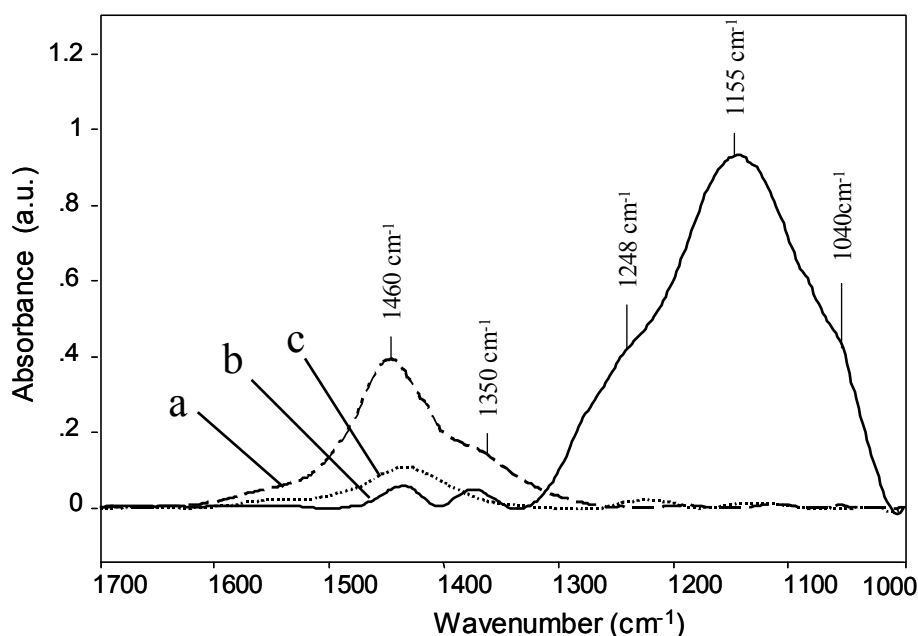


Figure 6.2: IR-spectra of a) the activated catalyst, after exposure b) to 400 ppm SO_2 and 5% O_2 at 350°C for 30 min. and c) to 400 ppm SO_2 and 2000 ppm C_3H_6 at 350°C for 30 min.

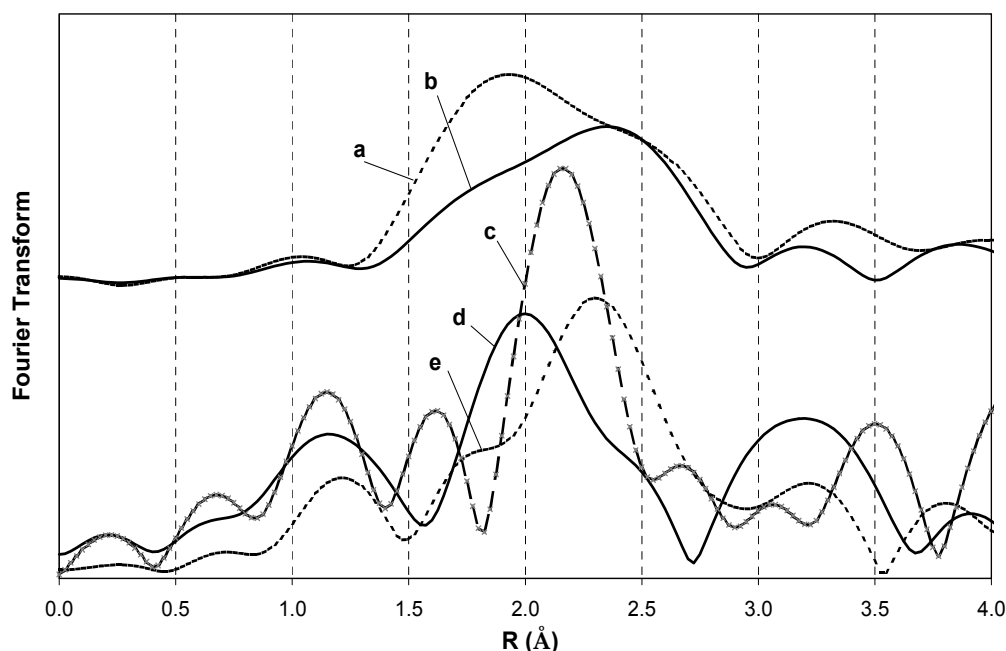


Fig. 6.3: Fourier transformed EXAFS at the Ba-L_{III} edge of the catalyst before and after exposure to SO₂/O₂: **(a)** NSR catalyst before exposure, **(b)** NSR catalyst after exposure, **(c)** BaCO₃, **(d)** BaO **(e)** BaSO₄.

The effect of SO₂/O₂ treatment on the local environment of the barium component was studied by *in situ* XAS of the Ba-L_{III} edge. Fourier transformed oscillations of the catalyst before and after 2h treatment with 400 ppm SO₂ and 5% O₂ at 350°C are compared to the reference materials of BaO, BaCO₃ and BaSO₄ in Fig. 6.3. The longer Ba-O distances of the catalyst observed after SO₂/O₂ treatment indicated changes in the local environment of Ba. The comparison of the Ba-O distances in the fresh catalyst and the reference samples indicated that barium exists as a mixture of BaO and BaCO₃ species. After exposure to SO₂ and O₂ the Ba-O distance of the catalyst is similar to the distance obtained for the BaSO₄ sample.

6.3.2 Interaction of SO_x with the oxidation/reduction function (Pt)

The oxidation state and the reducibility of Pt in the catalyst after treatment under lean and rich gas atmospheres were investigated by XANES and EXAFS at the Pt-L_{III} edge. XANES was used to examine the reducibility of Pt by H₂ for the

variously pretreated catalysts. Note, that this technique allows to specifically follow the reduction of Pt, while other techniques will lead to an integral signal, where other reducible components of the catalyst might contribute. The area of the peak above the Pt-L_{III} edge as a function of the temperature was used to describe the reduction of Pt with H₂ (Fig. 6.4 and Tab. 6.1).

In the fresh material Pt was reduced by H₂ between 150 and 200°C. A similar

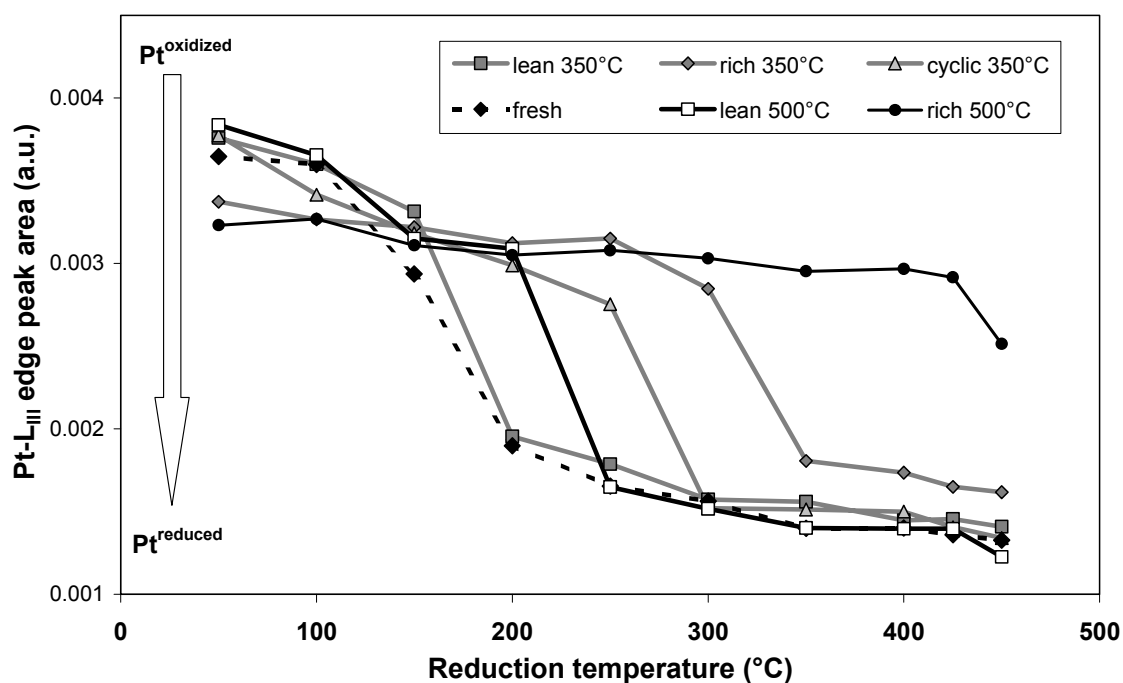


Figure 6.4: Area of the peak above the Pt-L_{III} edge during TPR in H₂ after different pre-treatment.

reduction behavior was observed for the catalyst pretreated under lean conditions (SO₂/O₂) at 350°C. For the material pretreated under lean conditions at 500°C, the cyclic pretreated material (SO₂/O₂, SO₂/C₃H₆) and the fuel-rich pretreated material (SO₂/C₃H₆) at 350°C a shift to higher reduction temperatures (from 230°C to 280°C up to 340°C) was observed. In contrast to the other samples investigated the rich pretreated material at 350°C was less reduced at the final temperature, while the fuel-rich pretreated material at 500°C was hardly reducible in hydrogen up to 450°C.

Table 6.1: Reduction temperature in H₂ of the different pretreated NSR catalyst.

Pretreatment	Gas composition	Reducibility	Reduction temperature
Fresh		++	160°C
Lean 350°C	SO ₂ + O ₂ at 350°C	++	180°C
Cyclic 350°C	SO ₂ + O ₂ /C ₃ H ₆ at 350°C	++	280°C
Rich 350°C	SO ₂ + C ₃ H ₆ at 350°C	+	335°C
Lean 500°C	SO ₂ + O ₂ at 500°C	++	230°C
Rich 500°C	SO ₂ + C ₃ H ₆ at 500°C	-	> 450°C

The local environment of Pt in the differently pretreated samples of the catalyst before TPR in H₂ was investigated by EXAFS to gain a better understanding of the sulfur species formed. The distance between Pt and its first neighbor (Fig. 6.5) in the fresh, lean and cyclic pretreated materials was 2 Å. Note that these distances are not corrected for the phase shift and, thus, are shifted to lower values. Distances above 2 Å were found in both samples pretreated in SO₂/C₃H₆ at 350°C and 500°C, which indicated structural changes in the neighborhood of the Pt atoms in presence of sulfur during fuel-rich conditions.

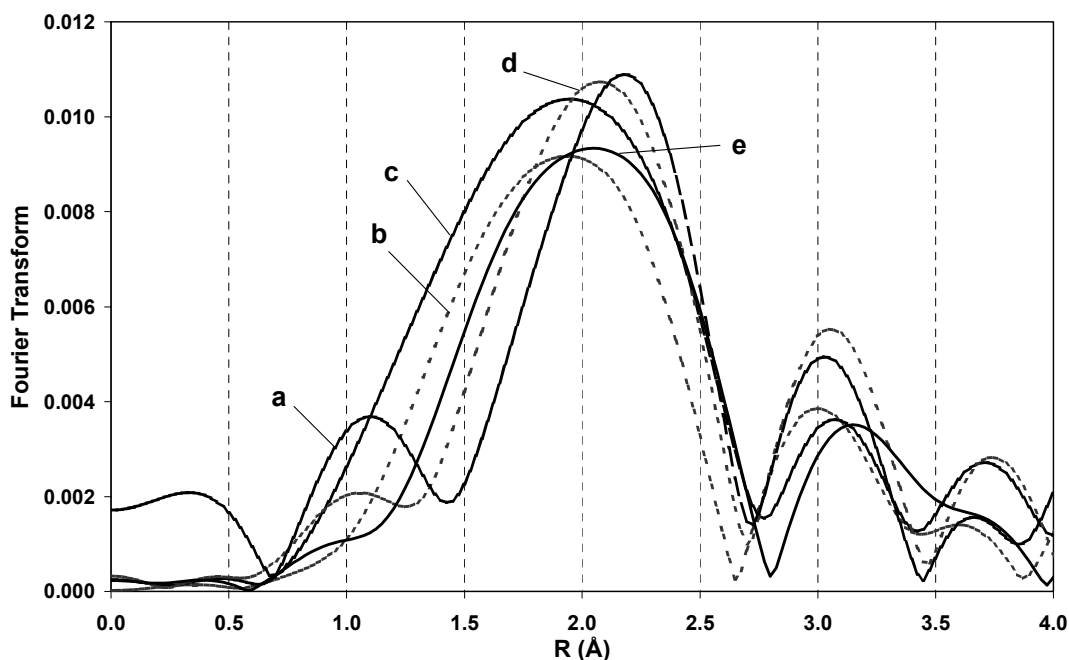


Fig. 6.5: Fourier transformed EXAFS at the Pt-L_{III} edge of the catalyst before TPR: (a) Pt-foil (ref.), (b) untreated catalyst, (c) after SO₂/O₂ pretreatment at 350°C, (d) after SO₂/C₃H₆ pretreatment at 350°C, (e) after SO₂/C₃H₆ pretreatment at 500°C.

6.4 Discussion

The results give a clear evidence for two possible pathways for the deactivation of NSR catalysts by sulfur. IR studies of the catalyst treated under lean conditions (400 ppm SO₂/ 5% O₂) at 350°C mainly showed sulfur species adsorbed on the support and on the storage component. Initially, bands for sulfates on the surface of barium were observed, while after further SO₂/O₂ exposure, bulk barium sulfates and aluminum sulfates were detected, which clearly indicated the migration and transformation of the surface sulfates into bulk sulfates. After regeneration of the catalyst with C₃H₆ (2000 ppm) at 350 C for 20 min significant changes in the intensities of the characteristic sulfate bands were not observed, which revealed that bulk sulfates were stable during the reduction in propene. Exposure of the fresh catalyst to rich conditions (SO₂/C₃H₆) showed only a negligible formation of sulfur species on the support and on the storage component, therefore, the deactivation of the storage component occurred mainly under lean reaction conditions. The comparison of the distance between Ba and the next neighbor (oxygen) in the references materials and the catalyst treated under lean conditions confirmed the formation of BaSO₄ on the catalyst after treatment with SO₂ under oxidizing conditions.

The distance between Pt and its first neighbor in the untreated, oxidized and cyclic pre-treated materials, was found to be less or equal to 2 Å (all distances were not corrected for the phase shift), while distances above 2 Å were found after pre-treatment in SO₂/C₃H₆ at 350°C and 500°C. The increasing distances clearly revealed the formation of Pt sulfide species [11, 12] during treatment under reducing conditions. Note, that in order to obtain a sufficient time resolution during the TPR experiments the XAS were measured only up to 8 Å⁻¹, which does not allow a detailed structural analysis of the Pt particles from the oscillations. XANES recorded during hydrogen TPR confirmed the lower reducibility of these platinum sulfide species as temperatures up to 450°C were necessary to (partly) reduce the poisoned metal particles under H₂ atmosphere. Sulfur species permanently

deactivating the Pt were not formed under lean condition, where the reduction behavior was comparable to that of the untreated material.

The differences in the reduction of the two fuel-rich pretreated materials clearly revealed a temperature dependency of the deactivation by sulfur. At 350°C mainly surface Pt-S species were formed, which could be removed during fuel-rich reaction conditions. The temperature increase to 500°C seems to accelerate the migration of the surface Pt-S into the bulk phase. As the catalyst could be regenerated under cyclic reaction conditions sintering of the Pt particles and masking of the Pt surface with mobile sulfate species seem to be only minor effects in the deactivation of the Pt component. The proposed deactivation pathways under lean and fuel-rich conditions are summarized in a general scheme given in Fig. 6.6.

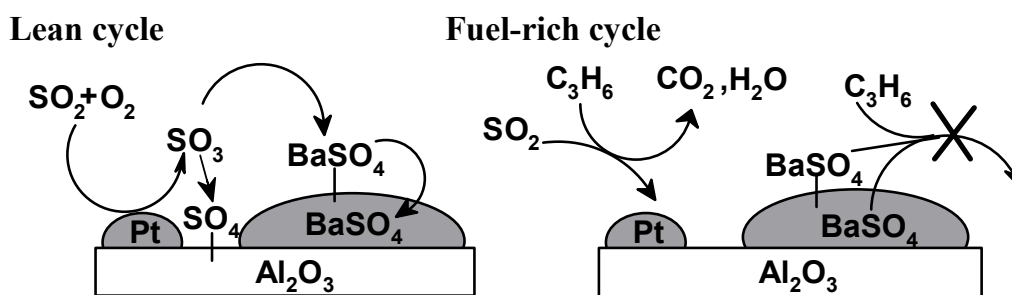


Figure 6.6: Proposed general scheme of the main pathways for the deactivation on a storage reduction catalyst. Lean cycle: Formation of surface sulfates on the storage component with a subsequent accumulation in the bulk. Fuel-rich cycle: Formation of sulfur species on the oxidation/reduction component. Regeneration of Ba-sulfates failed under working conditions

6.5 Conclusions

The results clearly reveal the existence of two pathways of deactivation for NO_x storage reduction catalysts. Under lean conditions (exposure to SO₂ and O₂) surface sulfates are formed on the storage component barium, which subsequently migrate into the bulk phase. These species are hardly reducible by C₃H₆ up to 550°C and block permanently Ba sites, which in turn leads to a decrease of NO_x storage capacity during successive cyclic treatments. A second pathway of

deactivation by sulfur species occurs during fuel-rich (reducing) conditions. Sulfides seem to be formed on the platinum particles, which block the metal surface and, thus, hinder the further reduction function of the metal as revealed by the lower reducibility (higher hydrogen reduction temperature) of the noble metal.

Acknowledgements

The authors would like to thank the European Union for funding of this project STORECAT; Brite/EuRam BRPR-CT98-0613. XAS experiments were supported by the EC, Contract Nr. II98-018 on the beamlines E4 and X1 at HASYLAB, DESY, Hamburg, Germany.

References

- [1] V. Pitchon, A. Fritz, *Appl. Catal. B*, **13** (1997) 1.
- [2] K. Katoh, T. Kihara, T. Asanuma, M. Gotoh, N. Shibagaki, *Toyota Techn. Review*, **44** (1995) 27.
- [3] N. Miyoshi, S. Matsumoto, K. Katoh, T. Tanaka, J. Harada, N. Takahashi, K. Yokota, M. Sugiura, K. Kasahara, *SAE Paper* 950809, 1995.
- [4] N. Miyoshi, S. Matsumoto, T. Tanaka, N. Takahashi, H. Shinjoh, T. Iijima, K. Yokota, T. Suzuki, H. Suzuki, K. Yamazaki, T. Tanizawa, S. Tateishi, K. Kasahara, *Catal. Today*, **27** (1996), 63.
- [5] P. Engström, A. Amberntsson, M. Skoglundh, E. Fridell, G. Smelder, *Appl. Catal. B*, **22** (1999) L241.
- [6] H. Mahzoul, J.F. Brilhac, P. Gilot, *Appl. Catal. B*, **20** (1999) 47.
- [7] R.A. Schoonheydt, J.H. Lunsford, *J. Catal.*, **26** (1972), 261.
- [8] M.A. Babaeva, A.A. Tsyganenko, V.N. Filimonov, *Kinetics and Catalysis*, (1985), 787.
- [9] M. Waqif, O. Saur, J.C. Lavalley, Y. Wang, B.A. Morrow, *Appl. Catal. B*, **71** (1991) 319.
- [10] O. Saur, M. Bensitel, A.B.M. Saad, J.C. Lavalley, C.P. Tripp, B.A. Morrow, *J. Catal.*, **99** (1986) 104.
- [11] M. Vaarkamp, J.T. Miller, F.S. Modica, D.C. Koningsberger, *J. Catal.*, **163** (1996) 294.
- [12] M. Vaarkamp, J.T. Miller, F.S. Modica, G.S. Lane, D.C. Koningsberger, *J. Catal.*, **138** (1992) 675.

Chapter 7

Summary and conclusions

7.1 SUMMARY AND CONCLUSION

Demands for a global reduction of CO₂ emission have led to the development of more fuel efficient combustion technologies. Lean burn and diesel engines are effective technologies for a reduced fuel consumption of motor vehicles. These engines, however, produce oxygen rich exhaust gases and conventional standard three way catalytic converters (TWCs) cannot efficiently reduce NO_x under a surplus of oxygen. The most promising approach for the reduction of NO_x under lean-burn conditions is based on the concept of NO_x storage-reduction (NSR), where the engine is operated in a mixed lean/rich operation mode. The major problem of NSR catalysts is, however, their low tolerance to sulfur containing fuels, which lead to a rapid decrease in the storage capacity. The reduction of the amount of sulfur in the fuel down to a technically sulfur-free level (~ 10 ppm) will help to preserve the activity of NSR catalysts. However, a slow poisoning effect occurs even with a fuel containing only small amounts of sulfur (<10 ppm). Therefore, improvements to catalyst design and technology will be required to create systems, which either totally preclude the possibility of sulfur poisoning or significantly facilitate regeneration.

A detailed knowledge of the NO_x storage and reduction mechanism and the SO_x deactivation mechanism is important for the design of NSR catalyst with an improved sulfur tolerance. The aim of this thesis was to describe elementary reaction steps for NO_x storage and release on a commercial NO_x storage reduction catalysts and to investigate the sulfur deactivation of this catalyst in more detail.

In chapter 3, the adsorption and reduction mechanisms of NO_x on alkali and alkaline earth metal exchanged zeolite Y (i.e. NaY and BaY) used as model storage components have been explored by *in situ* IR spectroscopy. Ionically bound nitrates and nitrites on the exchanged metal cation sites are the main species

formed during adsorption of NO and NO₂. Extra framework alumina was identified as additional sorption site forming small concentrations of bridging, chelating and monodentate nitrates. N₂O₄ and NO⁺ were found to be reaction intermediates during the NO_x adsorption process. The direct oxidation of NO₂ with reactive oxygen from the zeolite surface is facilitated by the formation of nitrates *via* the disproportionation reaction of N₂O₄ to NO⁺ and NO₃⁻. NO⁺ was found to act as precursor for the creation of nitrites. The nitrate species showed a thermal stability between 150 and 450°C. During the temperature increase less stable nitrite/nitrate species are transformed into Ba-nitrates showing the highest thermal stability. The stability of surface nitrates/nitrites was found to be lower, if NO instead of NO₂ is present in the feed during temperature increase. For the interaction of surface NO_x species with propene two pathways are proposed. At low temperatures, NO⁺ was identified as the active NO_x surface species reacting with propene to nitriles. At higher temperatures the reduction of surface nitrates/nitrites occurred *via* organic nitro/nitrito species, carboxylic species and isocyanates.

Based on the information obtained for the NO_x adsorption reduction mechanism on the metal exchanged Y zeolites the research was focused on the storage mechanism on a commercial NSR catalyst described in Chapter 4. During adsorption of NO mainly linear and bridged bonded nitrites of Ba-O-N-O-Ba type were formed on Al- and Ba-oxide components. Nitrites were detected during the initial phase of the NO/O₂ and NO₂ adsorption, whereas with further exposure nitrates were the dominant surface species. Using the different surface species and reaction intermediates identified by IR spectroscopy a series of sequential reaction steps during the sorption of NO_x on a NSR catalyst was derived. Initially, NO is stored in the form of nitrites on the storage component (Ba-oxide). NO₂ formed by oxidation on the noble metal component (Pt) either sorbs molecularly by forming nitrate species or dissociatively by forming nitrites. After a certain concentration of NO_x is adsorbed, the transformation and further oxidation of the surface nitrites into

surface nitrates by NO_2 occurs. The stability of the NO_x surface species was found to increase in the order: Al-nitrites < Ba-nitrites < Al-nitrates < Ba-nitrates.

The deactivation mechanism of a commercial NSR catalyst by sulfur dioxide is investigated and discussed in Chapter 5 and 6. Flow reactor studies and high temperature XRD was used to explore the influence of SO_2 exposure on the catalytic performance (Chapter 5). Both, the storage capacity and the oxidation/reduction function of the catalyst were deactivated by SO_2 exposure under lean (oxygen-rich) and rich (reducing) conditions. Deactivation of the storage component indicated by a loss of the NO_x storage capacity occurred mainly by the formation of Ba-sulfates accumulating in the bulk. They possess a high thermal stability ($>800^\circ\text{C}$) and could not be removed under working conditions typically for a NSR catalyst. For the oxidation function only a temporarily deactivation during lean exposure was observed. During the exposure under rich conditions, an adsorption of SO_2 on the noble metal is proposed via the formation of sulfide deposits by the reaction with C_3H_6 . The oxidation of these sulfur species with a subsequent spillover to the storage component during lean conditions could accelerate the deactivation of the storage capacity.

To investigate the interaction of sulfur dioxide with the storage component and the oxidation/reduction component in more detail *in situ* IR and X-ray absorption spectroscopy measurements were performed. The results clearly reveal the existence of two pathways of deactivation exist for NO_x storage reduction catalysts. Under lean conditions (exposure to SO_2 and O_2) surface sulfates are formed on the storage component, which subsequently migrate into the bulk phase. These species are hardly reducible by C_3H_6 up to 550°C and blocks permanently Ba sites, which in turn leads to a decrease of NO_x storage capacity during successive cyclic treatments. A second pathway of deactivation by sulfur species is proposed during fuel-rich (reducing) conditions. Sulfides seems to be formed at 350 and 500°C on platinum, which block the metal surface and hinder the further reduction function

of the metal as evidenced by a lower reducibility (higher hydrogen reduction temperature) of the noble metal.

7.2 SAMENVATTING EN CONCLUSIES

De vraag naar globale vermindering van CO₂ emissies hebben geldi tot de ontwikkeling van meer brandstofzuinige verbrandings technieken. Arme verbranding en diesel motoren zijn effectieve technologieën voor een lagere energie consumptie voor mobiele voertuigen. Deze motoren produceren een zuurstof rijk uitlaatgas en de conventionele standaard drie-weg katalysatoren (TWCs) kunnen niet efficiënt NO_x reduceren bij een surplus aan zuurstof. De meest belovende ontwikkeling voor de reductie van NO_x in arme verbrandig condities is gebaseerd op het concept van NO_x adsorptie-reductie (NSR), waarbij de mototr opereert in een afwisselende arm/rijk modus. Het grootste probleem van NSR katalysatoren is de lage tolerantie ten opzichte van zwafel houdende brandstoffen, welke een sterke afname in de adsorptie capaciteit tot gevolg hebben. Een afname van de hoeveelheid zwafel in de brandstof tot een technisch zwafel vrij niveau (<10 ppm) helpt bij het behoudt van de aktiviteit van de NSR katalysator. Hoewel zelfs bij deze lage concentraties aan zwafel vertoond de katalysator tekenen van een langzame deactivering. Dus zijn verbeteringen aan de katalysator gewenst die danwel de katalysator verhinderen te deactiveren of de mogelijkheid voor een regeneratie bevatten.

Een gedetailleerde kennis van de NO_x adsorptie en reductie mechanismen en het SO_x deactiverings mechanisme is van belang bij het ontwerp van een NSR katalysator met een verbeterede SO_x tolerantie. Het doel van dit proefschrift was het beschrijven van de elementaire reactie stappen van de NO_x adsorptie en desorptie op een commerciële NO_x adsorptie-reductie katalysator en om inzicht te verwerven in de deactivering door SO_x van deze katalysator.

Hoofdstuk 3 beschrijft een *in situ* infrarood spectroscopy studie van adsorptie en desorptie mechanismen voor NO_x op alkali en aardalkali uitgewisseld zeoliet Y (i.e. NaY en BaY) welke als model staan voor de adsorptie componenten. Ionisch gebonden nitraten en nitrieten op de uitgewisselde metaal kation posities zijn de overheersende vorm voor adsorptie van NO en NO_2 . Buiten structurelijke alumina vormde een extra adsorptie capaciteit voor kleine hoeveelheden aan overbruggende-, chelaterende- en monodentale nitraten. N_2O_4 en NO^+ bleken reactie intermediaren te zijn tijdens het NO_x adsorptie proces. De directe oxidering van NO_2 met reactief zuurstof van het zeoliet oppervlak is mogelijk door de vorming van nitraten via de disproportionerings reacties van N_2O_4 naar NO^+ en NO_3^- . NO^+ bleek zich te gedragen als voorloper voor de vorming van nitraten. De nitraten bleken thermisch stabiel tussen 150 en 450°C . Tijdens het verhogen van de temperatuur werden minder stabiele nitraten/nitrieten omgevormd tot Ba-nitraten welke meer thermisch stabiel zijn. De stabiliteit van oppervlakte nitraten/nitrieten bleek lager wanneer NO, in plaats van NO_2 , is aanwezig in de voeding tijdens het verhogen van de temperatuur. Twee routes zijn voorgesteld voor de interactie van oppervlakte NO_x species met propeen. Bij lage temperaturen bleek NO^+ de actieve NO_x species welke reageert met propeen tot cyanides. Bij hogere temperaturen blijkt de reductie van nitraten/nitrieten plaats te vinden via organische nitro/nitrito verbindingen, carboxyl species en isocyanaten.

Gebaseerd op de informatie verkregen over de NO_x adsorptie reductie mechanismen op het uitgewisselde Y zeoliet wordt in hoofdstuk 4 een studie beschreven naar de adsorptie mechanisme op een commerciële NSR katalysator. Tijdens de adsorptie van NO werden hoofdzakelijk lineaire en overbruggend gebonden nitrieten van het Ba-O-N-O-Ba type gevormd op Al- en Ba-oxide componenten. Nitrieten werden gedetecteerd tijdens de beginfase van de NO/ O_2 en NO_2 adsorptie terwijl bij langere blootstelling nitraten de dominante oppervlak species vormden. Gebruik makend van de verschillende oppervlakte species en

reactie intermediaren, aangetoond m.b.v. infrarood spectroscopy, een serie van opeenvolgende reactie stappen werden uitgevoerd tijdens de sorptie van NO_x op een NSR katalysator. Aanvankelijk adsorbeerd NO inde vorm van nitrieten op de opslag component (Ba-oxide). NO_2 dat gevromd word door oxidatie over de oxidatie component (Pt) adsorbeerd moleculair door de vorming van nitraten of dissociatief door de vorming van nitrieten. Nadat een bepaalde concentratie aan NO_x is geadsorbeerd geschied de oxidering van oppervlakte nitrieten tot nitraten met behulp van NO_2 . De stabiliteit van de NO_x oppervlakte species neemt toe in de volgende orde: Al-nitrieten < Ba-nitrieten < Al-nitraten < Ba-nitraten.

Het deactivering mechanisme van de commerciële NSR katalysator door zwafeldioxide is bestudeerd en wordt beschreven in hoofdstuk 5 en 6. Buis reactor studies en hoge temperatuur XRD experimenten zijn uitgevoerd om de invloed van blootstelling aan SO_2 op de activiteit van de katalysator (Hoofdstuk 5). De adsorptie capaciteit en de oxidatie/reductie functie van de katalysator werden beide verminderd in de aanwezigheid van SO_2 on arme verbranding (oxiderend) en rijke verbranding (reducerend) condities. Deactivering van de opslag component, geïdentificeerd door een vermindering vande opslag capaciteit, vindt hoofdzakelijk plaats door de vorming van Ba-sulfaten welke zich ophopen in de bulk. Deze zijn thermisch zeer stabiel ($>800^\circ\text{C}$) en konden niet worden verwijderd onder, voor de NSR normale, proces condities. Voor de oxiderings functie alleen een tijdelijke deactivering geobserveerd tijden de arme verbrandings condities. Tijdens de blootstelling in rijke verbrandings condities wordt de adsorptie van SO_2 voorgesteld door de vorming van zwafel afzetting tijdens de reactie met propaan. De oxidering van deze zwafel verbindingen en een daaropvolgende ‚spillover‘ naar de adsorptie component tijdens de arme verbrandings condities kan de deactivering van van de adsorptie component versnellen.

Om de interactie van zwafeldioxide met de adsorptie component en de oxidatie/reductie component in groter detail te bestuderen zijn in situ IR en Röntgen adsorptie metingen uitgevoerd. De resultaten tonen duidelijk het bestaan van twee routes voor de deactivering van NO_x adsorptie-reductie katalysator. In arme verbrandings condities (in de aanwezigheid van SO₂ en O₂) worden sulfaat species op het oppervlak gevormd van de adsorptie component welke vervolgens migreren naar de bulk fase. Deze verbindingen zijn nauwelijks te reduceerbaar met propeen tot 550°C en vormen een permanente blokkering voor de Ba posities wat dus een directe vermindering van adsorptie capaciteit tot gevolg heeft tijdens de meerdere cyclische behandelingen. Een tweede route voor de deactivering door zwafel verbindingen vindt plaats tijdens de rijke verbrandings condities (reducerend). Sulfides lijken te worden gevormd tussen de 350 en 500°C op platina, wat een blokkering vormd voor het metaal oppervlak en daarmee de reductie functie hinderen, wat blijkt uit de verminderde reduceerbaarheid (hogere waterstof reductie temperatuur) van het edel metaal.

7.3 ZUSAMMENFASSUNG UND SCHLUBFOLGERUNGEN

Die Notwendigkeit der Reduzierung des globalen Kohlendioxid-Ausstosses führte zur Entwicklung von effizienteren und verbrauchsärmeren Verbrennungstechnologien. Magermix- und Dieselmotoren sind effektive Technologien zur Verringerung des Treibstoffverbrauchs von Automobilen. Diese Motoren verursachen jedoch sauerstoffreiche Abgase. Dieser Überschuss an Sauerstoff führt dazu, dass herkömmliche Standard-Dreiwege-Katalysatoren (TWCs) die anfallenden Stickoxide nicht effizient genug reduzieren können. Eine der zukunftsreichsten Entwicklungen zur Reduktion von Stickoxiden unter Magermixbedingungen basiert auf dem Konzept von NO_x -Speicher-Reduktionskatalysatoren (NSR), bei dem der Motor in einer alternierenden mageren/fetten Arbeitsweise gefahren wird. Ein wichtiger Nachteil dieser NSR Katalysatoren ist jedoch die hohe Empfindlichkeit gegenüber schwefelhaltigem Treibstoff, was zu einer schnellen Abnahme der Speicherkapazität führt. Die Verringerung der Schwefelkonzentration im Treibstoff auf ein technisch schwefelfreies Niveau ($\sim 10\text{ppm}$) wird dazu beitragen die Aktivitätsdauer von NSR Katalysatoren zu erhöhen. Jedoch lässt sich ein langsamer Vergiftungseffekt auch bei geringen Schwefelkonzentrationen ($< 10\text{ ppm}$) feststellen. Deshalb sind Verbesserungen in der Katalysatorbeschaffenheit und -technik notwendig um Systeme zu entwickeln, die entweder eine mögliche Schwefelvergiftung vollkommen vermeiden oder eine verbesserte Regeneration des deaktivierten Katalysators aufweisen.

Um NSR Katalysatoren mit einer verbesserten Schwefeltoleranz zu entwickeln, ist eine genaue Kenntnis der Mechanismen der Stickoxid-Speicherung und -Reduktion sowie der Deaktivierung durch Schwefeloxide wichtig. Das Ziel der vorliegenden Arbeit war es, die elementaren Reaktionsschritte des NO_x Speicherprozesses für

einen kommerziellen NO_x-Speicher-Reduktions-Katalysator zu beschreiben und die Schwefeldeaktivierung detailliert zu untersuchen.

In Kapitel 3 wurden die Adsorptions- und Reduktionsmechanismen von NO_x auf mit Alkali- und Erdalkalimetallen ausgetauschten Y Zeolithen (NaY and BaY), die in diesen Untersuchungen als Modellspeichermaterialien fungierten, mittels *in situ* IR Spektroskopie untersucht. Es konnte gezeigt werden, dass ionisch gebundene Nitrate und Nitrite an ausgetauschten Metallkationzentren die vorherrschende Verbindung darstellen, die während der Adsorption von NO und NO₂ gebildet werden. Als zusätzliches Adsorptionszentrum konnten nicht im Gerüst eingelagerte Aluminiumoxidpartikel identifiziert werden, die mit NO_x in geringem Maße (ein- und zweizentren-)verbrückende und einfach-gebundene Nitrate bilden. N₂O₄ und NO⁺ konnten als Reaktionszwischenprodukte während der Adsorption von NO_x festgestellt werden. Die direkte Oxidation von NO₂ mit reaktiven Sauerstoffatomen auf der Zeolithoberfläche wird durch die Bildung von Nitraten über die Disproportionierung von N₂O₄ zu NO⁺ und NO₃⁻ unterstützt. Das gebildete NO⁺ fungiert als Vorstufe für die Bildung von Nitriten. Die gebildeten Nitrate zeigten eine thermische Stabilität zwischen 150 und 450°C. Während einer Temperaturerhöhung wurde eine Umlagerung von weniger stabilen Nitriten und Nitraten in Bariumnitraten, welche die höchste thermische Stabilität aufweisen, beobachtet. Die Stabilität der Oberflächennitrite und -nitrate erniedrigte sich unter NO Gasatmosphäre im Vergleich zu einer NO₂ Gasatmosphäre. Für die Wechselwirkung von Stickstoffoxidverbindungen auf der Oberfläche mit Propen können aufgrund der gefundenen Ergebnisse zwei Reaktionswege vorgeschlagen werden. Bei niedrigen Temperaturen konnte NO⁺ als aktive NO_x Verbindung identifiziert werden, welches mit Propen zu Nitrilen reagiert. Bei höheren Temperaturen erfolgt die Reduktion der Oberflächennitrate/-nitrite über organische Nitro- und Nitritverbindungen, Carboxylverbindungen und Isocyanate.

Basierend auf den Erkenntnissen über den Mechanismus der Stickoxidspeicherung und -reduktion an mit Metall getauschten Y Zeolithen wurde der Speichermechanismus an einem kommerziellen NSR Katalysator untersucht (Kapitel 4). Es zeigte sich, dass die Adsorption von NO bevorzugt durch die Bildung von einfach und verbrückt gebundenen Nitriten vom Typ Metall-O-N-O-Metall auf der Aluminium- und Bariumoxidoberfläche erfolgt. Während der Adsorption von NO/O₂ bzw. NO₂ konnten Nitrite nur am Beginn des Adsorptionsprozesses nachgewiesen werden, wohingegen mit weiterer Adsorptionszeit Nitrate die vorherrschende Oberflächenverbindung darstellten. Die verschiedenen Oberflächenverbindungen und Reaktionszwischenprodukten, die mittels IR Spektroskopie nachgewiesen werden konnten, ermöglichten eine Folge von sequentiellen Reaktionsschritten während der Speicherung von Stickoxiden auf einem NSR Katalysator abzuleiten. Zu Beginn wird NO als Nitrit auf der Speicherkomponente (BaO) sorbiert. NO₂, welches durch Oxidation an der Edelmetallkomponente (Pt) gebildet wurde, adsorbiert entweder molekular unter der Bildung von Nitraten oder dissoziativ unter der Bildung von Nitriten. Nachdem eine gewisse Konzentration an adsorbiertem NO_x erreicht ist, erfolgt eine Umlagerung und Oxidation der Oberflächennitrite durch NO₂ in Oberflächennitrate. Für die Stabilität der NO_x-Oberflächenverbindungen wurde folgende Reihung gefunden: Al-Nitrite < Ba-Nitrite < Al-Nitrate < Ba-Nitrate.

Die Untersuchungen des Deaktivierungsmechanismus an einem kommerziellen NSR Katalysator werden in Kapitel 5 und 6 diskutiert. Reaktorstudien und Hochtemperatur-Röntgenpulverdiffraktometrie wurden herangezogen, um den Einfluss von Schwefeldioxid auf die katalytische Leistung des NSR Katalysators zu untersuchen (Kapitel 5). Sowohl die Speicherkapazität als auch die Oxidations-/Reduktionsfunktion des Katalysators wurden durch SO₂ unter mageren (sauerstoffreichen) und fetten (reduzierenden) Bedingungen deaktiviert. Die Deaktivierung der Speicherkomponente, die sich in einem Verlust der NO_x

Speicherkapazität zeigte, wurde vorrangig durch die Bildung von Bariumsulfaten und deren Anreicherung im Katalysatorvolumen verursacht. Die hohe thermische Stabilität der Bariumsulfatverbindungen ($>800^{\circ}\text{C}$) verhindert eine Regenerierung des Katalysators unter für NSR Katalysatoren typischen Reaktionsbedingungen. Für die Oxidationsfunktion wurde eine reversibel Deaktivierung unter mageren Bedingungen gefunden. Unter fetten Reaktionsbedingungen kann eine Anlagerung von SO_2 am Edelmetall durch die Reaktion mit Propen unter der Bildung von Sulfiten angenommen werden. Die Oxidation dieser Schwefelverbindungen mit einem nachfolgenden Wechsel zur Speicherkomponente unter mageren Reaktionsbedingungen kann zu einer schnelleren Deaktivierung der Speicherkapazität beitragen.

Für eine genauere Untersuchung der Wechselwirkung von Schwefeldioxid mit der Speicherkomponente und der Oxidations-/Reduktionskomponente wurde *in situ* IR Spektroskopie und Röntgenabsorptionspektroskopie herangezogen. Die Ergebnisse zeigen deutlich, dass für die Deaktivierung von NO_x Speicher-Reduktionskatalysatoren zwei unterschiedliche Reaktionswege existieren. Unter mageren Reaktionsbedingungen (sauerstoffreiche Atmosphäre) werden Oberflächensulfate gebildet, die nachfolgend in das Volumen der Speicherkomponente wandern. Diese Verbindungen sind mit Propen bei Temperaturen bis 550°C kaum zu reduzieren und blockieren folglich irreversibel Bariumzentren, was sich in einer Abnahme der NO_x Speicherkapazität unter für NSR Katalysatoren typischen Reaktionsbedingungen zeigt. Ein zweiter Reaktionsweg für die Deaktivierung des Katalysators durch Schwefelverbindungen kann für fette (reduzierende) Reaktionsbedingungen vorgeschlagen werden. Die geringere Reduzierbarkeit (Reduktion mittels Wasserstoff bei höherer Temperatur) von Platin kann durch die Bildung von Sulfiden erklärt werden, welche die Metalloberfläche blockieren und dadurch eine weitere Reduktionsfunktion verhindern.

Acknowledgements

Looking back on the last four years during my PhD, there are quite a lot people who are part of the success and finalizing of this thesis. First of all, I would like to thank Prof. J.A. Lercher to offer me the PhD position. Thank you, Johannes, for the supervision and guidance of this work. You managed very well to push me to edges, which sometimes appeared to me insuperable. I am grateful for these experiences, which have certainly influenced my own life in a significant way. I also want to thank my dutch and german scientific supervisors, Seshan and Andy. Andy, thank you for the guidance of this work and the discussions (at the university and during XAFS measurements in Hamburg) and also for the careful revision and correcting of the thesis at the end. After a warm up period at the beginning it was nice and a great benefit for me to cooperate with you. Seshan, my dutch workleader, thank you for your guidance and your helpfulness and calmness especially during the more difficult parts of this PhD. I also want to thank Prof. Lefferts for the critical discussions during the last two years. Thank you, Leon, for your suggestions and remarks, which helped a lot to improve the quality of this work.

I would also like to thank my colleagues in the labs in Twente and Munich, who were part of my daily life during the last four years. Marco, thanks a lot for your introduction in the “secrets” of IR spectroscopy and for your readiness to help at any time during my stays in Enschede. To Bert for all the help in solving any administrative problems and financial matters. To all other members of the KPM group, Cis, Jan, Laurent, Sergio, Gerhard, Jean Pierre, Laszlo D., Laszlo L., Karin, Vilmos, Gautam, Cristina, Katia, and all the others many thanks for the visible or invisible help and the nice discussions in and outside the lab.

Thanks also to the two other members of the “Twente triplet” in Munich, Bertha and Martin. Many problems concerning our “outlaw status” were much easier to handle by the mexican-dutch-german connection.

To the colleagues (past and present) of the TC II group in Munich, Jan-Olaf, Josef, Reni, Xaver, Alex H., Steve, Andreas F., Andreas M., Su, Maria, Thomas, Alex G., Martin N., Hilton, Jochen, Fr. Schüler, Fr. Herrmann, Vannhu, Gabi, Iker, Christian, Hendrik, Hiroaki, Adam, Shoroung, Jan K., Florencia, Toshi, Xuebing, Oriol, Jenö, thanks for the support, the nice atmosphere and the fellowship at work and during the social events.

Dank gilt auch meinen Eltern, die durch ihre Unterstützung und ihr Vertrauen mir diesen Werdegang erst ermöglicht haben.

Meiner Frau Margit danke ich für ihre Liebe, ihr Verständnis und ihre Aufmunterungen in schwierigeren Zeiten. Besonderer Dank gilt meiner Tochter Rebekka und meinem Sohn Samuel, deren Liebe, Lachen, Zufriedenheit und Unbekümmertheit mir immer wieder zeigen, was den wahren Sinn des Lebens ausmacht.

But nevertheless, the show must go on ...

*Christian
October 2002*

Curriculum Vitae

Christian Sedlmair was born on May 4, 1972 in Buchloe, Germany. After graduating from high school in 1991 and civil service, he started his study in chemistry at the Technical University of Munich, Germany. He worked on his diploma thesis, entitled *Alkali and Alkaline Earth Metal Y Zeolites as Sorbents for CO₂ and NO₂* at the Institute for Technical Chemistry II at the Technical University of Munich, Germany under supervision of Prof. J.A. Lercher. In September 1998 he received his master degree (Diplom-Chemiker).

After graduation he started to work as a PhD student with Prof. J.A. Lercher at the University of Twente, The Netherlands and the Technical University of Munich. The main results of this research on the NO_x storage mechanism and SO_x deactivation on a commercial NO_x storage reduction catalyst are described in this thesis.

List of Publications

Studies on the deactivation of NO_x storage-reduction catalysts by sulfur dioxide

Sedlmair Ch., Seshan K., Jentys A., Lercher J. A. *Catal. Today* **75**, 413 (2002).

Catalytic reduction of NO_x in oxygen-rich gas streams, Deactivation of NO_x storage-reduction catalysts by sulfur dioxide

Sedlmair Ch., Seshan K., Jentys A., Lercher J. A. "Material Aspects in Automotive Catalytic Converter", Ed. H. Bode, Wiley-VCH, Weinheim, 2002, p.223-228.

Elementary steps of NO_x adsorption and surface reaction on a commercial storage-reduction catalyst

Sedlmair Ch., Seshan K., Jentys A., Lercher J. A. submitted to *J. Catal.*

An in situ IR study of the NO_x adsorption/reduction mechanism on modified Y zeolites

Sedlmair Ch., Seshan K., Jentys A., Lercher J. A. submitted to *Phys. Chem. Chem. Phys.*

Influence of sulfur dioxide on the catalytic performance of a commercial NO_x storage-reduction catalyst

Sedlmair Ch., Seshan K., Jentys A., Lercher J. A., in preparation.

Oral Presentations

Netherlands' Catalysis and Chemistry Conference NCCC III, March 4-6, 2002, Noordwijkerhout

Mechanistic aspects of the sulfur sensitivity of NO_x storage-reduction catalysts

Sedlmair Ch., Seshan K., Jentys A., Lercher J. A.

3rd European Workshop on Environmental Catalysis, Maiori, Italy, May 2-5, 2001

Studies on the Deactivation of NO_x Storage-Reduction Catalysts by Sulfur Dioxide

Sedlmair Ch., Seshan K., Jentys A., Lercher J. A.

34. Deutsche Katalytiker Tagung, Weimar, Germany, March 21- 23, 2001

Untersuchungen zur Vergiftung von NO_x Speicher-Reduktions-Katalysatoren durch Schwefeldioxid

Sedlmair Ch., Seshan K., Jentys A., Lercher J. A.